

TRANSPARENT GRAPHENE ANODES FOR ORGANIC LIGHT EMITTING
DIODES

A THESIS SUBMITTED TO
THE GRADUATE SCHOOL OF NATURAL AND APPLIED SCIENCES
OF
MIDDLE EAST TECHNICAL UNIVERSITY

BY

PARISA SHARIF

IN PARTIAL FULFILLMENT OF THE REQUIREMENTS
FOR
THE DEGREE OF DOCTOR OF PHILOSOPHY
IN
MICRO AND NANOTECHNOLOGY

JULY 2021

Approval of the thesis:

**TRANSPARENT GRAPHENE ANODES FOR ORGANIC LIGHT
EMITTING DIODES**

submitted by **Parisa Sharif** in partial fulfillment of the requirements for the degree
of **Doctor of Philosophy in Micro and Nanotechnology, Middle East Technical
University** by,

Prof. Dr. Halil Kalıpcılar
Dean, Graduate School of **Natural and Applied Sciences**

Prof. Dr. Almıla Güvenç Yazıcıoğlu
Head of the Department, **Micro and Nanotechnology**

Prof. Dr. Ahmet Oral
Supervisor, **Physics , METU**

Prof. Dr. Ali Çırpan
Co-Supervisor, **Chemistry , METU**

Examining Committee Members:

Prof. Dr. Oğuz Gülseren
Physics, Bilkent

Prof. Dr. Ahmet Oral
Physics, METU

Assoc. Prof. Dr. Alpan Bek
Physics, METU

Assoc. Dr. Emrullah Görkem Günbaş
Chemistry, METU

Prof. Dr. Coskun Kocabas
Materials Engineering, University of Manchester

Date: 14.07.2021

I hereby declare that all information in this document has been obtained and presented in accordance with academic rules and ethical conduct. I also declare that, as required by these rules and conduct, I have fully cited and referenced all material and results that are not original to this work.

Name Last name : Parisa Sharif

Signature :

ABSTRACT

TRANSPARENT GRAPHENE ANODES FOR ORGANIC LIGHT EMITTING DIODES

Sharif, Parisa

Doctor of Philosophy, Micro and Nanotechnology

Supervisor : Prof. Dr. Ahmet Oral

Co-Supervisor: Prof. Dr. Ali Çırpan

July 2021, 92 pages

This thesis presents a novel method for fabrication of OLEDs on a specific flexible PET substrate with graphene anodes, demonstrating low sheet resistance, high work function, and an extremely high luminance. Firstly, a single-layer graphene growth process with chemical vapor deposition (CVD) method is optimized. Flexible anodes are then fabricated by stacking 7-layers of graphene films and doped with nitric acid to reduce the sheet resistance. Modified few layer graphene anodes by $29 \Omega/\square$ sheet resistance and 84% transparency are used to fabricate OLEDs with a new family of thermally activated delayed fluorescence (TADF) materials. Observation of TADF in conjugated systems redefined the molecular design approach to realize highly efficient OLEDs in the early 2010s. Enabling effective reverse intersystem crossing (RISC) by minimizing the difference between singlet and triplet excited state energies (ΔE_{ST}) has been proven to be a widely applicable and fruitful approach, which resulted in the unproduction of numerous OLED devices with remarkable external quantum efficiencies (EQE). Here, a new series of TADF materials (Se-TADFs) with heavy-atom selenium is used as emitters in OLED structure. One of these materials, **SeDF-B**, resulted in pure blue emission with EQEs approaching 26%. Additionally, flexible graphene-based electrodes were developed for OLEDs

and revealed similar performance with indium tin oxide (ITO) on glass in most cases while, remarkably, suppressing ITO/Glass in pure blue OLED devices. These devices highlight the first-ever TADF based OLEDs that utilize graphene-based anodes in the literature.

Keywords: Graphene anode, TADF, OLEDs

ÖZ

ORGANİK IŞIK YAYAN DİYOTLAR İÇİN ŞEFFAF GRAFEN ANOTLARI

Sharif, Parisa
Doktora, Mikro ve Nanoteknoloji
Tez Yöneticisi: Prof. Dr. Ahmet Oral
Ortak Tez Yöneticisi: Doç. Dr. Ali Çırpan

Temmuz 2021, 92 sayfa

Mevcut çalışma düşük levha direnci, yüksek iş fonksiyonu ve yüksek parlaklık özellikleri sergileyerek bükülebilir bir alt taş üzerinde OLED üretiminde yeni bir metod ortaya koymaktadır. İlk olarak, kimyasal buhar biriktirme (CVD) metodu ile tek katman grafen büyüme süreci optimize edilmiştir. Daha sonra, esnek anotlar yedi kat grafen üst üste birleştirilerek ve levha direncini azaltmak için nitrik asit ile katkılanılarak üretilmiştir. $29 \Omega/\square$ levha direnci ve %84 şeffaflığa sahip modifiye edilmiş birkaç katmanlı grafen anotları TADF OLED'lerin üretiminde kullanılmıştır. Konjuge sistemlerdeki TADF gözlemi, 2010'ların başında yüksek verimliliğe sahip OLED'lerin moleküler dizaynına ilişkin yaklaşımı yeniden tanımlamıştır. Tekli ve üçlü uyarılmış hâl enerjileri (ΔEST) arasındaki farkı minimize ederek efektif RISC için imkan sağlamaktadır ve olağanüstü yüksek EQE özelliğine sahip çeşitli OLED cihazların üretimiyle sonuçlanan geniş çapta uygulanabilir ve verimli bir yaklaşım olarak kanıtlamıştır. Burada ağır-atom selenyumlu yeni bir TADF malzemeler serisi OLED yapısında ışık yayıcı olarak kullanılmıştır. Söz konusu malzemelerden biri olan SeDF-B %26'ya yaklaşan EQE değerinde saf mavi ışık yaymıştır. Buna ek olarak, OLED için esnek grafen bazlı elektrotlar geliştirilmiş ve bu elektrotlar çoğu zaman cam üzerindeki ITO'lara benzer performans göstermiştir, dahası saf mavi

OLED'lerdeki ITO/Cam elektrodunu belirgin bir şekilde geçmiştir. Bu cihazlar literatürde ilk grafen bazlı TADF OLED'ler olarak yer almaktadır.

Anahtar Kelimeler: Grafen, TADF, OLED

To my parents, and dear brother

ACKNOWLEDGMENTS

First of all, I would like to thank my supervisor, Prof. Dr. Ahmet Oral and co-supervisor Prof. Dr. Ali Cirpan for guidance, advice, criticism, encouragements, financial support and sharing their knowledge and experience without stinting. Their comments, suggestions and discussions were very valuable for me.

I am grateful to Prof. Dr. Gorkem Gunbas for his invaluable help, time, and support during that exciting and stressful process. This thesis would not have been possible without his support, great patience, and invaluable feedback.

This work is partially funded by Scientific and Technological Research Council of Turkey under grant number TUBİTAK 115F604.

I also would like to thank Professor Tofig Memmedli for design and fabrication of lab equipment and for his guidance and encouragement. I also want to express my appreciation to Professor Erol Yildirim for his theoretical collaboration in design and characterize of TADF materials.

I would like to give my special thanks to my committee members, Prof. Oguz Gulseren and Prof. Alpan Bek. I really appreciate their support, time, and valuable knowledge during this thesis. My deepest gratitude for the guidance they provided me as part of my thesis committee. I want to thank to Prof. Coskun Kocabas upon my last-minute request. I would like to thank very much for accepting to be a member of the PhD Thesis Committee.

I also want to thank to my friend Omer Caylan and his supervisor Prof. Goknur Buke for their help and support in lab operations, graphene growth experiments setting up, and materials characterizations. He is an outstanding role model not only as a scientist with hard-working ethic and extensive experiences but as a person with a great personality.

This work was heavily dependent on teamwork, and it would not have been possible without friendship, help and support of my great teammate Eda Alemdar, who train and help me in OLED fabrication. I was very lucky to have such a hardworking, adaptive, determined, and kind-hearted partner during my thesis study which became not only good colleague, but great friend. I would like to thank my friends in organic chemistry lab Dr. Gonul Hizalan, Mert Can Erer, Soner Ozturk and in their help and support in device fabrication and synthesizing the organic materials.

I would also like to express my special thanks to Mustafa Yasa for his support, sharing his knowledge, and his help in graphical abstract designing.

Special thanks are given to my research group members, Ercan Karagoz, Muammer Kozan, Kubra Cerit and Arash Badami for their emotional support, help in experiments, friendship , help and support not only at the university but also in my personal life as well.

I greatly thank many friends at METU who made my life very happy and exciting. My special thanks should be given to Mona Bora, Melisa Es, Salar sedani, Kerim Yusefi, Milad Gasemi, Naser Beyraghi, Wiria Soltani, Zeynab Eftekhari and Gence Bektas with whom I have spent countless time together.

I would also like to thank Yalciner Yalcin for his support, understanding, and encouragement during this stressful process, and I really appreciate his help for improving myself.

I would like to express my sincere thanks to my parents, Rahim and Parvin Sharif for their endless love, patience and supports throughout my life. I am also grateful to my brother, Pouria Sharif for his continuous support and encouragement.

TABLE OF CONTENTS

ABSTRACT	v
ÖZ.....	vii
ACKNOWLEDGMENTS.....	x
TABLE OF CONTENTS	xii
LIST OF TABLES	xiv
LIST OF FIGURES.....	xv
CHAPTERS	
1 INTRODUCTION.....	1
2 LITERATURE REVIEW.....	7
2.1 Graphene.....	7
2.1.1 Synthesis methods of graphene	11
2.1.2 Characterization methods of graphene	17
2.1.3 Transfer methods.....	20
2.2 Organic Light Emitting Diode (OLED).....	23
2.2.1 Application of OLEDs.....	25
2.2.2 OLED classification	27
2.2.3 Flexible OLEDs.....	32
3 GRAPHENE GROWTH	37
3.1 Synthesis of graphene with CVD method.....	37
3.1.1 Copper as a catalyst metal	38
3.1.2 Precleaning (Acid Pretreatment)	40
3.1.3 Growth of graphene.....	42

3.1.4	Oxidation Technique.....	45
3.1.5	Raman Spectrum of SLG.....	46
3.1.6	Scanning Electron Microscopy image of SLG.....	47
3.1.7	HEMS measurement.....	48
3.1.8	Transmission measurement.....	49
3.1.9	Work function Measurement.....	51
3.2	Transfer of CVD-Grown graphene.....	53
3.2.1	Fishing technique.....	54
3.2.2	Lamination technique.....	55
3.3	Doping of graphene.....	55
4	GRAPHENE BASED OLEDs.....	59
4.1	TADF Materials.....	59
4.1.1	Molecular Design, Computational Studies, and Synthesis.....	60
4.2	Device fabrication and characterization.....	65
4.3	Graphene based OLEDs with commercial materials.....	79
5	CONCLUSION.....	81
	REFERENCES.....	83
	CURRICULUM VITAE.....	93

LIST OF TABLES

TABLES

Table 2.1 Summary of graphene-based OLED papers in literature.	34
Table 2.2. Comparison between the TADF blue OLEDs in literatures and the OLEDs of this work.....	35
Table 3.1 Summary of graphene growth result	43
Table 4.1 Summary of OLED characteristics of champion devices, (average in parenthesis).....	76

LIST OF FIGURES

FIGURES

Figure 1.1. (a) Structure of graphene. (b) Structure of graphene in graphite	1
Figure 1.2. (a) Performance of a graphene-based touch screen. (b) A foldable graphene screen. (c) Graphene-based touch screen vs. ITO-based touch screen. [8]	3
Figure 2.1. Graphene as a basic structure of other graphitic forms.[9].....	8
Figure 2.2. Fermi energy for an undoped graphene crystal[13].....	10
Figure 2.3. Procedure of graphene synthesis with Scotch tape [14].....	12
Figure 2.4. Procedure of graphene synthesis with LPE method. [17]	13
Figure 2.5. Procedure of graphene synthesis with epitaxial growth on SiC. [19] ..	14
Figure 2.6. Procedure of CVD growth of graphene on (a) Ni, (b) Cu. [24]	15
Figure 2.7. (a) Raman Spectrum of Graphite vs SLG, (b) Raman spectrum of graphene with different layers [31].....	18
Figure 2.8. (a–e) SEM images of few-layer graphene after growth for 5, 10, 20, 40, and 60 minutes. (f–g) SEM images of the regions at high magnification [33].....	19
Figure 2.9. Optical transmittance measurement of graphene sheets transferred to glass for graphene with 1, 2, and 3 layers [34].	20
Figure 2.10. Process flow of PMMA-assisted transfer of CVD graphene films. [35]	22
Figure 2.11. Graphene transfer by using Lamination technique [36]	23
Figure 2.12. A simple structure of OLED [37]	24
Figure 2.13. OLED's application in electronic display technology, (a)Smartphone, (b) OLED TV, (c) Digital Camera, (d) Wearable device. [40] [41]	26
Figure 2.14. OLED light panel [43].....	27
Figure 2.15. Schematic image of, (a) Charge recombination, (b) Spin combination [44].....	28
Figure 2.16. Working principles of 1 st , 2 nd and 3 rd generations of OLEDs. [45]....	30
Figure 3.1. (a) CVD system 1, (b) CVD system 2, (c) CVD system 3.	38
Figure 3.2. (a) Graphene on electroplated Copper, (b) Graphene on cold rolling Copper.....	39

Figure 3.3. (a) Raman spectrum and optical image of graphene on electroplated Copper, (b) Raman spectrum and optical image of graphene on cold rolling Copper.	40
Figure 3.4. (a) Surface of copper before annealing, (b) Surface of copper after annealing.....	41
Figure 3.4. Summary of graphene growth process.....	44
Figure 3.5 (a) Oxidation technique, (b) Optical image of graphene/Cu foil with inconstant surface, (c)) Optical image of graphene/Cu foil with uniform surface.	45
Figure 3.7. Raman spectrum of single layer graphene.	46
Figure 3.8. SEM images of single layer graphene on copper substrates before the transfer, with different magnifications.	47
Figure 3.9. (a) Description of van der Paw method, (b) Measuring the electronic properties of graphene with four probe measurement.....	49
Figure 3.10. The optical transmission measurement of single layer and seven-layer graphene.	50
Figure 3.11. UPS spectrum[64]	52
Figure 3.12. UPS spectrum of SLG.....	53
Figure 3.13. Process flow of Photoresist-assisted transfer method.	54
Figure 3.14. Process flow of lamination-assisted transfer technique.	55
Figure 3.15. Schematic description of Interlayer and last layer-doped of graphene.	57
Figure 3.16. The 7LG/PET samples which doped with interlayer doping and last layer doping method.	57
Figure 4.1. a) Structural formula of small molecules SeDF-G, SeDF-B, and SeDF-YG. b) Electrostatic potential surface (ESP) and frontier molecular orbital surfaces (HOMO, and LUMO) for the SeDF-G, SeDF-B, and SeDF-YG TADF materials in the equatorial and axial conformation of selenium substituted PTZ donor, c) Luminescence images of SeDF-G, SeDF-B, and SeDF-YG in chloroform recorded under UV irradiation at $\lambda_{ex}=365$ nm (above), Absorption and normalized	

photoluminescence (PL) spectra of SeDF-G, SeDF-B and SeDF-YG in chloroform at room temperature (below).....	61
Figure 4.2. Optimized lowest energy conformations for SeDF-G, SeDF-B and SeDF-YG TADF materials.	62
Figure 4.3. Synthetic pathways for the TADF materials (SeDF-G, SeDF-YG, SeDF-B): Reagents and Conditions: (a) SeO ₂ , I ₂ , 180 °C, 48%; (b) bromobenzene, AlCl ₃ , rt □ 90 °C; (c) Pd ₂ (dba) ₃ , (t-Bu) ₃ P, NaO-tBu, Toluene, 125 °C, 82%; (d) NaH, DMF, 60 °C, 28%.	63
Figure 4.4. Time Resolved PL spectra for SeDF-G, SeDF-B and SeDF-YG.....	64
Figure 4.5. Cross-section of process flow of graphene-based graphene.....	65
Figure 4.6. The J-V characteristic and luminance vs voltage curve of HIL thickness optimization with (1:1), (1:2), (1:3) ratios.	67
Figure 4.7. The J-V characteristic and luminance vs voltage curve of ETL thickness optimization.	69
Figure 4.8. Electroluminescence vs wavelength graph for different ETL thicknesses	70
Figure 4.9. Device architectures of (a) ITO-based and (b) graphene-devices and energy band alignments of (c) ITO-based devices and (d) graphene-based devices.	71
Figure 4.10. OLED characteristics, a Current Efficiency and EQE (%) vs. Luminance of devices ITO- SeDF-G , ITO- SeDF-B , and ITO- SeDF-YG , b . Current density–voltage–luminance (J–V–L) characteristics of ITO-based OLEDs.....	73
Figure 4.11. a . Current Efficiency and EQE (%) vs. Luminance of devices Gr-SeDF-G, Gr-SeDF-B, and Gr-SeDF-YG, b . Current density–voltage–luminance (J–V–L) characteristics of graphene-based OLEDs.	74
Figure 4.12., Photographs of ITO based and graphene-based OLED devices (A: SeDF-G / ITO, B: SeDF-G /Gr, C: SeDF-B / ITO, D: SeDF-B / Gr, E: SeDF-YG / ITO, F: SeDF-YG / Gr). b , Chromaticity diagram of OLED devices. c , Electroluminescence vs. wavelength graphs of devices: (SeDF-G / ITO and SeDF-	

G / Gr), (SeDF-B / ITO and SeDF-B / Gr), (SeDF-YG / ITO and SeDF-YG / ITO).	78
Figure 4.13. a. Luminance vs voltage plot of PFOPV thickness optimization, b. Electroluminescence spectrum of device, c. Chromaticity diagram of device, d. Current density–voltage–luminance (J–V–L) characteristics of graphene-based OLEDs.	80

CHAPTER 1

INTRODUCTION

Graphene is a two-dimensional (2D-material) and nanoscale allotrope of carbon with several important features, namely light transmission and electrical conductivity, is a promising material for different application. Graphene is a 2D planar sheet of sp^2 connected carbon atoms. It could also be described as being made up of benzene rings separated from their hydrogen atoms. In graphene, the carbon-carbon bond (sp^2) length is approximately 0.142 nm. Graphite's interlayer spacing distance is also 0.335 nm.[1] Figure 1.1 illustrates the graphene structure.

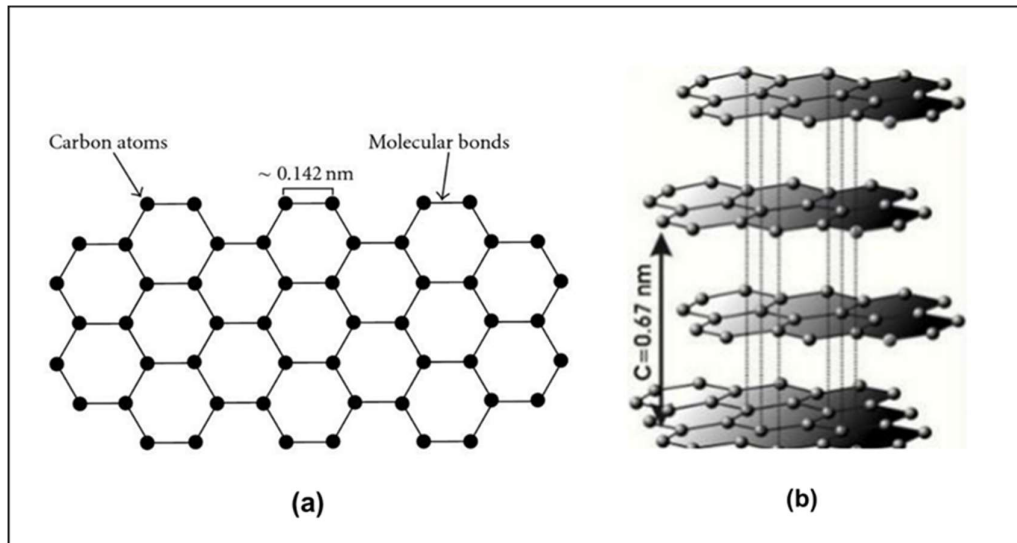


Figure 1.1. (a) Structure of graphene. (b) Structure of graphene in graphite

Since its discovery by Andre Geim and Kostya Novoselov in 2004, graphene has acquired a great deal of attention due to its remarkable and one-of-a-kind qualities,

which have attracted the attention of scientists worldwide. Graphene exhibits a significant specific surface area (2630 m² /gr), a high Young's modulus (nearly 1 TPa), a high intrinsic charge mobility (200000 cm² /V.s), a high thermal conductivity (5000 W/m.K), and a considerable optical transmittance (97.7%). Transparent conductive electrodes, batteries, super capacitors, graphene-based electronics, fuel cells, solar cells, membranes, transistors, biosensors, molecular gas sensors, and composite materials are just a few of the possibilities for graphene.

Graphene can be synthesized in a variety of ways. There are two types of methods: top-down methods and bottom-up methods. Micromechanical cleavage was one of the top-down approaches used to discover graphene. Hummers technique, Tour method, chemical and thermal reduction of graphene oxide, sonochemical liquid phase exfoliation, microwave, and electrochemical exfoliation of graphite are all basic top-down approaches. The main bottom-up methods are CVD (chemical vapor deposition) and SiC thermal decomposition.

Scientists' main goal is to create defect-free graphene with few layers. It is difficult to synthesize graphene in large scales with few layers using top-down methods. Graphene in large scale is largely used in electronic applications. Bottom-up graphene production methods may be more useful for these types of applications. Bottom-up techniques involve the formation of single layers of graphene on top of a substrate. Bottom-up techniques include chemical vapor deposition (CVD) epitaxial growth of graphene on a substrate, pyrolysis, solvothermal synthesis, and thermal decomposition of silicon carbide (SiC) wafers under ultrahigh vacuum conditions. It is hard to obtain graphene without substrate because without a supporting substrate, it is almost impossible to grow graphene.

Numerous research have been carried on how to use graphene in certain applications. For molecular-scale electronics, graphene is a good choice. Graphene can also be used in the field effect transistor as a semiconductor layer [2]. Capacitors, sensors, and electronic lenses can all be manufactured out of graphene. [3]

Along with electronic application, graphene is a useful material for photonics and optoelectronics applications that demand the combination of electronic and optical properties [4]. Because of its remarkable transparency and low sheet resistance, graphene is employed as a transparent conductor in optoelectronic applications. Graphene can also be used as transparent conducting films in solar cells. Graphene is an excellent material for flexible devices[5]–[7]. Many studies have been done to replace ITO (Indium Thin Oxide) in touch screens and organic light emitting devices (OLEDs) with graphene. Figure 2.2 depicts the use of graphene on screens.

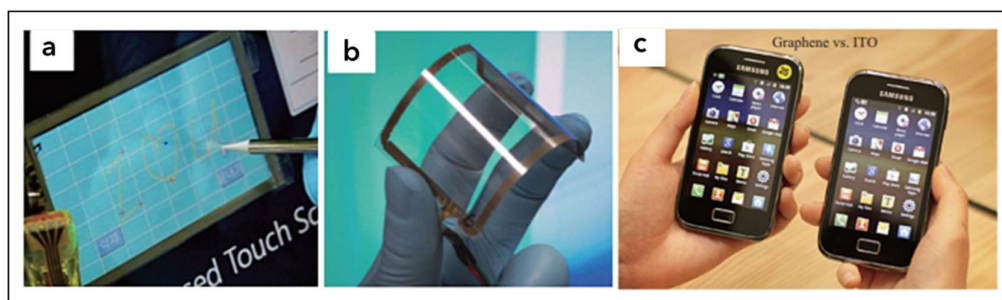


Figure 1.2. (a) Performance of a graphene-based touch screen. (b) A foldable graphene screen. (c) Graphene-based touch screen vs. ITO-based touch screen. [8]

As previously stated, graphene has been proposed as a possible transparent and flexible substitute to the widely used indium tin oxide (ITO) anodes in OLEDs applications. [5] [6][7]Organic lighting diodes (OLED), thanks to their combination of High-efficient electroluminescence and compatibility with a broad range of materials, are an outstanding electronic display and solid-state lighting devices. During the past two decades, extensive research has improved electroluminescence, lifetime, and color range of OLEDs. Transparent and conductive anode is a crucial component of OLED devices. ITO has long been utilized as a transparent conductor, although it has significant drawbacks. First, because of the costs of indium and the low-performance deposition process used, ITO may be too costly for use in OLEDs.

Second, metal oxides like ITO are brittle, making them unsuitable for flexible substrates. Third, indium has been shown to diffuse into the active layers of OLEDs, resulting in performance loss over time. Alternatively, graphene has unique electrical, mechanical, and optical properties and making it a good choice for flexible OLED-based displays and lighting. Regardless of its great potential as a transparent anode, graphene has low work function (4.4 eV) and high sheet resistance (300 Ω/sqr) that limits its use in practical optoelectronic applications. Low work function limitation of graphene causes give arise of a high injection barrier between graphene anode and overlaying organic materials, resulting an undesirable hole injection between these layers. Furthermore, the high sheet resistance of pristine graphene causes high turning-on voltage and reducing the luminous efficiencies of OLEDs. Emerging new methods for overcoming these drawbacks are critical to achieving effective graphene anodes. Several methods for overcoming the disadvantages of pristine graphene for OLED applications have been reported by different research groups.

In this thesis, the fabrication and characterization of transparent conductive graphene anodes are reported. The direct synthesis of large-scale graphene films employing chemical vapor deposition on thin copper layers is explained, as well as two methods for patterning and transferring the films to different substrates. To achieve applicable anode, a method to reduce the sheet resistance of graphene is indicated and numerous tunable polymers have been explored to improve the WF of graphene OLEDs. A conducting polymer (PEDOT: PSS) is applied to engineer the surface, hence generating a WF gradient between the graphene and overlying organic layers. Furthermore, this thesis presents innovative methodologies for designing and manufacturing high-performance OLEDs for next-generation devices. The first section shows high-performance OLEDs with graphene as an anode and a four-layer device architecture. To accomplish effective charge balance and exciton confinement in the emissive layer of the device, these devices use three novel TADF materials (SeDF-G, SeDF-B and SeDF-YG).

Overall, this work is demonstrated outstanding and functional graphene based-OLEDs, which are comparable to ITO a OLEDs.

CHAPTER 2

LITERATURE REVIEW

This chapter introduces the background information relevant to graphene and graphene-based Organic Light Emitting Diode (OLED). The overview of the first part of chapter discusses recent advances in synthesis, characterization, and transfer methods of graphene, followed by fabrication and properties of graphene-electrodes. The second part of the chapter summarizes different kinds of OLEDs.

2.1 Graphene

Graphene is the first material in the class of the two-dimensional (2D) crystalline material which have been identified and characterized recently. It is a single atom thick layer of carbon packed which are covalently bonded to other carbon atoms with a bond distance of 0.142 nm, forming a hexagonal (honeycomb) lattice. Furthermore, interlayer spacing distance between graphene layers in graphite structure is 0.335 nm. This honeycomb lattice is the basic structure of other carbon allotrope, it can be stacked to creat 3D graphite, rolled to create 2D carbon nanotubes and wrapped to creat 0D fullerenes. (See figure 2.1.)

Andre K. Geim and Konstantin S. Novoselov were awarded the Nobel Prize in Physics in 2010 for their advancement on graphene. They were able to produce and characterize graphene.

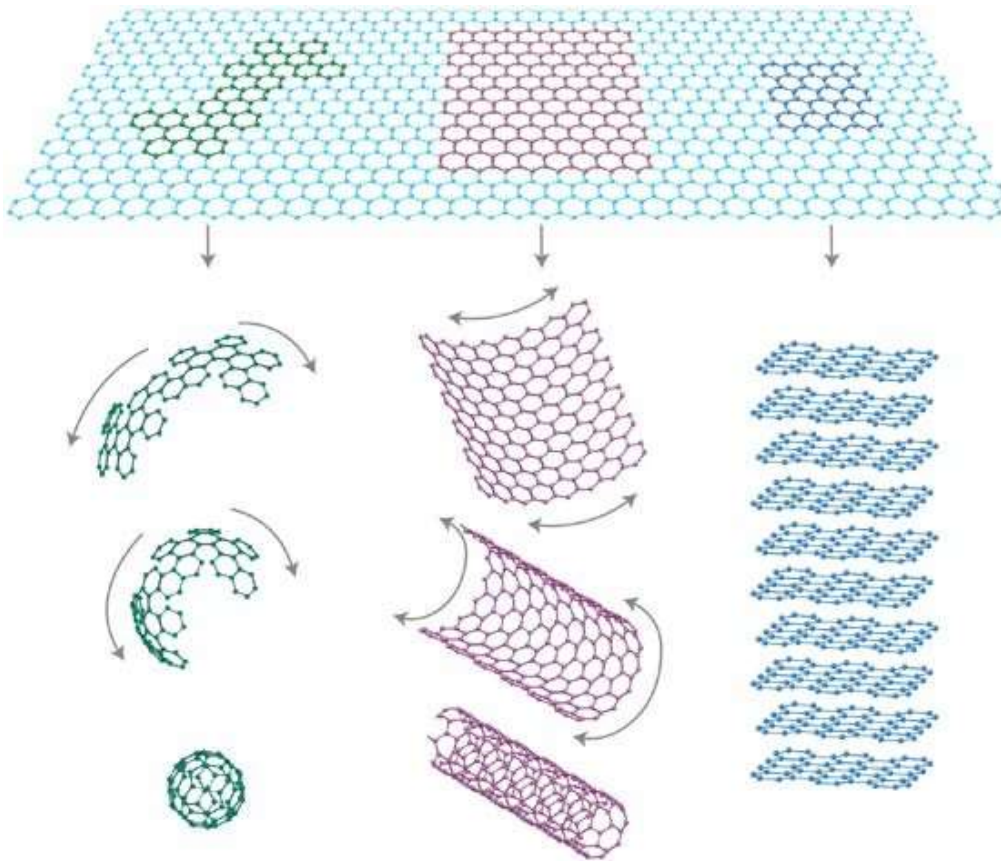


Figure 2.1. Graphene as a basic structure of other graphitic forms.[9]

This novel material has a number of unique features that make it appealing for both basic research and future uses. For example, the electrical characteristics of this 2D-material provide an uncommon quantum Hall effect. [10][11] It is a transparent, one-atom-thick conductor. It also brings up parallels with particle physics, such as an unusual sort of tunneling suggested by Swedish physicist Oscar Klein.[12] Graphene also has a number of unique mechanical and electrical properties. It possesses several unique mechanical and electrical features. It has a far higher tensile strength than steel and is extremely stretchy. It has excellent thermal and electrical conductivity and can be utilized as a flexible conductor. Graphene has a unique electrical structure compared to other three-dimensional materials. [13] It has six double cones on its

Fermi surface, as seen in Figure 2. The Fermi level is located at the connecting points of these cones in intrinsic (undoped) graphene. Intrinsic graphene's electrical conductivity is relatively low because the material's density of states is zero at that point. However, the fermi level can be change by applying an electric field, causing the material to become either n-doped (with electrons) or p-doped (with holes) depending on the polarity of the electric field. Adsorbing water or ammonia on the surface of graphene can also be used to dope it. Doped graphene has the potential to have a high electrical conductivity, possibly even higher than copper at ambient temperature. Adsorbing water or ammonia on the surface of graphene can also be used to dope it. Doped graphene has the potential to have a high electrical conductivity, possibly even higher than copper at ambient temperature. Figure 1 shows the energy, E , of graphene excitations as a function of the k_x and k_y wave numbers in the x and y directions. The Fermi energy of an undoped graphene crystal is represented by the black line. The energy spectrum near this Fermi level is defined by six double cones with a linear dispersion relation.

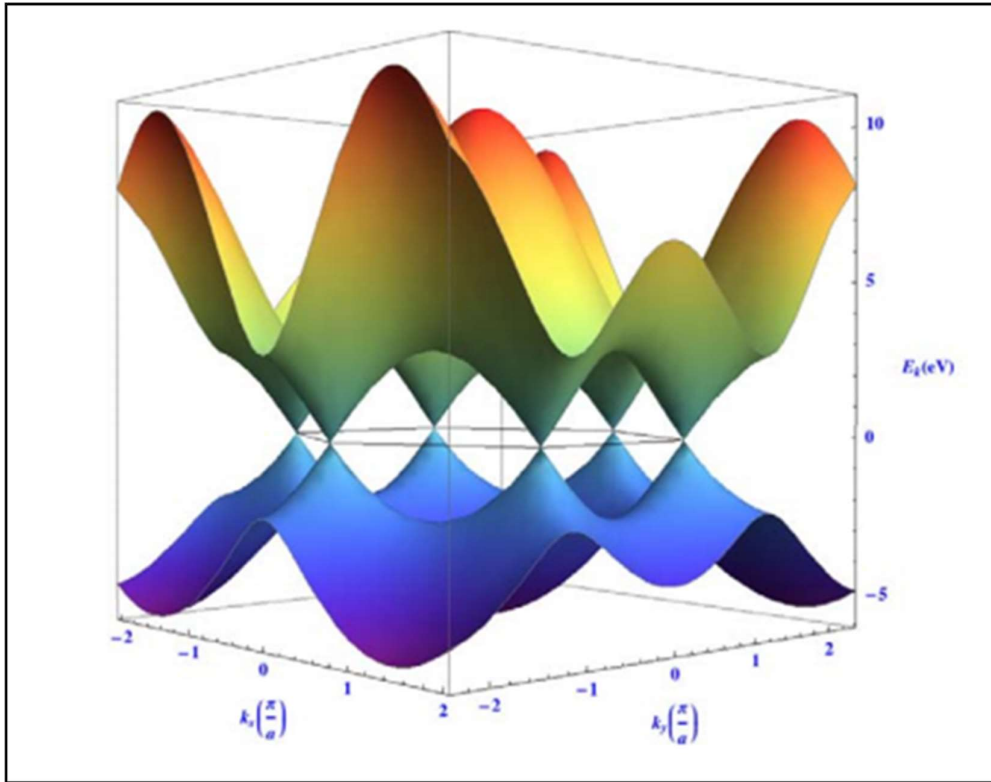


Figure 2.2. Fermi energy for an undoped graphene crystal[13].

Graphene is practically transparent. In the optical region it absorbs only 2.3% of the light. This number is in fact given by $\pi \alpha$, where α is the fine structure constant that sets the strength of the electromagnetic force. In contrast to low temperature 2D systems based on semiconductors, graphene maintains its 2D properties at room temperature. Graphene also has several other interesting properties, which it shares with carbon nanotubes. It is substantially stronger than steel, very stretchable and can be used as a flexible conductor. Its thermal conductivity is much higher than that of silver.

2.1.1 Synthesis methods of graphene

It is necessary to isolate the two-dimensional graphene layer in order to investigate the physical properties of graphene. Due to the one-atom thickness of the graphene, this is a challenging process. However, over the last decade, several reliable methods for achieving one-atom-thick single layer graphene have been established. As explained earlier, these methods are classified into top-down and bottom-up approaches. At the moment, there are four primary methods for synthesizing graphene, including mechanical exfoliation, liquid phase exfoliation, epitaxial growth, and chemical vapor deposition. In the following paragraphs, we will provide a brief overview of these methods, highlighting their benefits and drawbacks.

2.1.1.1 Mechanical exfoliation

Mechanical exfoliation (commonly referred to as the scotch-tape method) was the first technique used to isolate a single graphite monolayer. Its mechanism is straightforward and is based on repetitive peeling of graphite. This procedure begins by binding graphite to adhesive tape and then bending the two adhesive sides against the small crystals (Figure 2.3). Flakes are divided into two separate flakes after pulling the tape away. Thinner pieces can be obtained by repeating the splitting procedures several times. And then, the parts are stuck to the silicon wafer with the silicon dioxide film on top of it, and then the tape is taken away. In the end, can already see graphene due to optical contrast differences.

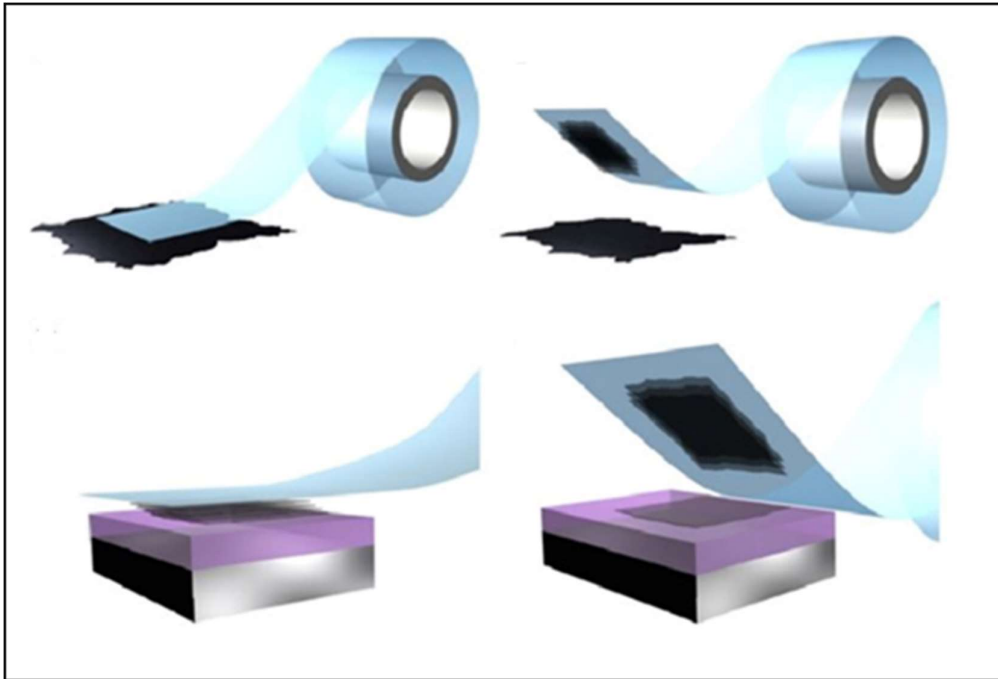


Figure 2.3. Procedure of graphene synthesis with Scotch tape [14]

Despite its simplicity, the method is not suitable for large-scale production, but it is still a simple method for studying the fundamental electronic properties of graphene over a small area. In graphene-based field effect transistors, this approach provides the highest carrier mobilities ($200,000 \text{ cm}^2 \text{ V}^{-1} \text{ s}^{-1}$). [15]

2.1.1.2 Liquid phase exfoliation (LPE)

In the liquid phase exfoliation (LPE) process, graphite is exfoliated in various medium using ultrasound or shear forces to obtain graphene sheets. The van der Waals forces that hold graphite together are weak, hence breaking these bonds is not challenging. To minimize the interfacial tension energy between graphene layers and solvent, a suitable liquid solution with equivalent surface energy to graphene should

be utilized. Hernandez and collaborators dispersed graphite in NMP and then separated the non-exfoliated graphite using ultrasonication.[16] (See figure 2.4)

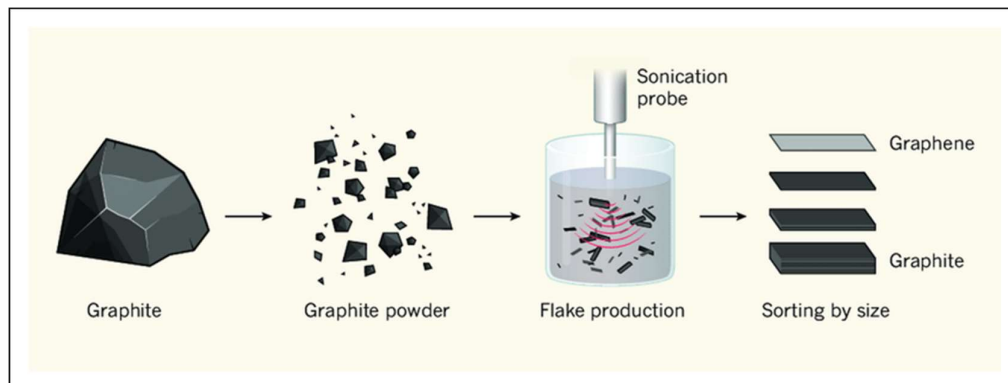


Figure 2.4. Procedure of graphene synthesis with LPE method. [17]

Controlling the flaked size of graphene in LPE is quite complicated. Moreover, it can be problematic to find the appropriate solvents, surfactants, and liquid stabilizers. However, it is a simple and inexpensive technique. Additionally, it has a significant potential for expansion into large scale production.

2.1.1.3 Epitaxial growth of graphene on SiC

Epitaxial growth on crystalline silicon carbide wafers is another method for growing graphene. When c-SiC is exposed to heat under vacuum, the silicon near the surface is sublimated, but the carbon atoms remain in their solid state. Carbon will reorganize and graphitization is obtained when the material is heated to 1300 °C or higher.[18] This approach allows for the growth of graphene sheets with a relatively large area, and devices based on epitaxially grown graphene on SiC can perform at high frequencies. On the other hand, significant drawbacks in the technology continue, such as the expensive cost of SiC substrates and the demand for ultra-high vacuum

chambers. The schematic of graphene growth on SiC substrate is shown in figure 2.5.

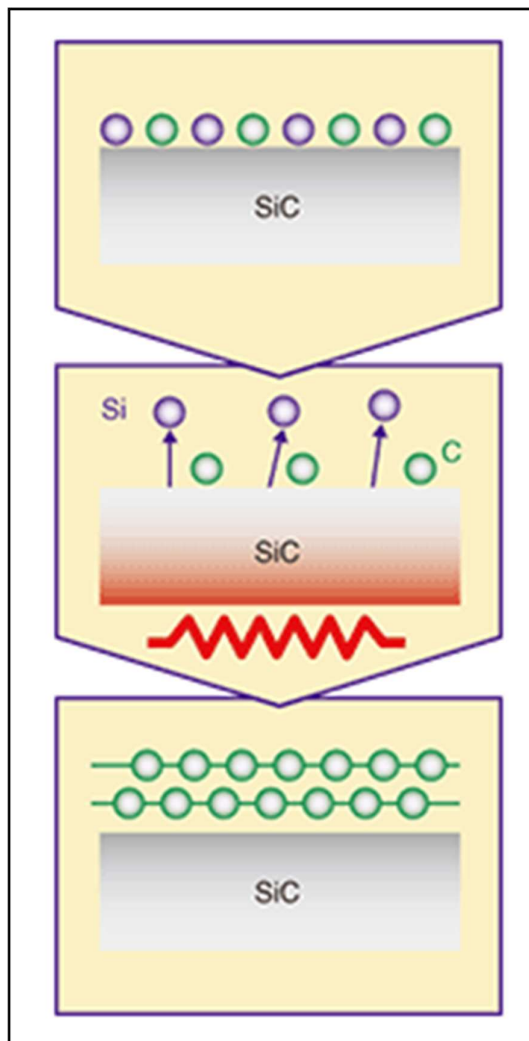


Figure 2.5. Procedure of graphene synthesis with epitaxial growth on SiC. [19]

2.1.1.4 Chemical vapor deposition (CVD)

Chemical vapor deposition (CVD) is one of the most widely used synthesis processes in graphene science. Scalability to large area, cost effectiveness, and easy to use are the major benefits of the CVD synthesis when compared to other

techniques. CVD-synthesized graphene samples with large area were exhibited and used as transparent electrodes in electronic application.[20] To obtain graphene layer via CVD method, a catalyst substrate is required for the thermal decomposition of carbon atoms from the hydrocarbon gas flowing across the CVD tube furnace. Although nickel and copper are commonly used as catalyst substrates (figure 2.6), the use of transition metals such as Au [21], Pt [22], and Pd [23] in CVD synthesis has also been exhibited. When compared to mechanically exfoliated graphene films, the transport parameters of CVD grown graphene layers are not better. This is because the metallic substrates that the graphene grows have a polycrystalline lattice. Although, large area single crystal graphene can be obtained with the efficient optimization of gases using in CVD method.

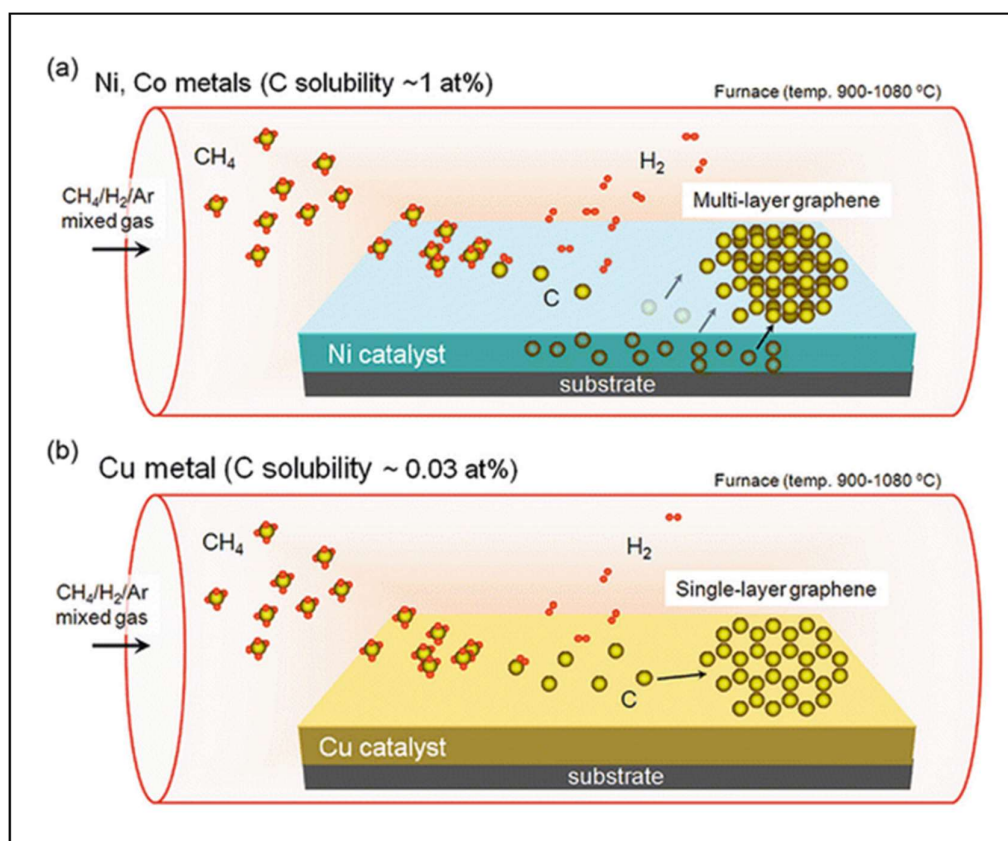


Figure 2.6. Procedure of CVD growth of graphene on (a) Ni, (b) Cu. [24]

High quality graphene films with consistent transport properties are crucial for broad optoelectronic applications. Countless advancements in the quality of graphene films obtained by CVD synthesis have been announced in literature [25][26]. Graphene growth is self-limited on copper substrates due to the limited solubility of carbon in copper. This feature of copper enables the direct synthesis of single layer graphene. Copper foils are a cost-effective and scalable substrate for graphene growth that can be produced in large quantities. The surface quality and the transfer process influence the graphene layers' productivity and durability. On the other hand, c Copper foils that are commercially available, have remarkably rough surfaces as a result of the rolling process. Thick scratches caused by the rolling process have negative impacts during the graphene transfer process. One of the most important criteria for obtaining high quality graphene layers is the morphology of the copper surface²³. In order to achieve uniform and high-quality surface coverage of graphene, defects , contaminations, and grain boundaries should be carefully healing[26]. Various techniques have been reported for the healing of copper surfaces. Electropolishing is one of these methods for smoothing copper surfaces [27]. In comparison to the unpolished copper substrates, their Raman spectroscopy spectrum revealed a higher quality graphene layer. A similar electrochemical polishing technique was used in combination with high pressure annealing to fabricate single crystal graphene domains about 2mm in diameter[28]. As an alternative to these techniques, the use of hydrogen gas as an activator and etchant on surface of copper has been documented[29]. The shape and size of graphene domains could be precisely controlled by varying the flow rate of hydrogen gas in the process.

To explain why copper is a desirable substrate in graphene synthesis using the CVD method, studies have shown that the copper surface quality has a significant effect on the transport properties of the resulting graphene layer. For the synthesis of the graphene film, surface morphology and crystallography of the copper substrate also are important. According to Wood et al.[30], due to the higher diffusion rates of

carbon at the (111) surface, monolayer graphene is more likely to grow on copper surface than on other surfaces.

2.1.2 Characterization methods of graphene

Graphene can be characterized using a variety of techniques. The following are the basic methods:

2.1.2.1 Raman Spectroscopy

Raman spectroscopy is the most frequently used technique for characterizing the properties of graphene. It is used to characterize sp^2 and sp^3 hybridized atoms of carbon. Raman spectroscopy can also be used to calculate the number of layers in graphene. The G band at 1582 cm^{-1} and the 2D band at around 2700 cm^{-1} are prominent features in the Raman spectra of graphene, while the D-band appears around 1350 cm^{-1} in the case of disorder or defect in graphene.

The Raman spectrum represents valuable details about both of these atomic formation and electronic properties since graphene has no bandgap and most of the wavelengths of incoming radiation are resonant. The Raman spectra of SLG and graphite on a SiO_2/Si substrate are shown in Figure 2.7.a [31]. The 2D band distinguishes the Raman characteristics of SLG from those of graphite. The G band shifted to lower frequencies as the number of graphene layers increases. In general, the intensity ratio of the G and 2D bands indicates the number of graphene layers. In general, as the ratio of I_G to I_{2D} decreases, the number of layers in the graphene decreases [31]. As shown in figure 2.7.b , the 2D band becomes broader and more blue-shifted as graphene layer numbers increases from SLG to multilayer graphene.

Raman spectroscopy has the advantage of being independent of the substrate used in identifying the amount of graphene layers. This is due to the fact that the Raman spectrum seems to be a fundamental property of graphene [31].

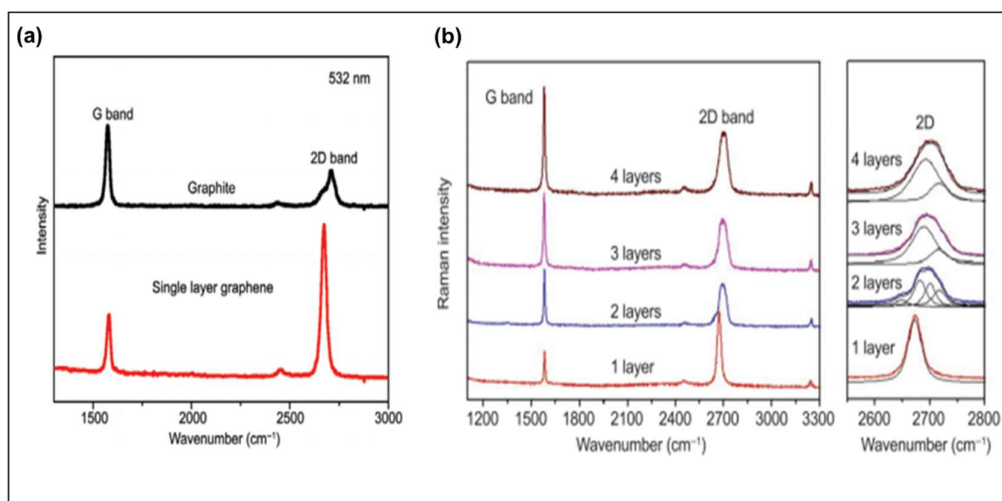


Figure 2.7. (a) Raman Spectrum of Graphite vs SLG, (b) Raman spectrum of graphene with different layers [31].

2.1.2.2 Scanning Electron Microscopy

Various techniques have been used to characterize the quality, the layer number, imperfections, and crystalline structures of graphene. Scanning electron microscopy (SEM) has become a non-contact, most often non-destructive, and remarkably more effective and easy technique for high-speed imaging, making it highly desirable for identifying micro/nano component of graphene such as wrinkles, grains, and grain boundaries, particularly in CVD grown graphene. Besides that, due to its one-atom thick structure of graphene, it is transparent to high acceleration voltage during imaging and make SEM a challenging technique for imaging graphene, particularly at the large-scale graphene applications [32].

Figure 2.8 shows the SEM images of CVD grown graphene/Cu surface at different growth durations. By increasing the growth duration, the graphene grains is enlarged [33].

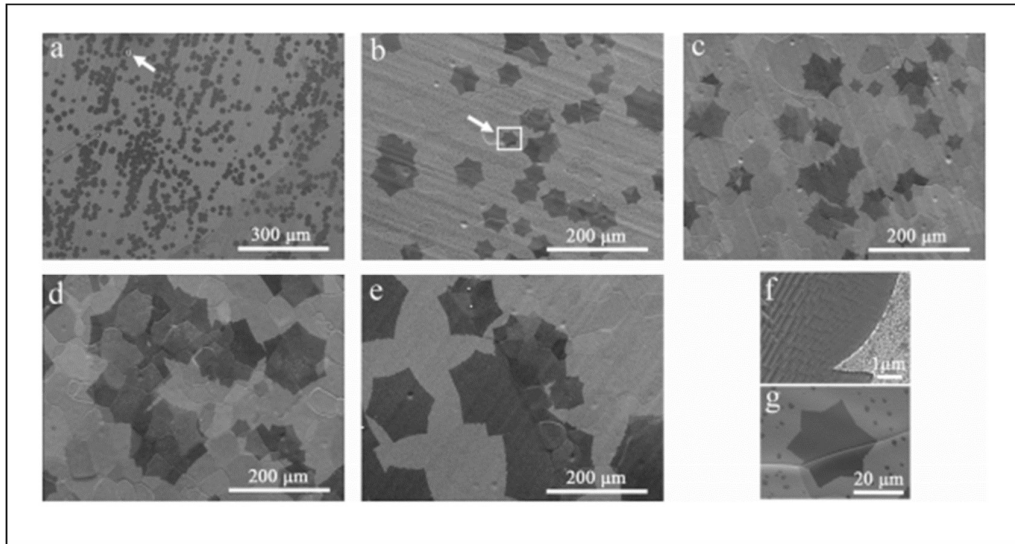


Figure 2.8. (a–e) SEM images of few-layer graphene after growth for 5, 10, 20, 40, and 60 minutes. (f–g) SEM images of the regions at high magnification [33].

2.1.2.3 Optical Transmission Measurement

Transmission measurement of graphene is a technique which used to calculate the number of graphene layers. Due to the fact that a SLG absorbs only 2.3 percent of light, 97.7 percent of light passes through it. [34]Conversely, the more the light absorption, and the less optical transparency becomes in the case of MLG. Therefore, because each layer absorbs 2.3 percent of light, a graphene sample made up of five layers would have an 11.5 percent absorption and an optical transparency of roughly 88-88.5 percent. The figure 2.9 shows the transparency of graphene samples with different thicknesses and layer numbers.

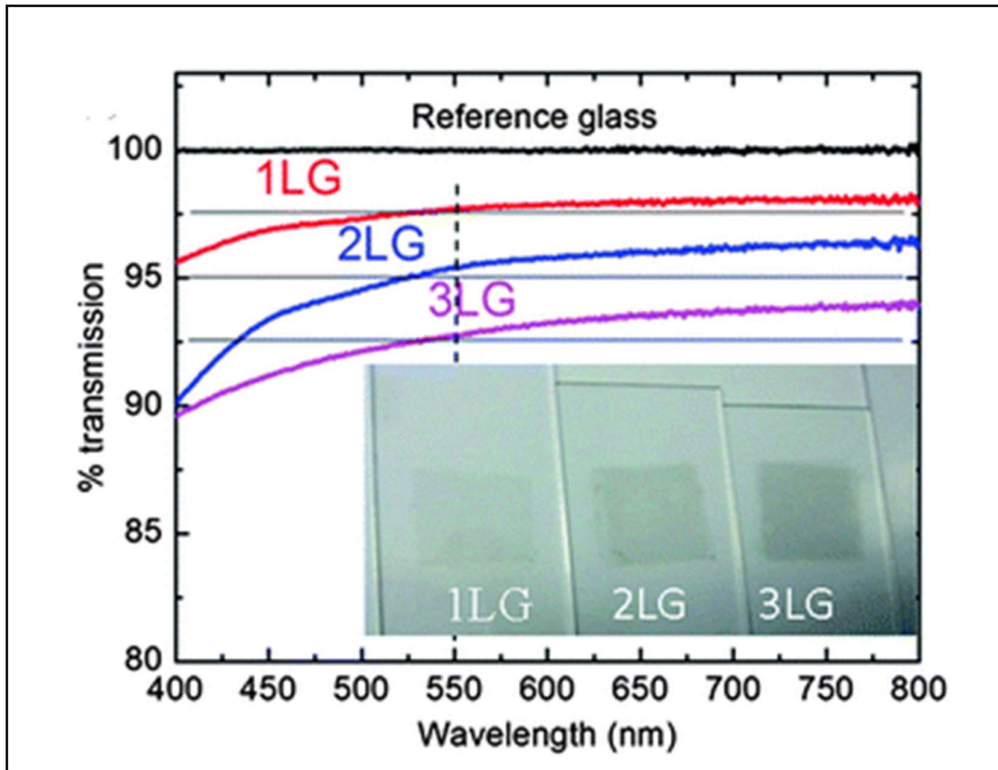


Figure 2.9. Optical transmittance measurement of graphene sheets transferred to glass for graphene with 1, 2, and 3 layers [34].

2.1.3 Transfer methods

Graphene transfer printing is important in CVD synthesis because electrical and optical properties of the graphene cannot be analyzed on transition metal substrates. There are two widely used transfer printing techniques for CVD graphene: polymer-assisted transfer method (Fishing method) and lamination transfer method. Furthermore, in order to use graphene in different applications such as optoelectronic or electronic applications, there is a need to transfer graphene to arbitrary substrates (glass, PET, and SiO₂/Si).

2.1.3.1 Polymer-assisted Transfer method

The development of polymer-supported transfer methods is emerging parallelly with and particularly for CVD grown graphene. The metal substrate on which graphene is synthesized is used as catalyzer and is typically undesirable after the synthesis is finished, so removing the metal is the essential step alongside the growth. Ni and Cu substrates could be etched away using $\text{Fe}(\text{NO}_3)_3$, FeCl_3 , or $(\text{NH}_4)_2\text{S}_2\text{O}_8$ without the need for polymers. Nevertheless, very thin graphene is too sensitive to be breaking and pulling during etching and transfer, depending on the graphene's synthesis quality. As a result, many scientists prefer to use polymer assisted transfer to make sure a secure transfer. Furthermore, the polymer support allowed for the transfer of large scales of graphene [35].

PDMS (polydimethylsiloxane), PMMA (polymethyl methacrylate) are a common type of polymer used as a support for CVD graphene transfer. Cu foil with CVD graphene is spin-coated with a polymer layer and then floated on top of the etchant solution. Finally, after Cu etching and removing the PMMA with acetone, a polymer/graphene layer fished onto a SiO_2/Si substrate achieves graphene on the aimed substrate [35]. The process flow of this method is shown in figure 2.10.

The difficulty to remove the full PMMA layer along the graphene layer, which influences the transport properties, is one of the method's drawbacks. Additionally, PMMA transfer method leaves random surface cracks. However, putting another coating of PMMA before removing the PMMA has been found to avoid the creation of cracks through the transfer.

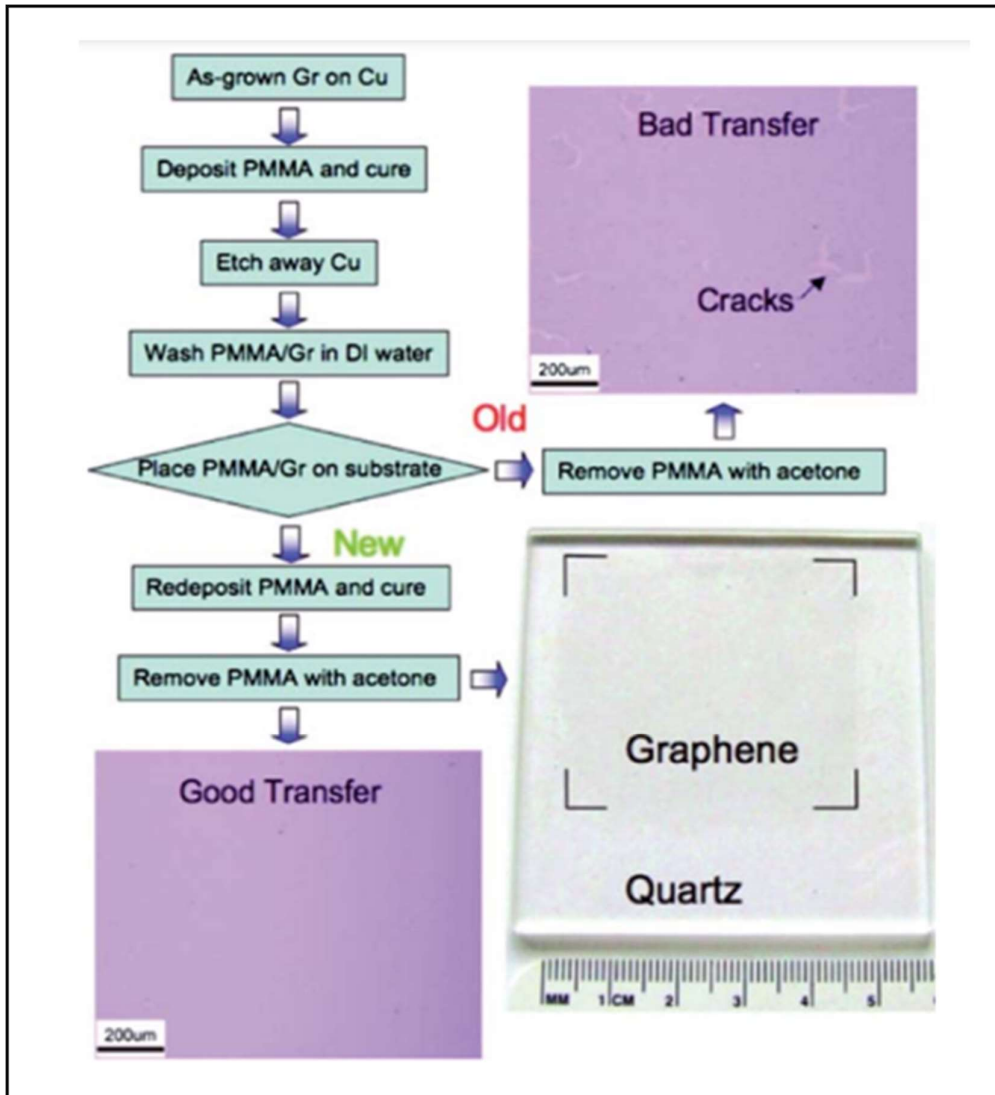


Figure 2.10. Process flow of PMMA-assisted transfer of CVD graphene films. [35]

2.1.3.2 Lamination transfer method

Graphene can be transferred directly on to wide range of flexible substrates using a lamination-based technique that eliminates the need for an intermediate "adhesive" layer. The procedure begins with the formation of graphene layer on top of a copper

foil. The Gr/Cu sheet are then placed between a covering paper layer and the desired flexible surface. This is loaded into a lamination machine, where the temperature is controlled, and the components are bonded together. After removing the paper, a Gr/Cu bonded to the target substrate were revealed. A copper etchant was used to dissolve (or etch away) the copper [36].

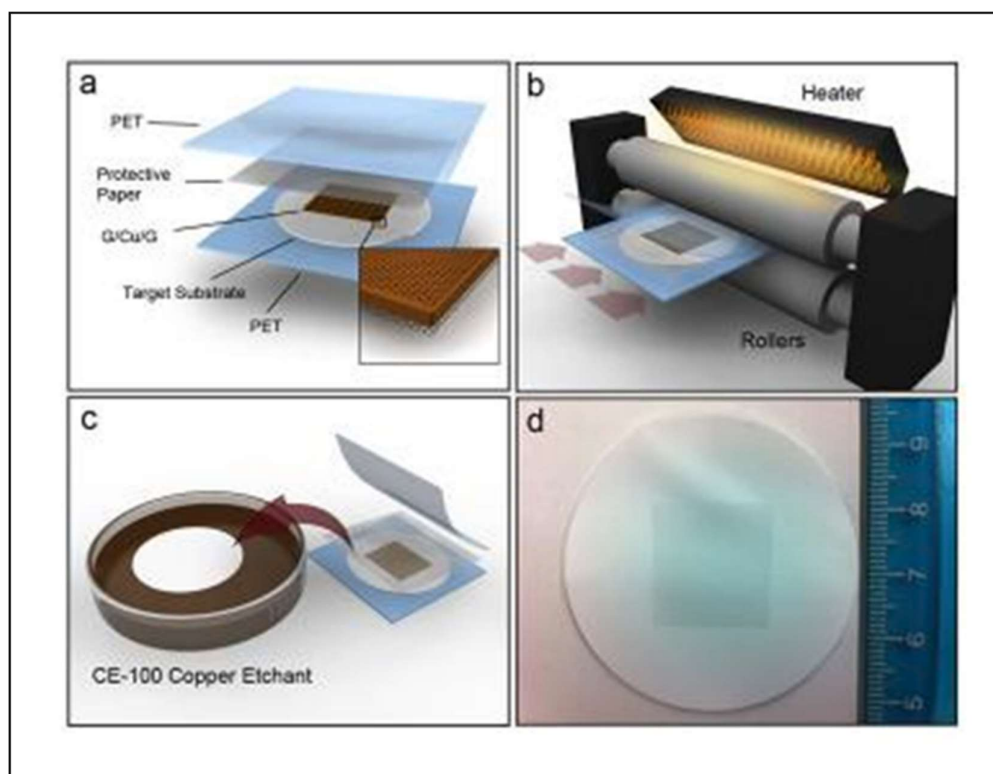


Figure 2.11. Graphene transfer by using Lamination technique [36]

2.2 Organic Light Emitting Diode (OLED)

Electroluminescence is the term used to describe the light emission from materials in the existence of an applied electric field. An anthracene crystal played a critical

role in recognizing this phenomenon in the 1960s. The efficient and low-powering OLEDs were obtained in 1987 from Kodak's Tang and van Slyke [37].

Typically, OLEDs are thin multilayer devices composed of organic semiconductor layers (see Figure 1). In a simplified device, charge carriers (electrons and holes) are obtained at the cathode and anode by applying an external voltage. The charge carriers are then injected into both the electron transport layers (ETL) and hole injection layer (HIL), respectively [38].

The development of OLEDs has been the focus of many studies including both academia and industry over the last two decades. OLED devices have been developed using three generations of emitter materials based on fluorescence (1st generation), phosphorescence (2nd generation) and thermally activated delayed fluorescence (3rd generation). Meanwhile, research into the new generation of OLEDs is underway [38].

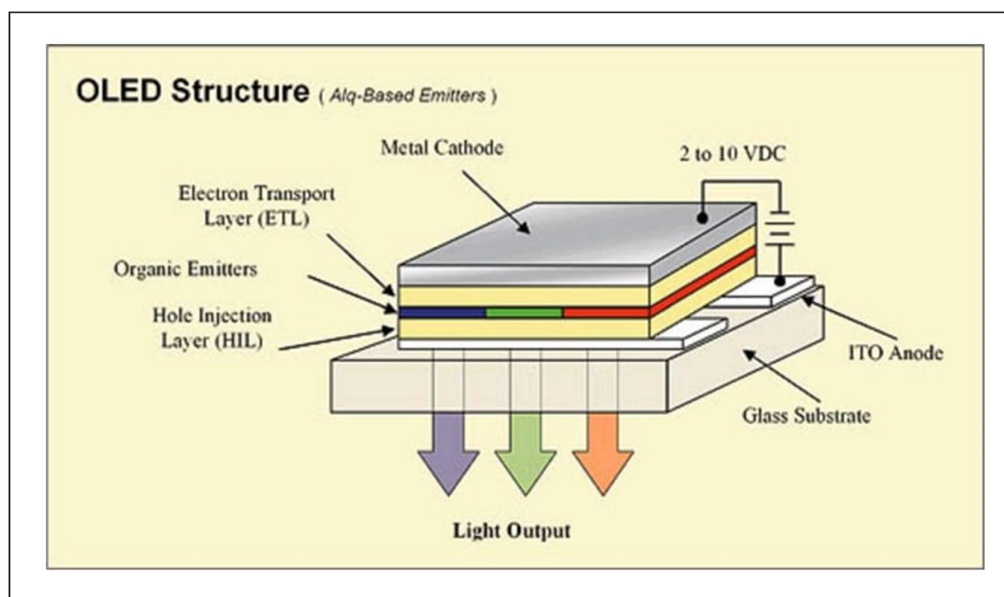


Figure 2.12. A simple structure of OLED [37].

Until now, the market for OLEDs has been primarily based on two large industries: electronic displays and solid-state lighting. Although OLEDs for displays have seen significantly more development and market infiltration than OLEDs for solid-state lighting, these also hold promise and are estimated to improve rapidly in the next decade as industries continue to invest in and develop the technology required for low-cost, large-scale manufacturing[39]

2.2.1 Application of OLEDs

OLEDs have emerged as a promising alternative to cathode ray tubes (CRTs) and light-emitting diodes (LEDs) in flat-panel displays in recent years. Furthermore, OLEDs allow for flexible display fabrication. Mainly utilized in digital devices such as high-end TV systems, computer screens and handheld systems such as smartphones, portable media, cameras, wireless gaming consoles or wearable devices. OLED displays are used for many sorts of functions. Such applications necessarily require a high level of durability and usability. In contrast to other screens, OLEDs are energy efficient while offering a high-quality display. The present OLED technology delivers excellent color accuracy, productivity, and stability of operation.

Since 2016, numerous smartphones with OLED displays have been introduced, such as those from Samsung, Oppo, One plus, Google, and Apple. LED screen display technology has advanced to OLED and QLED. To make their technologies smarter, all companies are currently focusing on OLED displays. Some firms, such as LG, have divided their TV screens into three categories: flat OLED displays, curved OLED displays, and OLED wallpaper. Digital camera screens and electronic viewfinders using OLED displays are in demand. Wearable devices usually involve multi-functional tools that incorporate OLED technology into their design. Wearable

devices benefit from OLED technology's thinner and foldable display portability. OLED's application is shown in figure 2.13.

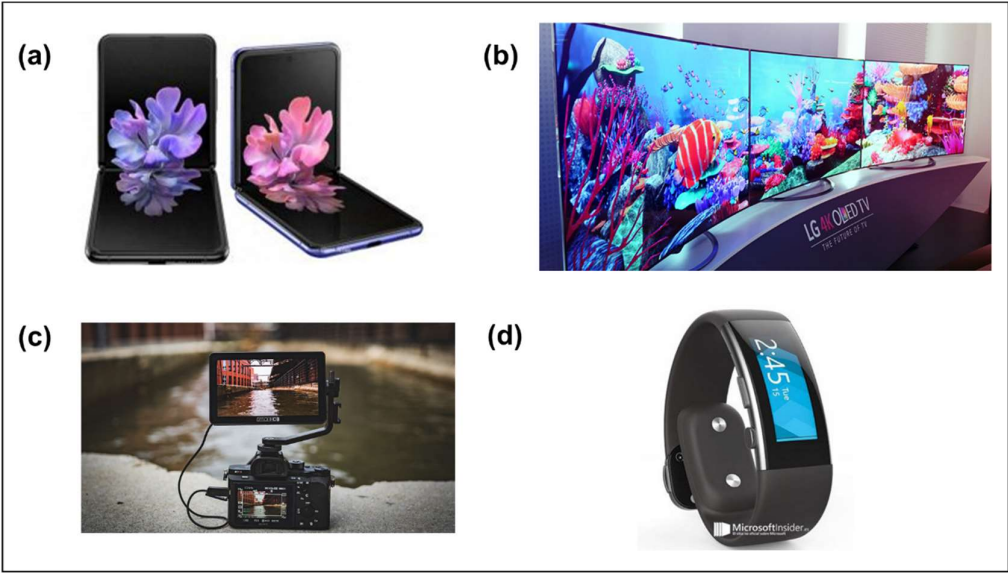


Figure 2.13. OLED's application in electronic display technology, (a)Smartphone, (b) OLED TV, (c) Digital Camera, (d) Wearable device. [40] [41]

OLED technology is gradually being applied in the last few years toward the lighting application domains, substituting conventional light lamps and LED bulbs. Large-area light panels are possible owing to OLED technology[42]. Foldable, transparent, and tint light panels are manufactured with OLEDs (see figure 2.14).



Figure 2.14. OLED light panel [43].

2.2.2 OLED classification

OLEDs can be produced in various of structures and emit light in a number of different emitters. The OLED emitter development presented in this thesis is divided into multiple “generations” based on the emission process that is employed to generate light. Fluorescent emitters are used in the first generation of OLEDs, phosphorescence is used in the second generation, and thermally activated delayed fluorescence (TADF) is used in the third generation[38]. The singlet excitons and triplet excitons generated by OLED devices are distributed in a 25 percent to 75 percent ratio in OLED devices. To achieve satisfying device performances with high EQEs, it is critical to develop and design light-emitting materials for OLEDs that would have the capability to sufficiently harvest the singlet excitons and triplet

excitons. In order to achieve this aim, three generations of emitters were designed and analyzed detailly.

The accumulation of excited states in an electroluminescence approach arises through the recombination of electrons and holes. They generate excitons in the OLED's emission layer as a result of Coulomb interaction (Figure 2.14). Due to the fact that both the hole and the electron have spins, four distinct spin combinations are achievable. Antiparallel spins yield a singlet while parallel spins yield a triplet, according to quantum mechanics. (See Figure 1b.) As a result, in a logical threshold, 25% of the excitons are singlets and 75% are triplets [44].

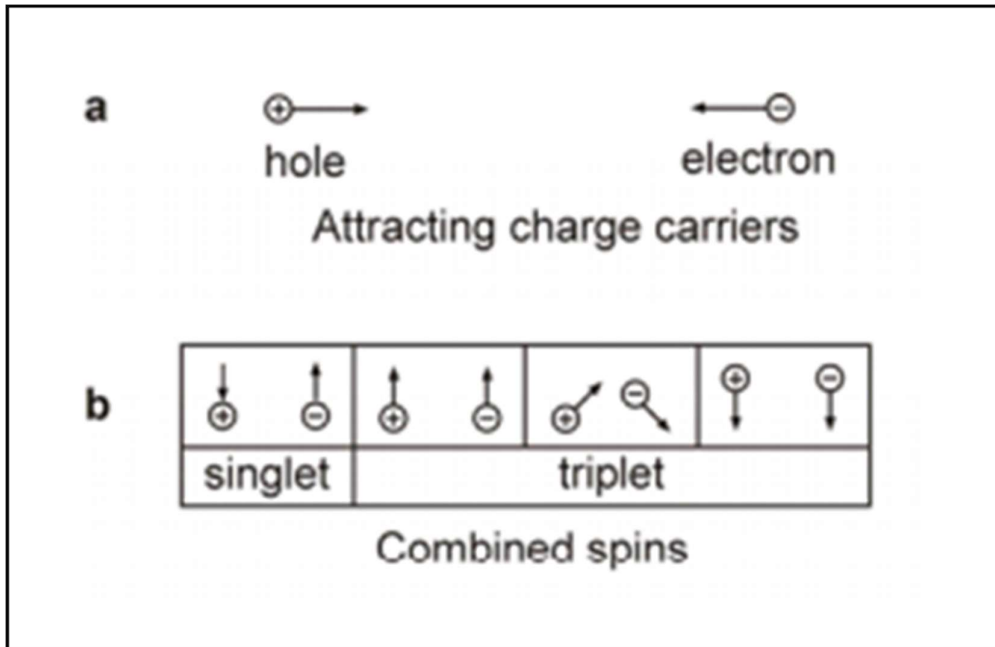


Figure 2.15. Schematic image of, (a) Charge recombination, (b) Spin combination [44].

The triplet problem is a major issue in the development of an efficient OLED because radiative decay from its triplet position (T_1) to the ground state singlet (S_0) is banned

due to angular momentum conservation. As a result, 75% of charges injected into the OLED are wasted, and the OLED's maximum internal quantum efficiency is limited to 25%.

The first approach to this issue was to switch from pure organic chemicals like those used in first-generation OLEDs to organic molecules that included heavy metals like iridium. The addition of heavy metals enhances the spin orbit coupling (SOC) among the exciton spin and orbital angular momentum. As a result of the SOC, the radiative transition from T1 to S0 is no more expressly banned, and the T1 state will become. The SOC also enhances ISC between the S1 and the T1, resulting in an even greater population of the T1 state. For OLEDs with this mechanism, 2nd generation or PhOLEDs, the internal quantum efficiency approaches 100%.[45]

Even though heavy-metal complex emitters are showing remarkable results and have been used in industrial electroluminescent products, the use of heavy-metal limits their much more growth in the market, considering environmental and cost concerns. As a result, the evolution of emitters that minimize the use of high-cost and environmentally hazardous elements while providing high QIEs has become a growing motivator. A promising solution is to switch from phosphorescent emitters to fluorescent emitters that exhibit a phenomenon known as Thermally Activated Delayed Fluorescence (TADF). TADF OLEDs will be covered in greater depth later.[45]

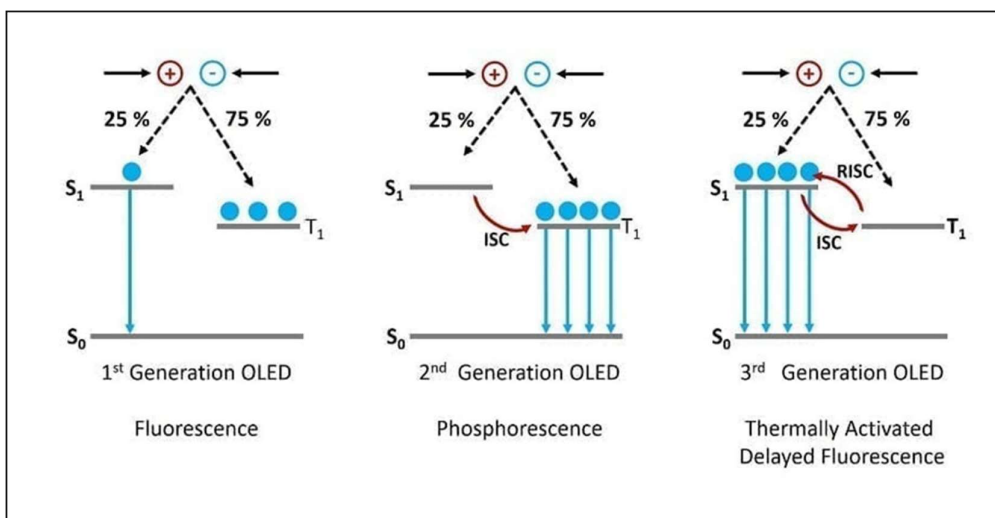


Figure 2.16. Working principles of 1st, 2nd and 3rd generations of OLEDs. [45]

2.2.2.1 First generation OLEDs: Fluorescent OLEDs

The first generation of OLEDs are referred to as fluorescent OLEDs as they are typically made of organic dyes. The transition between states with different electronic spin multiplicity (ISC) is non-radiative, and thus just the transition of singlet excitons to the singlet ground state (S_1 to S_0) is ideally permitted for fluorescence. As a result, only around 25% of the singlet excitons could be used to generate light. Without additional optical outcoupling, the EQE of OLEDs employing typical fluorescent emitters is limited to 5%. [38] The fluorescence OLED working principle is shown in figure 2.16.

2.2.2.2 Second generation OLEDs: Phosphorescent OLEDs

Phosphorescent heavy-metal complexes have been explored and manufactured as the second-generation emitters of OLEDs to obtain entry to the other 75% of excitons in

triplet states. Phosphorescent heavy-metal combinations have been explored and manufactured as the second-generation emitters of OLEDs to obtain entry to the other 75% of excitons in triplet states. The subsequent complexes can enhance radiative deactivation via phosphorescence from the lowest-lying triplet state to the ground state S_0 and enable ISC from the lowest-lying singlet state S_1 to T_1 through an improved spin-orbit coupling caused by heavy atoms such as iridium or platinum. Phosphorescent heavy-metal-based emitters have EQEs of up to 100 percent when employing a triplet-using method and relaxation mechanism.[38] Operating principle of phosphorescent OLEDs is shown in figure 2.16.

2.2.2.3 Third generation OLEDs: TADF OLEDs

The TADF technology is not new, since Perrin et al. first mentioned it in 1929, [46] and several others examined it during the 20th century.[47] This newfound efficiency was discovered in 2012 once Chihaya Adachi used the TADF technique to produce an efficient OLED without the use of phosphorescence.[48]

The following is a basic illustration of the TADF mechanism. The S_1 and T_1 states are intensely coupled in a TADF mechanism, allowing ISC among the two states. The molecules are also designed to reduce the emission spectrum in between S_1 and the T_1 (ΔE_{ST}) significantly to less than in conventional organic molecules. The molecules are also designed to reduce the emission spectrum in between S_1 and the T_1 (ΔE_{ST}) significantly to less than in conventional organic molecules. This small energy gap allows reverse crossing (RISC) when excitons on the T_1 are thermally activated and converted to S_1 (Figure 2.16, 3rd generation). While in the S_1 level, excitons can decay through the fluorescence to the S_0 ground level. Because RISC is a slow procedure the fluorescence from the formerly triplet excitons come delayed than the fluorescence from excitons in the S_1 state, leading to the term "delayed fluorescence." [45]

The TADF emitter 4CzIPN, which has become the prototype green TADF emitter, was first synthesized by Adachi group.[48] They demonstrated in their paper that once doped in a CBP host material at a rate of 0.1 wt. percent, they could produce OLEDs with an optimum EQE of 19.3 %. Recent research has demonstrated that using ambipolar host materials can boost the efficiency of these devices even further, and TADF OLEDs with EQEs of over 25% have been observed. DMC-DPS, which is a blue-emitting TADF material and yielded a maximum EQE of 19.5%, was synthesized by Zhang et al. in 2014.[49]

Investigation into TADF materials has produced results and equipment which have already matched the capabilities of smaller scale devices. However, there are still numerous challenges to overcome in the synthesis and usage of TADF materials. Producing a blue light-emitting TADF molecule with such a sensible lifetime is probably the biggest obstacle. The lack of a stable molecular design technique is another challenge in generating efficient TADF materials. The combination of dopant and host material, as well as the twisted molecular formation offer great basic starting ideas for new synthesis but identifying which molecules will prove the most efficient is difficult due to the complexity in estimating HOMO and LUMO energy levels.

2.2.3 Flexible OLEDs

OLEDs' manufacturing capabilities enable them to be manufactured on a wide range of substrates. OLEDs have been demonstrated with good efficiency on polyethylene terephthalate (PET), polyethersulfone (PES), and foldable glass. hence, alternative flexible anodes attracted significant attention from OLED community in recent years. ITO is the most common transparent anode for conventional OLEDs due to its superior optical and electrical properties. However, recent studies demonstrated

that ITO on polymer substrates is not a suitable candidate as transparent electrodes due to the brittle nature of ITO and the scarcity, thus the high cost of indium. Graphene—a flexible, transparent, 2D sheet of sp^2 -hybridized carbon atoms— has evolved into a promising alternative as an electrode material due to its remarkable electrical, mechanical, and optical properties. However, its low work function (4.4 eV) and high sheet resistance (300 Ω /sqr) limit its use in practical optoelectronic applications.[5] The low work function (WF) of graphene causes a significant injection barrier with the most overlaying organic emitters. In addition, the high sheet resistance of pristine graphene results in high turning-on voltages, thus reducing luminous efficiencies in OLEDs. Various approaches have been reported to overcome these disadvantages of graphene for OLED applications with appreciable success.[5]–[7], [50]–[52] However, a true ITO alternative for efficient OLEDs is yet to be achieved.

The last achievement in graphene-based OLEDs is summarized in Table 2.1. In all of these papers, graphene used as flexible anode and different methods are reported to modify the drawbacks of graphene as a flexible anode. Most of them, use chemical doping (HNO_3 doping) to reduce the sheet resistance of graphene and coat a GraHIL layer to engineer the low work function problem. The most-commonly used GraHIL layers are PEDOT:PSS and MoO_3 .

Table 2.1 Summary of graphene-based OLED papers in literature.

Year	Journal	Method of Doping	Pristine Gr Rs	Doped Gr Rs	WF engineering Method	Pristine graphene WF	Modified WF
2012	Nature Photonics	HNO ₃ or AuCl ₃	>300 Ω/□	30 Ω/□	GraHIL	4.4 eV	5.95 eV
2013	Nature Communication	OA/dichloroethene solution	1 kΩ/□	<200 Ω/□	PEDOT:PSS and MoO ₃	4.7 eV	6.1 eV
2014	Nature Scientific Report	5nm MoO ₃	700 Ω/□	50 Ω/□	5nm MoO ₃	4.7 eV	6.6 eV
2016	Nature Asia	HNO ₃ vapor for 150 s	>300 Ω/□	58.3±3.8 Ω/□	GraHIL composed of PEDOT:PSS and PFI	4.4 eV	5.95 eV
2016	Nature Communication	HNO ₃ aqueous solution or by its vapour	-	92.5±9.4 Ω/□	electrode architecture TiO ₂ layers	4.5 eV	-
2018	Nature Communication	PFSA Doping	352.7 ± 48.0 Ω/□	91.4 ± 30.1 Ω/□	PFSA Doping + GraHIL	4.7 eV	5.8 eV Just with PFSA

The comparison and last achievement in blue flexible OLEDs are also summarized and shown in Table 2.2.

Table 2.2. Comparison between the TADF blue OLEDs in literatures and the OLEDs of this work

Dopants	V_{on} (V)	L_{MAX} (cd.m⁻²)	η_C (cd.A⁻¹)	η_{EXT} (%)	CIE (x, y)	Ref.
<i>BPy-pC</i>	3.8	2183	5.0	4.2	(0.16, 0.13)	[53]
<i>BPy-pTC</i>	3.4	8610	16.3	9.4	(0.17, 0.27)	[53]
<i>BPy-p2C</i>	3.6	10800	20.8	11.0	(0.18, 0.28)	[53]
<i>BPy-p3C</i>	2.9	16700	56.5	23.9	(0.19, 0.32)	[53]
<i>BPy-p3C</i>	3.1	25850	35.2	14.5	(0.20, 0.36)	[53]
<i>BPy-p3C</i>	3.1	28660	25.3	9.9	(0.20, 0.38)	[53]
<i>DCzIPN</i>	3.5	26280	22.5	13.8	(0.15, 0.16)	[54]
<i>DMeCzIPN</i>	3.5	95743	46.6	23.8	(0.16, 0.28)	[54]
<i>sAC-sDBB</i>	3.3	4872	14.8	25.4	(0.151, 0.058)	[55]
<i>sAC-DBB</i>	3.4	2061	8.7	16.2	(0.166, 0.066)	[55]
<i>4-DPFCzAIAd</i>	3.4		67.1	28.2	(0.20, 0.36)	[56]
<i>TPh2Cz2DPhCzBN</i>	11.5	≥10000	140	32.4	(0.13, 0.16)	[57]
<i>tCbz-mPYRs</i>	4.5	≤100		8.7	(0.16; 0.12)	[58]
<i>TDBA-SAF</i>	-	-	23.7	28.2	(0.142, 0.090)	[59]
<i>DBA-SAB</i>	-	-	43.8	25.7	(0.144, 0.212)	[59]
<i>tCz-ND</i>	3.25	8424	22.17	17	(0.14, 0.16)	[60]
<i>MetCz-ND</i>	3.25	21459	31.98	17.6	(0.18, 0.32)	[60]
<i>PXZ-BIP</i>	2.82	-	57.9	21	(0.21, 0.37)	[61]
<i>2Cz2tCzBn</i>	-	9625	64.8	25.8	(0.21, 0.42)	[62]

CHAPTER 3

GRAPHENE GROWTH

Chemical vapor deposition is now one of the most widely used synthesis techniques in graphene science (CVD). The advantages of the CVD method are the scalability of the resulting graphene layers to a large area, low costs and easy to use. CVD produced graphene samples with very large areas were used as transparent electrodes in OLEDs. A catalyst substratum is needed to decompose the carbon atoms from the carbon feedstock gas that flows through the CVD chamber to form a graphene layer through the CVD synthesis. Due to the low carbon soluble limit in copper, the graphene growth procedure on copper substrates is self-limited. This copper property offers a straightforward synthesis of single layer graphene . Copper foils are cost-effective and scalable graphene growth substrates. The transport qualities of the produced graphene layer are strongly influenced by the quality of the copper surface.

This thesis describes the direct synthesis of large-scale graphene films on thin copper layers using chemical vapor deposition. Graphene is grown on top of copper foil using the CVD method, which uses a combination of methane and hydrogen gases. The flow rate of these gases has a significant impact on the quality of growth graphene. As previously stated, graphene has two drawbacks when compared to ITO: high sheet resistance and low work function. Finding the best gas flow rates allows us to reduce sheet resistance and improve the mobility of CVD-grown graphene.

3.1 Synthesis of graphene with CVD method

In CVD method with decomposition of CH_4 in assist of H_2 and Ar gases, the graphene grows on top of the Cu. During this thesis, some CVD process are designed to growth graphene. Right now, we have three working CVD system in our group.

One of them is one zone CVD system and the others are three zone CVD systems. We optimized all systems and tried to grow graphene. The results will be showed later. The figures of these three systems are shown below.

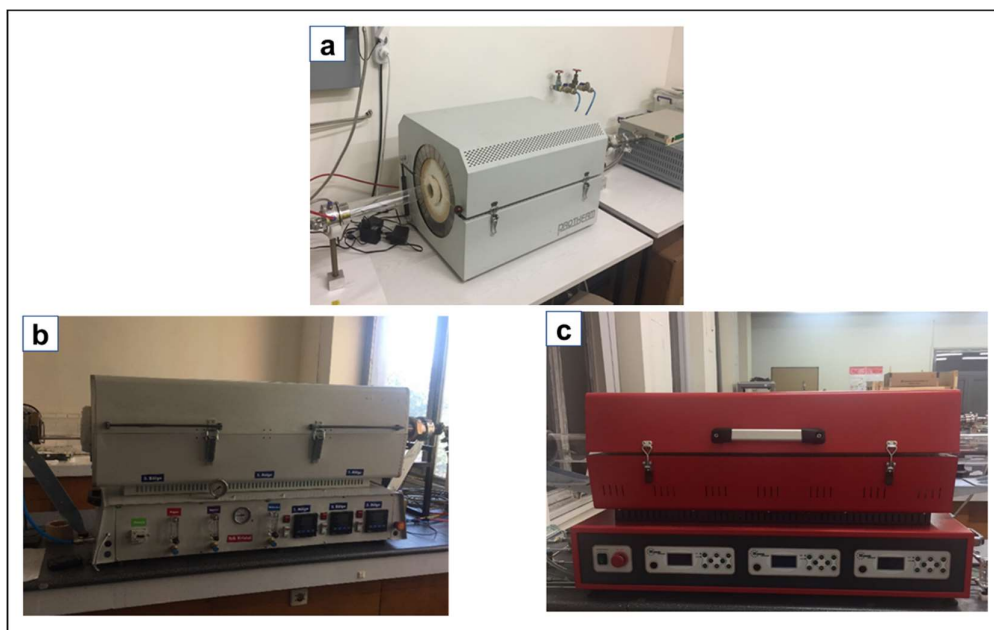


Figure 3.1. (a) CVD system 1, (b) CVD system 2, (c) CVD system 3.

The CVD system 3 is designed and fabricated by our group. In this new system all three zones are controlled by separate electronic controllers and the electronic gas flow meters are used to control gas flow rate more accurately.

3.1.1 Copper as a catalyst metal

As previously stated, copper is a promising catalyst substrate for CVD grown graphene, due to its self-limited graphene growth procedure. Furthermore, copper foils are cost-effective and scalable graphene growth substrates.

In this work, a 25 μm -thick cold rolling copper is used to achieve highly uniform large area graphene films. Cold rolling copper is a very suitable substrate to use in CVD grown graphene due to deformation in its grain structure. The microstructure of cold-rolled copper consists of long, thin, elongated cells with sharp boundaries. [63] These sharp boundaries become flat during when annealed and therefore achieves a uniform single-layer graphene. In compare with electroplated copper, . cold rolling copper do not have grain boundaries which enables to have uniform cover of graphene on top of the copper. Figure 3.2 shows the optical image of graphene/Cu sample on both electroplated copper and cold rolling copper after oxidation. Oxidation after growth is done to be ensure about the quality and uniformity of graphene (The oxidation technique will be described by detail in part 3...). As seen in figure 3.2.a, the grain boundaries act like obstacles and prevent the uniform growth of graphene. On the other hand, the surface of graphene/cold rolling copper is uniform (figure 3.2b).

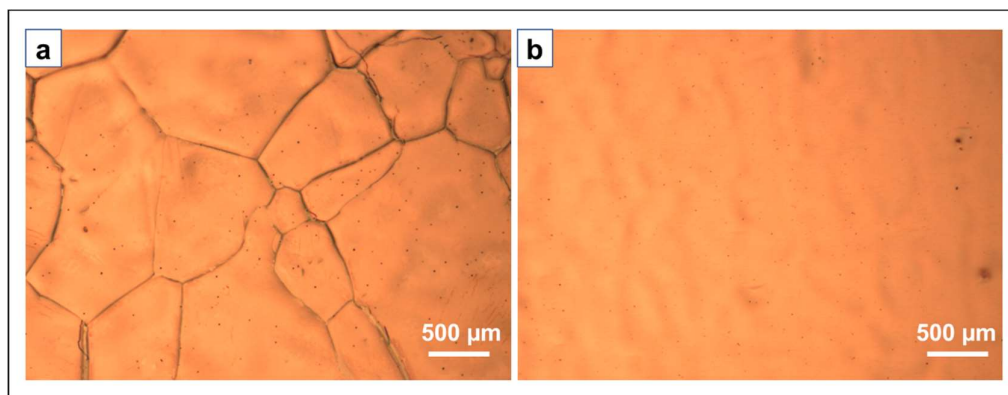


Figure 3.2. (a) Graphene on electroplated Copper, (b) Graphene on cold rolling Copper.

In order to better comparison between these two kinds of copper, the Raman spectrum of them is shown in figure 3.3. As obtained from Raman spectrum, the 2D

peak in graphene/cold rolling copper is sharper than graphene/electroplated copper. Although, Raman measurement of graphene on top of copper is not a reliable method due to the background peak of copper, but transfer of graphene on SiO₂ substrates is a time-consuming process and destructive method. On the other hand, characterize the samples via Raman directly on the copper foil is a nondestructive method and give an idea about the graphene layer number and quality.

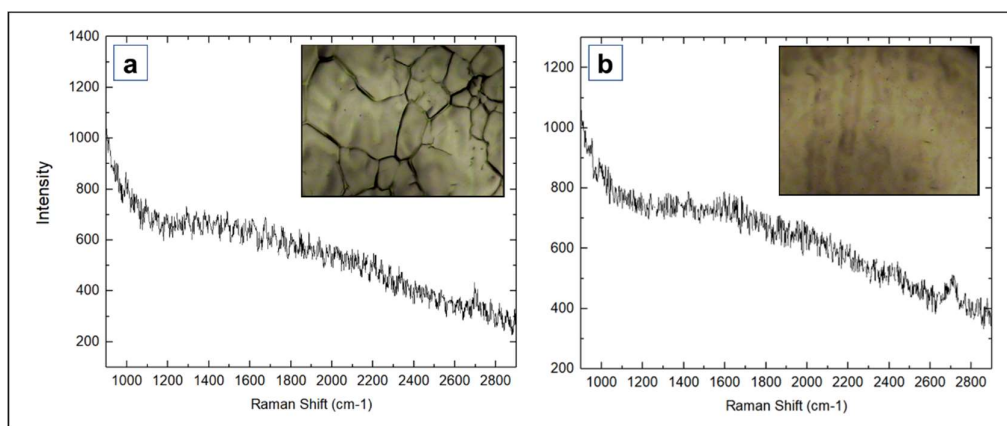


Figure 3.3. (a) Raman spectrum and optical image of graphene on electroplated Copper, (b) Raman spectrum and optical image of graphene on cold rolling Copper.

3.1.2 Precleaning (Acid Pretreatment)

A pure and uniform copper surface is required for the creation of high-quality graphene. In addition to causing the nucleation density of graphene to rise, rough surfaces and impurities contribute to the introduction of further defects. According to the literature [36], the acid treatments has a significant impact on the coverage and morphology of the CVD-grown graphene because it helps to remove the substrate oxide layer and surface Ca particles that are intrinsically existent on the copper foil.

In the literature, the following are the most widely accepted and effective cleaning methods:

1. Cleaning with acetone and ethanol: The sample was washed before deposition by immersing them in acetone and ethanol for ten minutes and in DI water for 5 minutes.

2. Cleaning with nitric acid: The foil was soaked in a nitric acid for 30 - 60 seconds. After cleanliness, the copper foil is immersed in DI water for additional washing, then cleaned using acetone and isopropanol for a short time before getting dried with N_2 . In this thesis, all of these methods were tried and optimized. Accordingly, a precleaning method was also investigated and done. In this method, copper foil is put in acetic acid for 10 minutes, then is washed in DI water for 10 minutes at the end is washed in ethanol for 10 minutes.

Washing with argon is added to process. After loading copper foils into furnace, samples are washed with argon gas for 10 minutes under vacuum. Besides this, annealing the copper foils under hydrogen flowing is done to etch oxide layer and get smooth and free-defect copper surface. The surface of the copper before and after annealing is shown in figure 3.4.

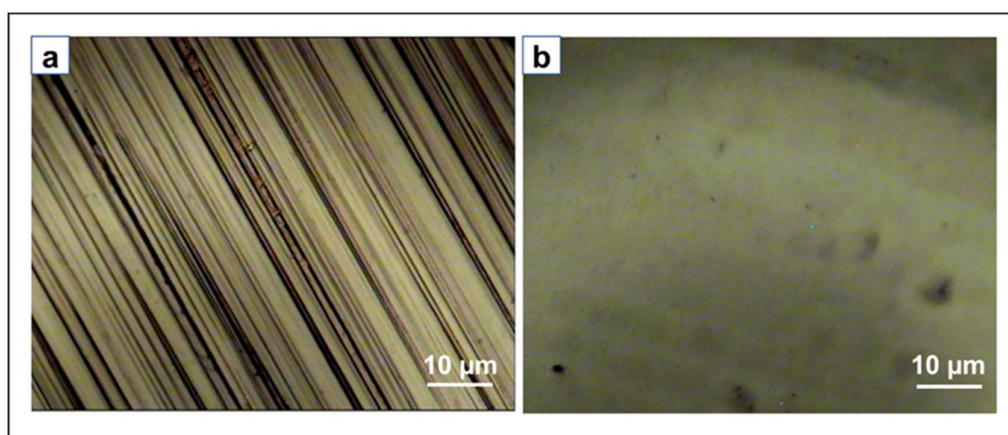


Figure 3.4. (a) Surface of copper before annealing, (b) Surface of copper after annealing.

3.1.3 Growth of graphene

The fabrication and characterization of Transparent Conductive Graphene Anodes are reported in this thesis. Here we will report the direct synthesis of large-scale graphene films using CVD method on thin copper layers. In CVD method, with combination of methane and hydrogen gases, the graphene is grown on top of the copper foil. The flow rate of these gases plays an important role in the quality of growth graphene. Several experiments have been done to find the best gas flow rates. As discussed before graphene has two disadvantages in compare with ITO, high sheet resistance and low work function. Finding the best gas flow rates helps us to decrease the sheet resistance and increase the mobility of CVD grown graphene. The results of these set of graphene growth experiments are summarized in Table1. As shown in table 1 the sheet resistance has decreased to 450Ω .

In literature the sheet resistance of graphene is around $300 \Omega/\square \leq R_s \leq 1 \text{ K}\Omega/\square$. Despite its high capability as a transparent conductor, graphene's practical usage as the anode of optoelectronic devices has been restricted, due to its low work WF (4.4 eV) and high R_s compared to ITO ($4.7 \leq \text{WF} \leq 4.9 \text{ eV}$ and $10 \Omega/\square$). Due to graphene's low WF, hole injection among the graphene anode and the upper organic layers is unfavorable due to the interface's high injection barrier. As an outcome, graphene-based OLEDs perform worse than ITO-based devices in terms of current efficiency. Furthermore, the poor conductivity of pristine graphene anodes reduces the device's luminous (power) efficiencies because it causes high operating voltages. To make workable graphene anodes, a method to overcome graphene's drawbacks (poor WF and high sheet resistance) must be discovered.

Table 3.1 Summary of graphene growth result

#of exp.	H2 (sccm)	Ch4 (sccm)	Ar (sccm)	Growth Temp. (°C)	Growth Dur. (min)	Anneal. Dur. (min)	Rs (Ω/\square)	Mobility
1	100	500	5000	1000	35	0	3920	31,2
2	100	100	5000	1000	35	0	5490	12,8
3	100	90	5000	1000	35	0	2950	357,4
4	100	80	5000	1000	35	0	1560	323,3
5	100	50	5000	1000	35	0	480	419,9
6	100	20	5000	1000	35	0	930	470,2
7	100	10	5000	1000	35	0	820	321,0
8	100	50	5000	1000	35	20	2290	152,2
9	100	50	5000	1000	35	10	580	463,1
10	100	50	5000	1000	25	0	460	814,4
11	100	50	5000	1000	15	0	1090	474,5
12	100	50	5000	1000	10	0	1670	356,8

As mentioned before, many methods and techniques were tried to growth graphene with CVD method. Every step of growth (copper precleaning, H₂/CH₄ gas flow ratio, Ar washing duration, H₂ annealing duration and temperature, growth duration and temperature and rapid cooling) optimization is done during this work. The most important point here to get a graphene with low sheet resistance and high mobility. In single layer graphene because of low charge concentration in compare of multilayer graphene, Rs is high but it's quality and uniformity are better than multi-layer graphene. Consequently, for OLED application, synthesizing single layer graphene play an important role. To achieve this, a set of experiments have been done. For single layer graphene the flow rate of hydrogen to methane should be 20, 30 times more.

After many experiments the gas flow rates are established to H₂:CH₄ (35:2) sccm. The growth duration is optimized to 30 minutes. The sharp 2D peak in Raman spectrum which shown in figure 3.3 approve the single layer nature of graphene.

The summary of graphene growth is shown in figure 3. As a supplemental characterization method, oxidation method is done which is described in following part.

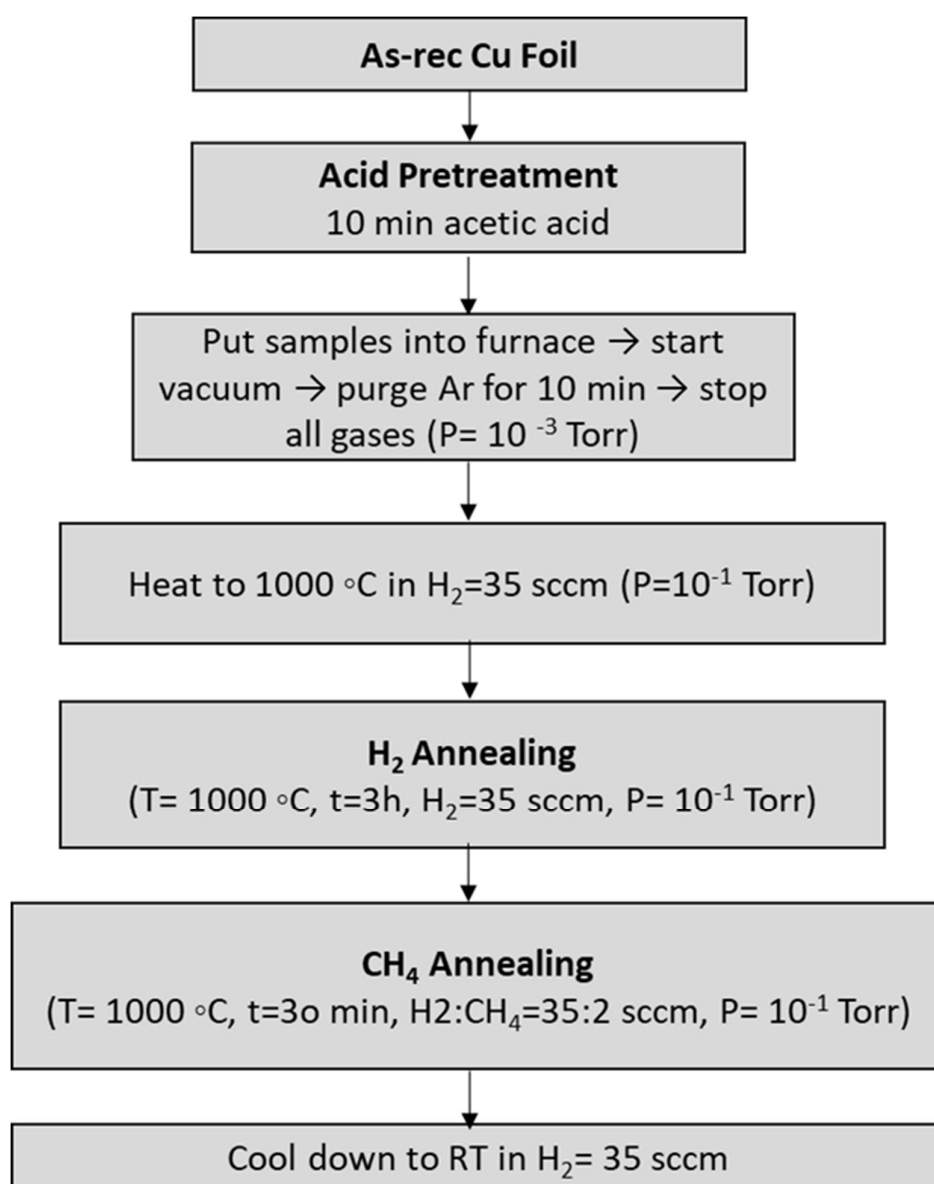


Figure 3.5. Summary of graphene growth process.

3.1.4 Oxidation Technique

Oxidation of graphene-copper foil is a technique which use to prove existents of graphene and show the uniformity of the graphene, in the lack of graphene after oxidation the copper will be oxidized, and the color will be changed. This color change can be recognized in optic images or SEM characterization.

Oxidation is done after growth in 200 °C for 5 minutes (Fig.3.5 (a)). Figure 3.5 (b) and (c) shows the optical images of a good quality graphene and bad quality graphene. The parts with orange color indicate the lack of graphene which have resulted with oxidizing of copper.

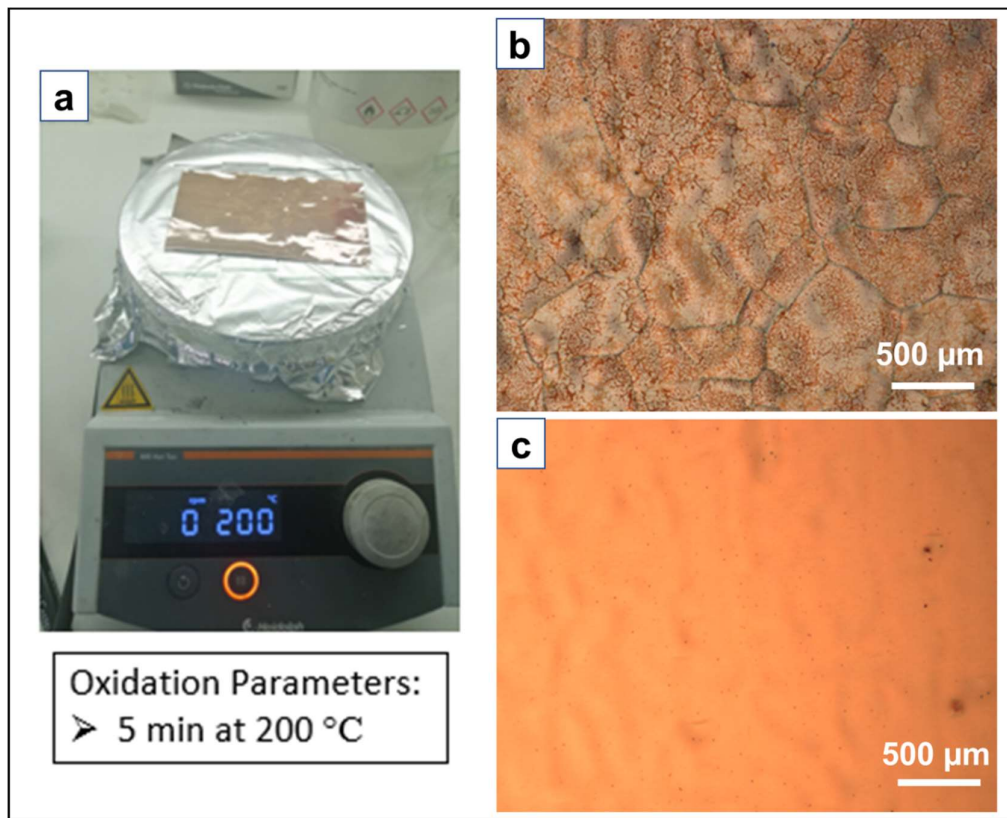


Figure 3.6 (a) Oxidation technique, (b) Optical image of graphene/Cu foil with inconstant surface, (c)) Optical image of graphene/Cu foil with uniform surface.

3.1.5 Raman Spectrum of SLG

As stated before, the most popular approach for characterizing graphene properties is Raman spectroscopy. The G band at 1582 cm^{-1} and the 2D band at about 2700 cm^{-1} are key features in the Raman spectra of graphene, while the D-band appears around 1350 cm^{-1} in the case of disorder or defect in graphene. The intensity ratio of the G-band and 2D-band in graphene's Raman spectrum can be used to determine the number of graphene layers. Single-layer graphene has a very strong peak in 2D-band. Furthermore, as the number of layers grows, the peak intensity in the G-band increases. The Raman spectrum of SLG which is transfer to SiO_2/Si is shown in figure 3.7. The sharp 2D peak in the Raman spectrum verifies the single layer nature of graphene film.

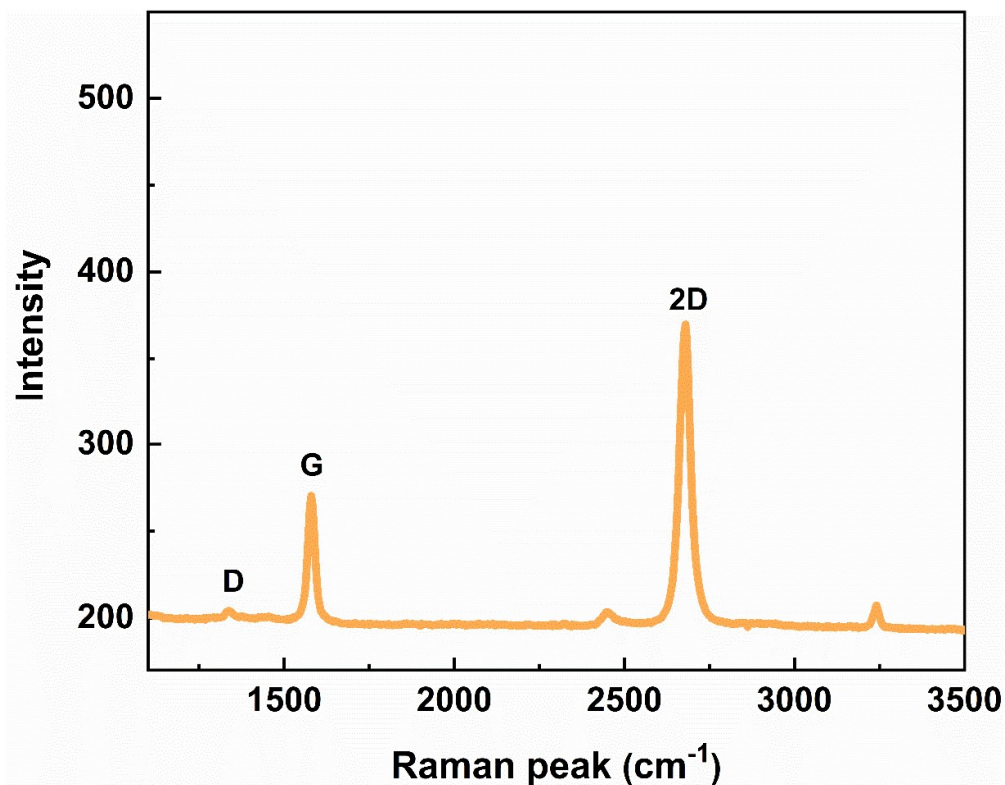


Figure 3.7. Raman spectrum of single layer graphene.

3.1.6 Scanning Electron Microscopy image of SLG

The morphology of graphene is analyzed by scanning electron microscopy (SEM). SEM image (Figure. 3.8) revealed no impurities on the surface of the graphene-copper film, and it is highly uniform.

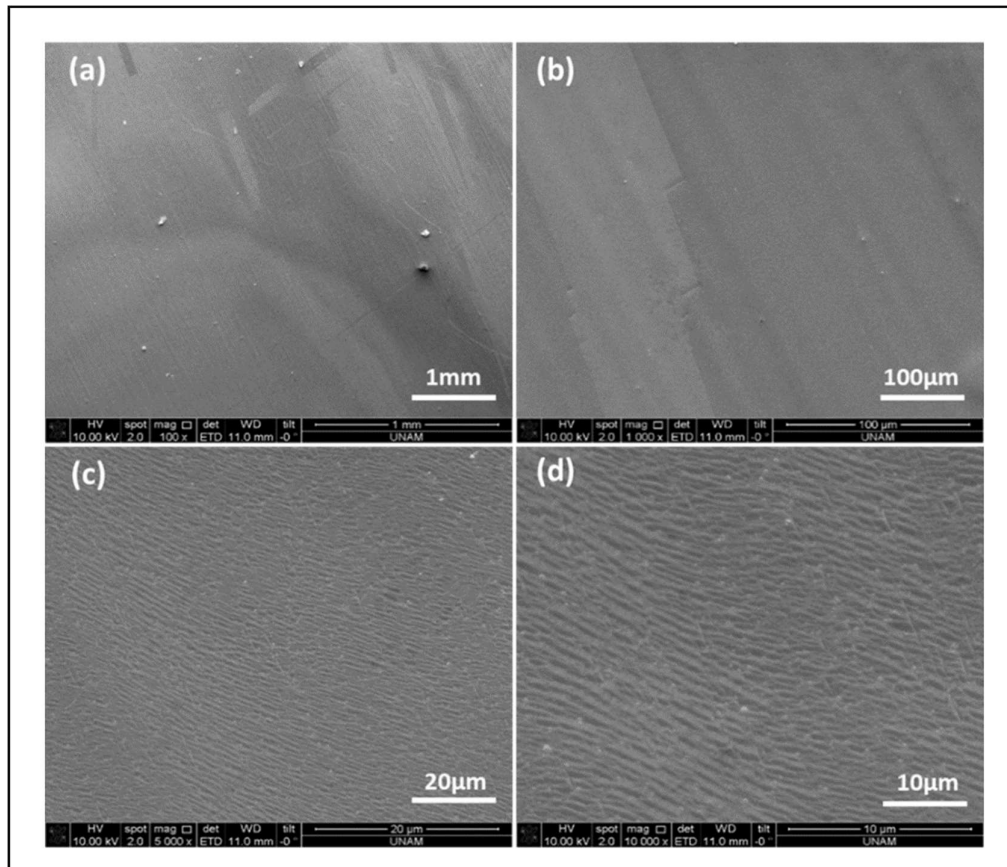


Figure 3.8. SEM images of single layer graphene on copper substrates before the transfer, with different magnifications.

3.1.7 HEMS measurement

Van der Pauw measurements are used to determine the sheet resistance of graphene films. The van der Pauw Technique uses a four-point probe that is put around the edge of the sample to determine the sample's average resistivity. Following the transfer of the graphene to the plastic, four ohmic contacts are created for use in this measurement. In this measurement, ezHEMS facility is used. The ezHEMS has four probes that measure the sample's inner and outer resistances. The sample figure is presented below. The ezHEMS system, which uses four probe measurements and a hall effect measurement, can provide interesting information about CVD-grown graphene, such as sheet resistance and charge carrier mobility.

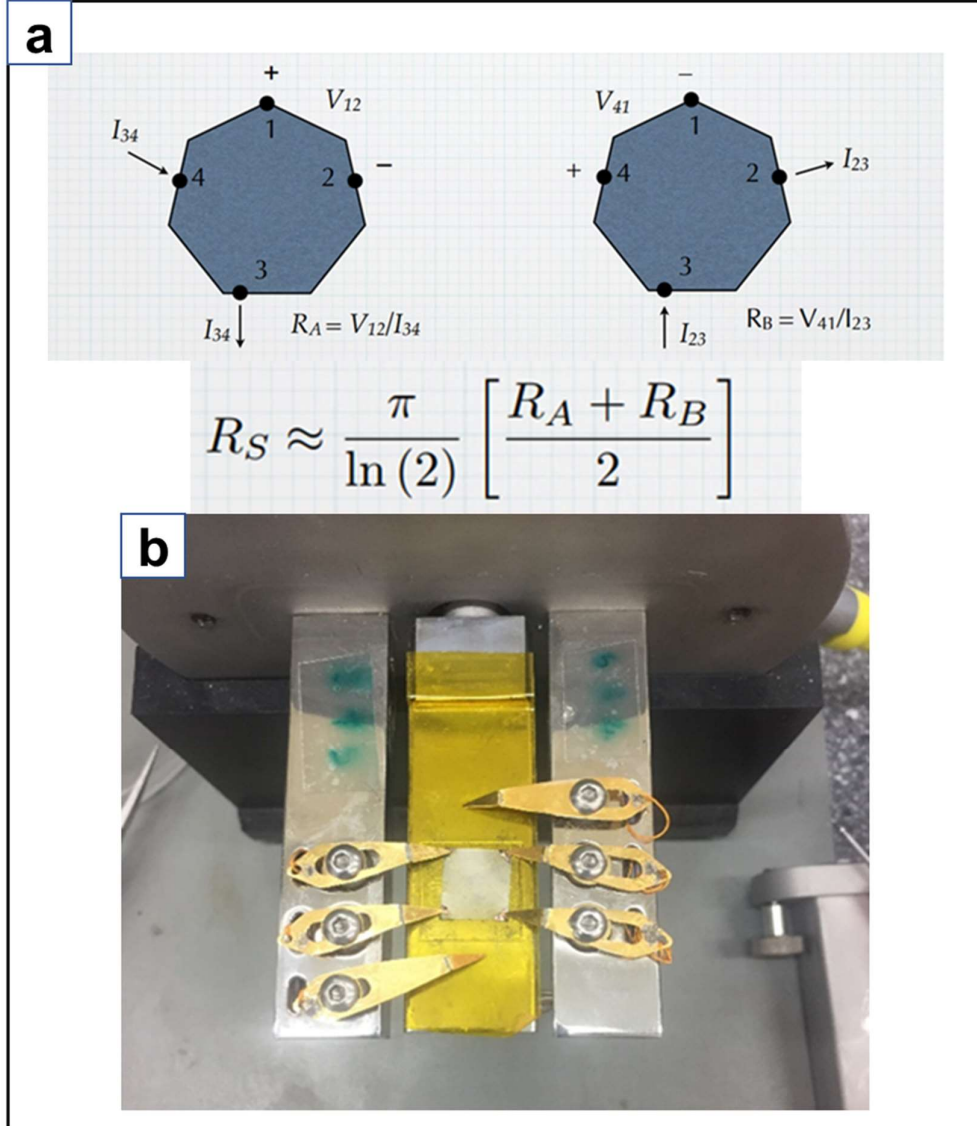


Figure 3.9. (a) Description of van der Pauw method, (b) Measuring the electronic properties of graphene with four probe measurement.

3.1.8 Transmission measurement

To measure the transmission and have an idea about the layer number of graphene the transmission measurement is done. Firstly, the transmission of plastic is

measured then the transmission of the transferred graphene to plastic is done. The difference between these two values gives us the number of layers. Every 2.29 % is counted as one layer.

The graphene is then transferred with a laminating machine to plastic. Transmission of plastic is measured as reference. Transmission of graphene on plastic is also measured. The difference of these two values gives us the number of layers of graphene. Our results are consistent with the literature, where a $\sim 2.3\%$ drop in transmittance was observed per graphene layer at 550 nm.

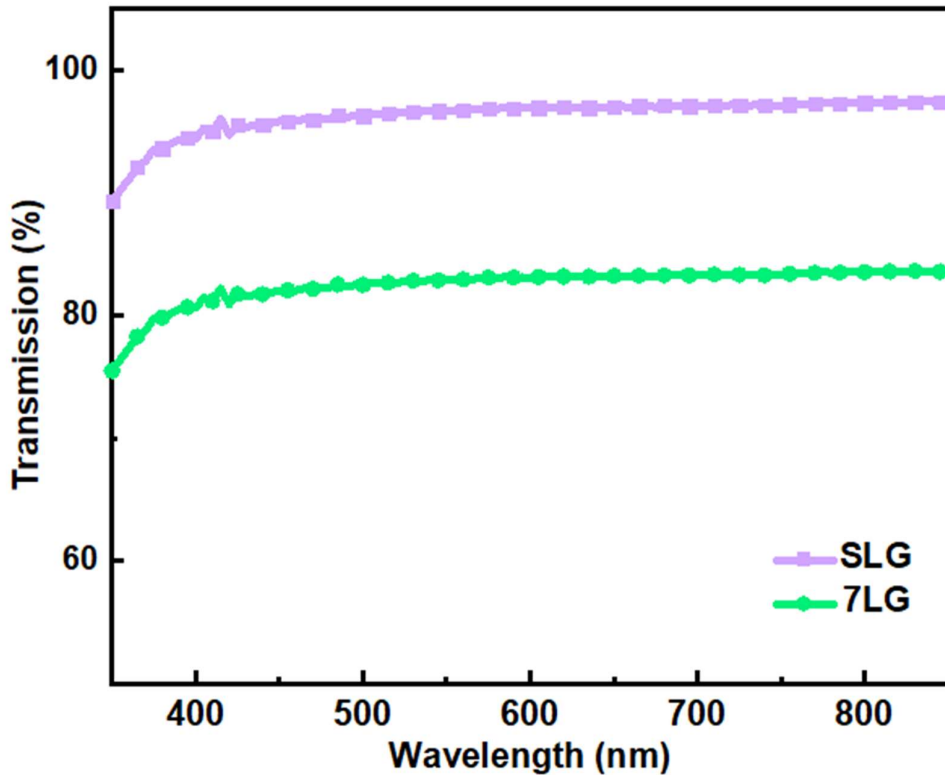


Figure 3.10. The optical transmission measurement of single layer and seven-layer graphene.

3.1.9 Work function Measurement

The OLED is made up of an active layer (an i-layer) sandwiched between two injectors that also serve as reflectors. What exactly does this imply? There's a hole injection layer that has to be both electron reflecting and hole injection. The electron injection layer, on the other hand, must inject electrons into the active layer while reflecting them back to itself.

This is necessary in order to confine the electrons and holes in the active layer so that they can radiatively recombine and emit photons.

To achieve this function, the hole injecting layer's valence energy level must be lower than the valence energy level of the active layer's homo-level, allowing the holes to readily slide down to the active layer. Simultaneously, its conduction energy level must be higher than that of the active layer in order to reflect electrons back to the active layer. As a result, knowing the work function value is critical before beginning OLED fabrication.

Work function measurements were done with UPS measurement. Work function is just the difference between the energy of the UV photons (21.21 eV for He I radiation) and the binding energy of the secondary edge.[64]

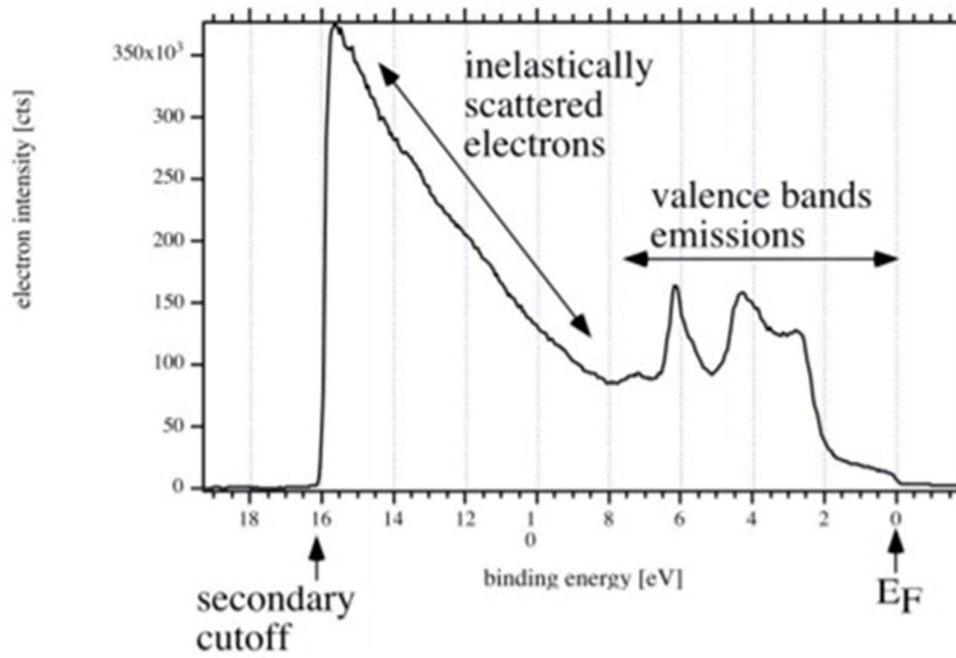


Figure 3.11. UPS spectrum[64]

The graphene WF in literature is around 4.2-5 eV, and the work function of SLG is measured around 4.4 eV. The UPS spectrum of SLG is shown in figure 3.4.

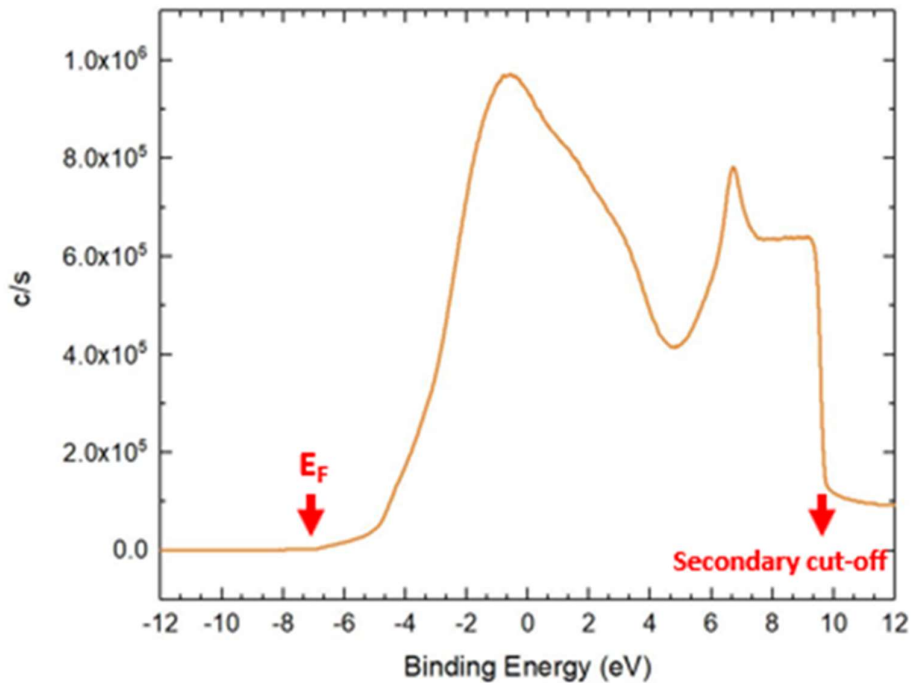


Figure 3.12. UPS spectrum of SLG

$E_F = 7$ eV, Secondary Cutoff = 9.85 eV

$WF = 21.21 - (7 + 9.85) = 4.36$ eV

In order to spectrum and calculation the work function of SLG is around 4.36 eV.

3.2 Transfer of CVD-Grown graphene

In order to characterize graphene with Raman spectroscopy it is required to transfer the graphene to the SiO_2/Si substrate. To do this, polymer assisted method (Fishing method) is used which is described by detail in part 2.1.3.1. For OLED application, since we need a transparent and flexible substrate, lamination technique is used to

transfer graphene to PET substrates. The details of these experiments is described in following parts.

3.2.1 Fishing technique

Instead of PMMA, photoresist (Az 5411) is used as an assist polymer. The graphene samples after growth on copper substrates is coated with photoresist, and then baked in vacuum oven for 24 hours under 60 °C. After photoresist bake, the samples are put in copper etchant solution (FeCl_3) to etch away the copper.

The suspended graphene/photoresist is fished by SiO_2/Si substrate, and photoresist is then developed with acetone. The process flow of this method is shown in figure 3.13.

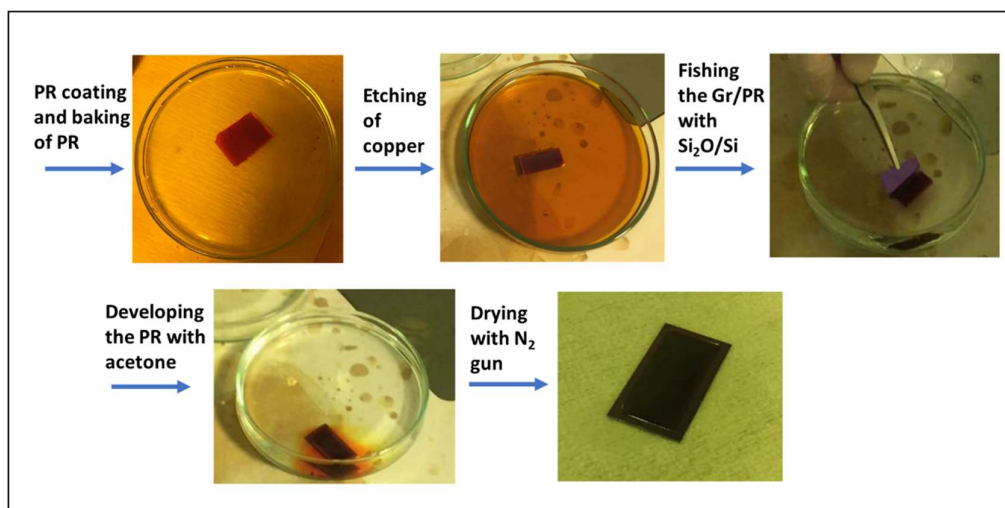


Figure 3.13. Process flow of Photoresist-assisted transfer method.

3.2.2 Lamination technique

In order to measure the electronic properties (sheet resistance and carrier mobility) and optical transparency of graphene, Lamination-assisted transfer method is used to transfer the graphene samples to PET substrate. This method also used to create Gr/PET anodes for OLED application. To do this, Gr/Cu samples sandwiched between a protect paper and PET substrate and put in lamination machine under 90 °C. The copper is then etched by FeCl_3 , and GR/PET is released. The process flow of this technique is shown in figure 3.14.

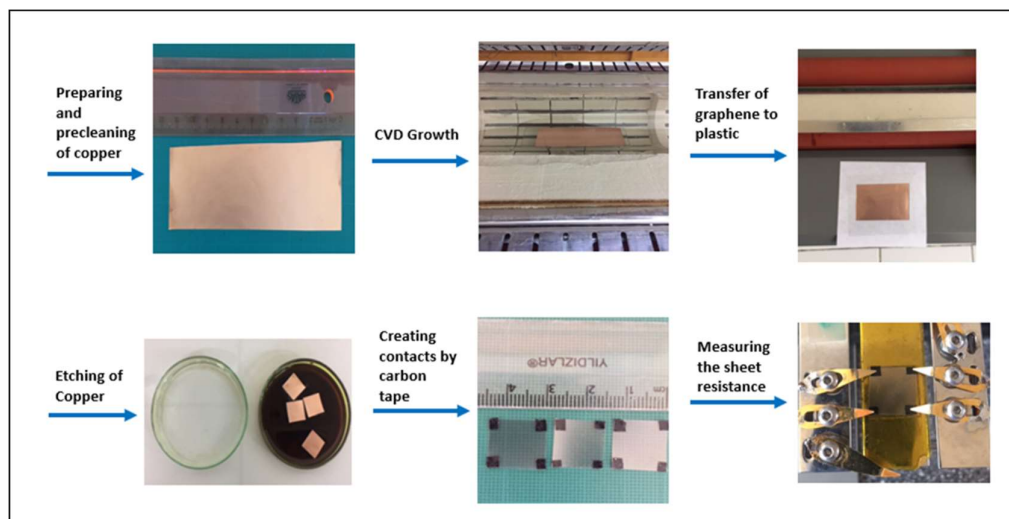


Figure 3.14. Process flow of lamination-assisted transfer technique.

3.3 Doping of graphene

The main drawback of graphene films compared to the ITO is their high sheet resistance. Therefore, an anode with low sheet resistance ($R_s < 100 \Omega$) is needed for high-performance OLED applications. Several different dopants have been used to enhance the electrical properties of pristine graphene on rigid substrates with

success.[5]–[7], [51] Doping materials can be classified into two main groups: (1) inorganic acids (most commonly HNO₃, HCl, H₂SO₄), and (2) transition metal halides (most commonly AuCl₃, FeCl₃), where both utilize charge transfer processes on the graphene surface (shift in Fermi level) towards enhancement of conductivity, thus lowering sheet resistance (Figure.3.15).

HNO₃, a p-type dopant for materials based on carbon can be used for the doping of graphene. According to equation 1, an electron can already be transferred from graphene to nitric acid; this reaction indicates a shift in the fermi level related with increasing graphene sheet conductivity and carrier concentration.



In this work, inspired by the doping studies for graphene on quartz substrates in literature,[65] two different approaches (inter-layer and last-layer doping) have been performed and optimized to reduce the high sheet resistance of multi-layer graphene films on PET. In the first approach, doping is performed for each layer separately, while, in the second approach, the graphene film is doped after the whole multi-layer stack is formed on the PET (see Figure.2c). Last-layer doping showed significantly better results, where graphene films with sheet resistance as low as 29.3 Ω/sqr were achieved.

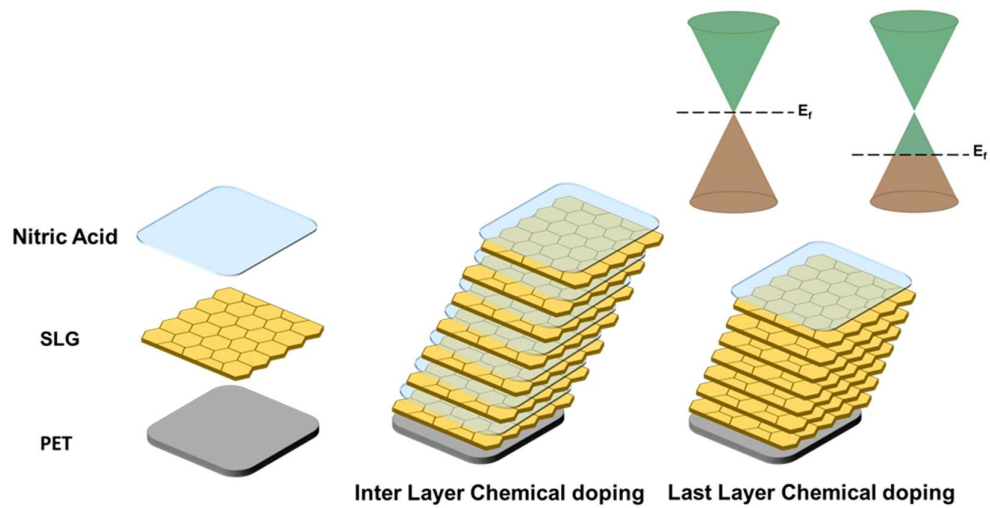


Figure 3.15. Schematic description of Interlayer and last layer-doped of graphene.

The photographs of samples that prepared with mentioned methods is shown in figure 3.16. The HEMS measurement results are shown in Table 3.2.

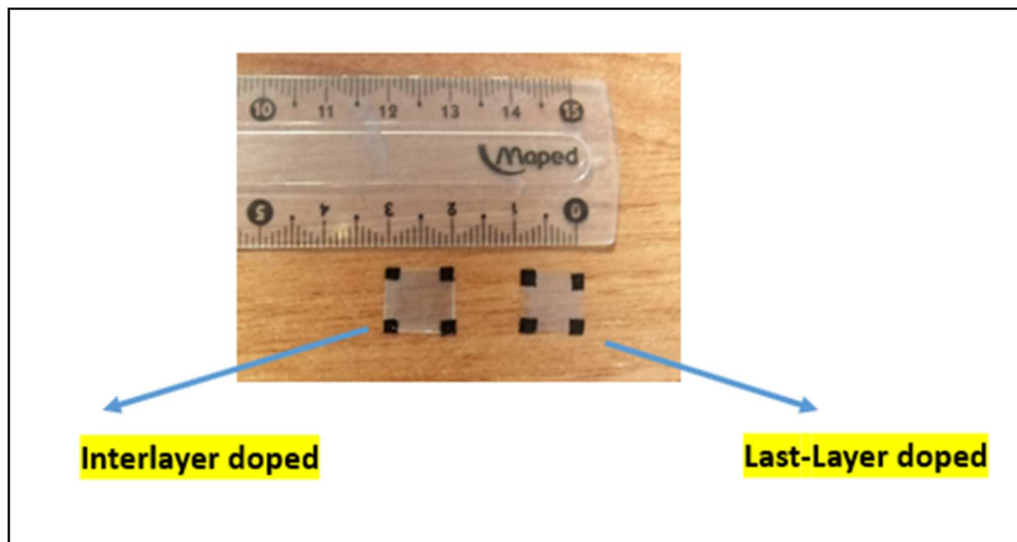


Figure 3.16. The 7LG/PET samples which doped with interlayer doping and last layer doping method.

Table3.2. Sheet resistance measurement results.

Doping Method	R_s (Ω/□)	Resistivity (Ωcm)	Conductivity (1/Ω)	Mobility (cm²/V_s)
Last-layer doped	29.3	79.05 x 10⁻⁵	12.64 x 10⁴	1785
Inter-layer doped	762.2	12.89 x 10⁻²	77.55 x 10¹	63.5

CHAPTER 4

GRAPHENE BASED OLEDs

To use graphene films as electrodes in flexible electronics, large-area synthesis and an efficient transfer method are essential. Large-scale synthesis of graphene films can be achieved using chemical vapor deposition (CVD). To form a graphene anode on a flexible substrate, multilayered graphene films were transferred to a PET substrate using lamination technique.

4.1 TADF Materials

In this thesis, a new family of TADF emitters (designed by Dr. Gorkem Gunbus and synthesis by Cirpan Research group) are used to develop TADF flexible OLEDs which they are TADF emitters with selenium incorporated the donor units that are orthogonal to the carefully selected acceptor units to increase HSO and minimize ΔE_{ST} simultaneously. The approach was proven fruitful with enhanced EQEs compared to similar TADF emitters with no heavy-atom utilization. Remarkably one of the derivatives resulted in pure blue emission with EQEs approaching 26%. Additionally, by carefully optimizing the growth, surface modification, and doping processes, graphene-based flexible anodes revealed similar performance to ITO/glass substrates. In pure blue OLED devices utilizing our TADF emitter SeDF-B, graphene/PET anodes developed in this work outperformed ITO/Glass electrodes. These graphene-based devices highlight the first-ever utilization of graphene anodes for OLEDs with TADF-based emissive layers.

4.1.1 Molecular Design, Computational Studies, and Synthesis

The new family TADF material design principle was based on the fact that increasing H_{SO} while simultaneously maintaining ΔE_{ST} should enhance λ , thus more effective RISC. Hence, we carefully selected high-performance OLED active materials reported in the literature and substituted the oxygen atoms in donor units with the selenium atom, which possesses significantly higher H_{SO} than oxygen[66] The possibility of utilizing large halogens was omitted since it was shown that long-term accumulation of the corresponding anions of the aforementioned halogens at metal interfaces is detrimental to OLED performance.[67]

Molecular structures of SeDF-G, SeDF-B, and SeDF-YG are shown in Figure 4.1a. Ultraviolet-visible (UV-Vis) absorption and photoluminescence (PL) spectra of SeDF-G, SeDF-B, and SeDF-YG in chloroform are indicated in Figure 1c. When benzophenone-based derivatives are compared, it is seen that the intramolecular charge transfer (ICT) peak observed around 350 nm of SeDF-G is stronger compared to SeDF-YG. Moreover, SeDF-G is highly emissive with lower FWHM than SeDF-YG. These outcomes are consistent with theoretical calculations and shed light on better OLED performance of SeDF-G over SeDF-YG.

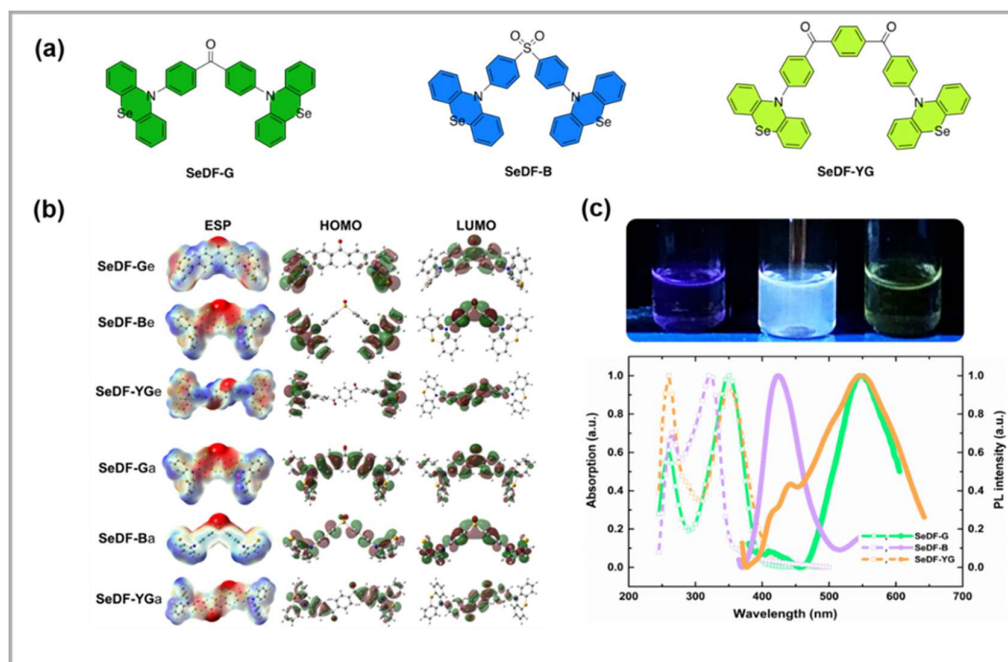


Figure 4.1. a) Structural formula of small molecules SeDF-G, SeDF-B, and SeDF-YG. b) Electrostatic potential surface (ESP) and frontier molecular orbital surfaces (HOMO, and LUMO) for the SeDF-G, SeDF-B, and SeDF-YG TADF materials in the equatorial and axial conformation of selenium substituted PTZ donor, c) Luminescence images of SeDF-G, SeDF-B, and SeDF-YG in chloroform recorded under UV irradiation at $\lambda_{ex}=365$ nm (above), Absorption and normalized photoluminescence (PL) spectra of SeDF-G, SeDF-B and SeDF-YG in chloroform at room temperature (below).

The lowest energy structures for the designed TADF materials presented two different conformations that are planar and vertical structures corresponding to quasi-axial (A) and quasi-equatorial (E) conformers, respectively (Figure 4.2). This indicates TADF materials with selenium substituted phenothiazine (Se-PTZ) derivatives have dual conformations due to the different C-N and C-Se bond lengths in the donor group as previously reported for PTZ.[68] The nearly orthogonal equatorial conformers resulted in the lower excited energy levels with a closer

singlet-triplet difference (TADF characteristics), axial conformers possess higher singlet energy level with stronger oscillator frequency with classical fluorescence characteristics.

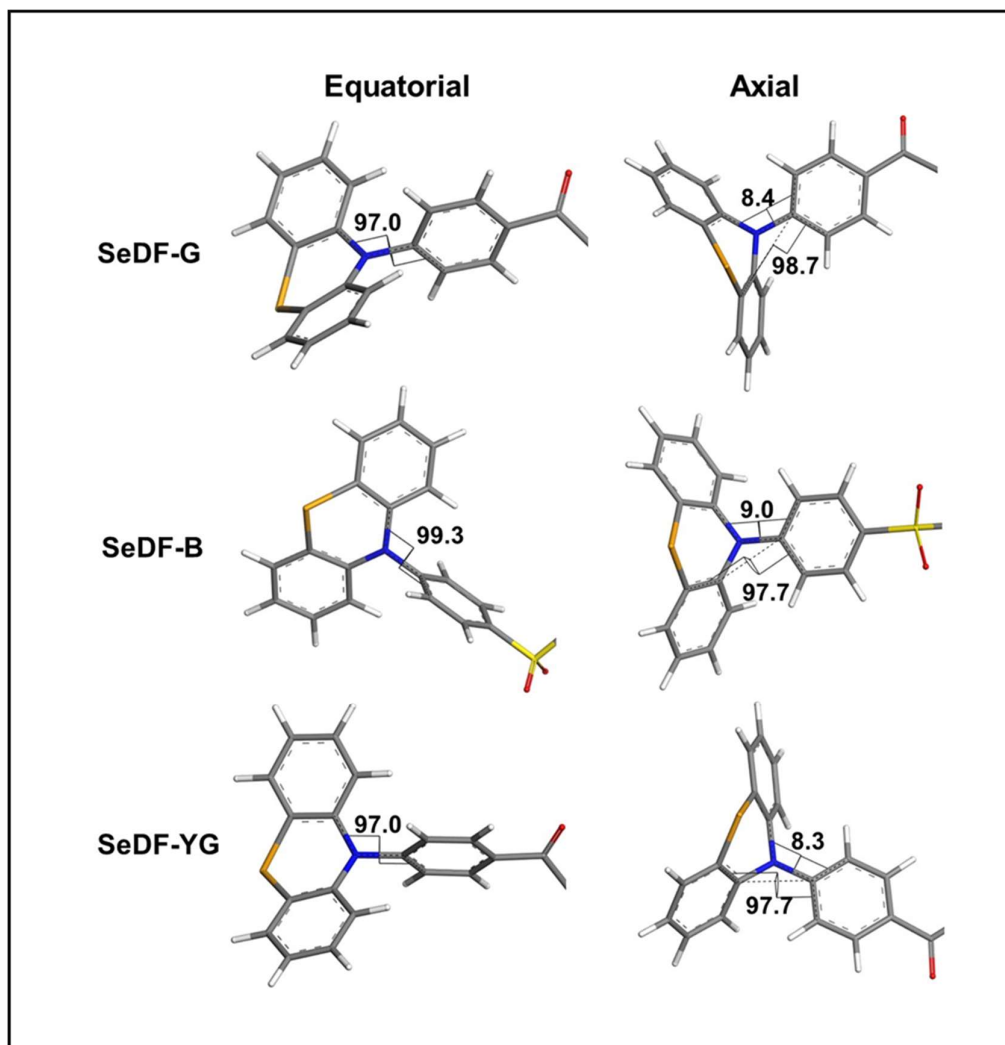


Figure 4.2. Optimized lowest energy conformations for SeDF-G, SeDF-B and SeDF-YG TADF materials.

We concluded that all three materials possess dual conformations where our calculations demonstrated that quasi-axial conformers are expected to show classical

fluorescence emission behavior, and the quasi-equatorial conformers have TADF characteristics. Similar to the previous studies conducted for PTZ, efficient OLED materials can be designed for Se-PTZ by utilizing the energy transfer between axial. With our main design principle and encouraging computational results in hand, we set out to synthesize these interesting targets. The synthetic pathway for the target molecules is given below.

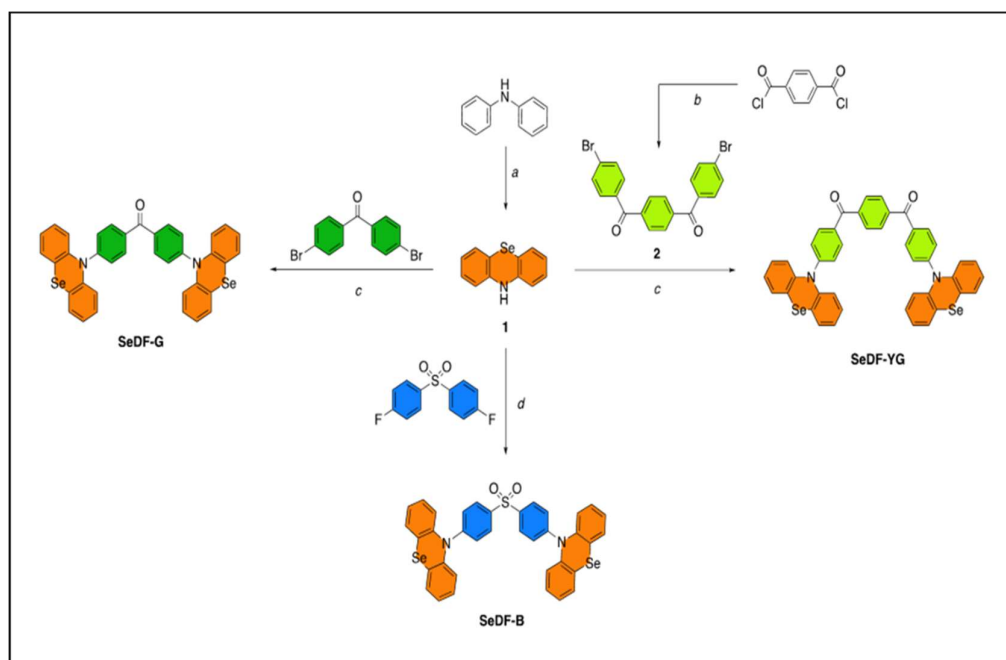


Figure 4.3. Synthetic pathways for the TADF materials (SeDF-G, SeDF-YG, SeDF-B): Reagents and Conditions: (a) SeO₂, I₂, 180 °C, 48%; (b) bromobenzene, AlCl₃, rt–90 °C; (c) Pd₂(dba)₃, (t-Bu)₃P, NaO-tBu, Toluene, 125 °C, 82%; (d) NaH, DMF, 60 °C, 28%.

The synthesis started with diphenylamine, and selenium incorporation was performed using SeO₂ and I₂ to get the target donor unit (1) in moderate yield.[20] Acceptor unit 2 was synthesized from commercially available terephthaloyl chloride

and bromobenzene using Friedel-Crafts chemistry. Compounds SeDF-G and SeDF-YG were realized by Buchwald-Hartwig coupling in good yields. Finally, SeDF-B was synthesized using commercial bis-(4-fluorophenyl)sulfone and donor 1 using NaH in DMF.

Transient time-resolved PL decays were investigated to verify the TADF character of the three emitters in the host-guest systems, and a large amount of excited-state energy transfer to the dopants was observed. (See figure 4.3)

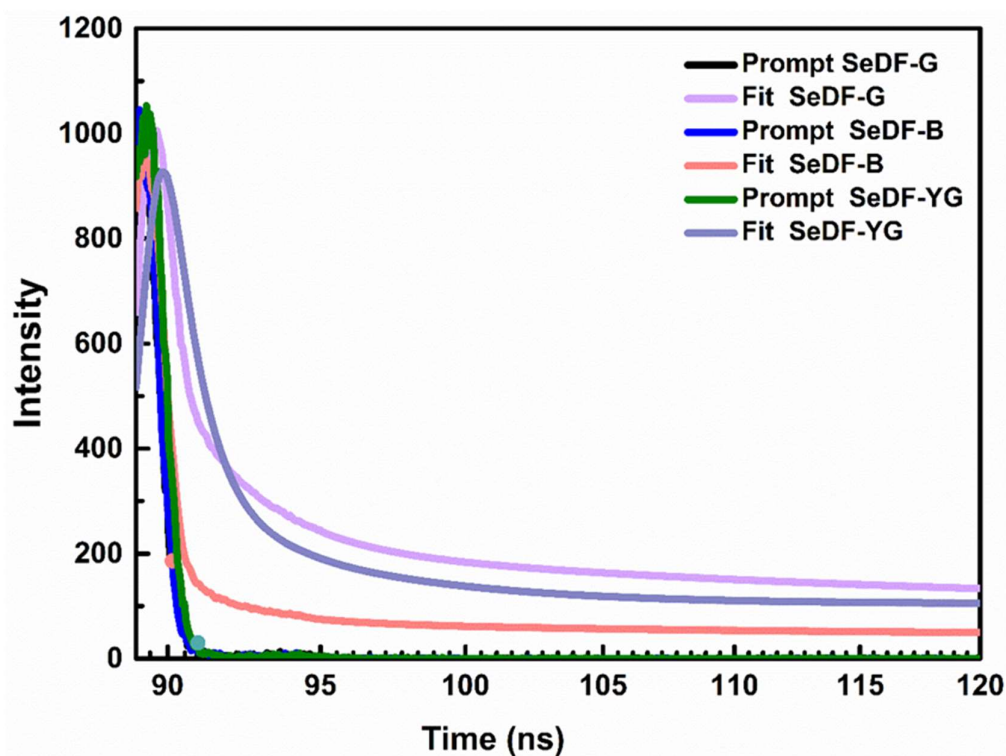


Figure 4.4. Time Resolved PL spectra for SeDF-G, SeDF-B and SeDF-YG

4.2 Device fabrication and characterization

To investigate the potential of graphene/PET anodes, TADF-based OLEDs were fabricated utilizing both graphene- and ITO-based anodes. The process flow of OLED fabrication is shown below.

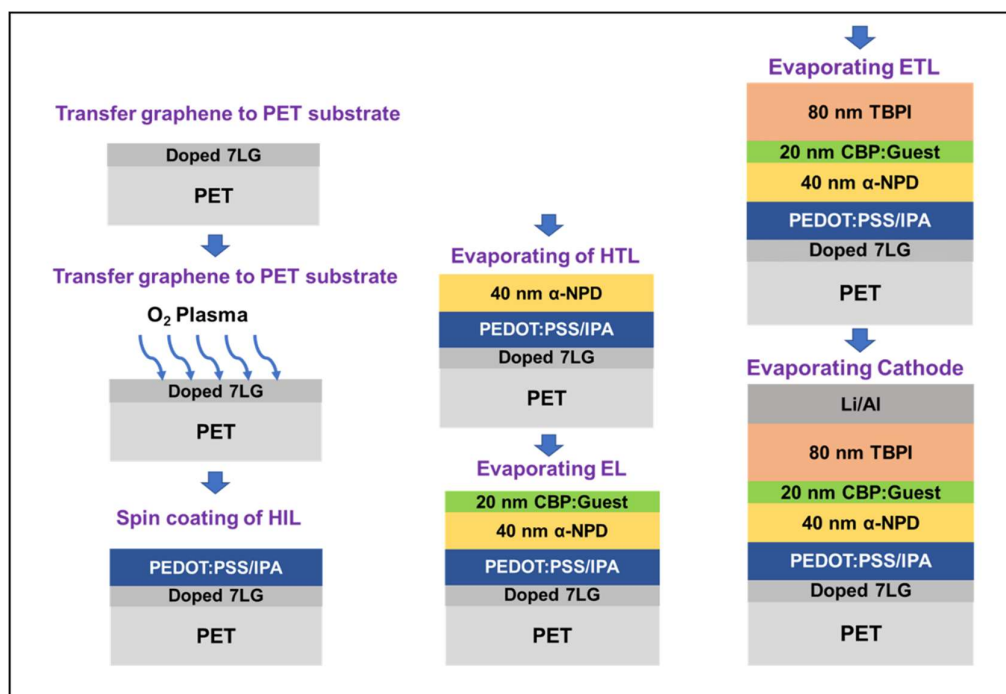


Figure 4.5. Cross-section of process flow of graphene-based OLED

As graphene's work function is lower than that of ITO, a hole injection layer (HIL) is necessary for the band alignment between the anode and hole transport layer (HTL) (α -NPD) towards enhancing the charge injection and charge transport properties, which are crucial for achieving high efficiency OLEDs.[69] Several methods have been reported for modifying the graphene anode, such as treatment with oxygen plasma, ultraviolet-ozone, and insertion of an ultra-thin buffer layer (MoO_3 , WO_3 , PEDOT: PSS and PFSA).[69] PEDOT:PSS was chosen as the HIL

layer since it has been well studied and shown to enhance the efficiency and lifetime of graphene-based OLEDs.[6], [69] To prevent the well-known wettability issue between graphene and PEDOT:PSS,[70] isopropyl alcohol (IPA) diluted PEDOT:PSS suspension was chosen as the HIL precursor. PEDOT:PSS/IPA ratio was optimized via fabrication and characterization of OLEDs (PET/Gr/PEDOT:PSS/**m-CBP:SeDF-G**/TBPI/LiF/Al) with different proportions. **SeDF-G** was chosen as the emissive layer dopant for optimization studies due to its ease of synthesis and higher yields. The optimization result of HIL is shown in figure 4.6.

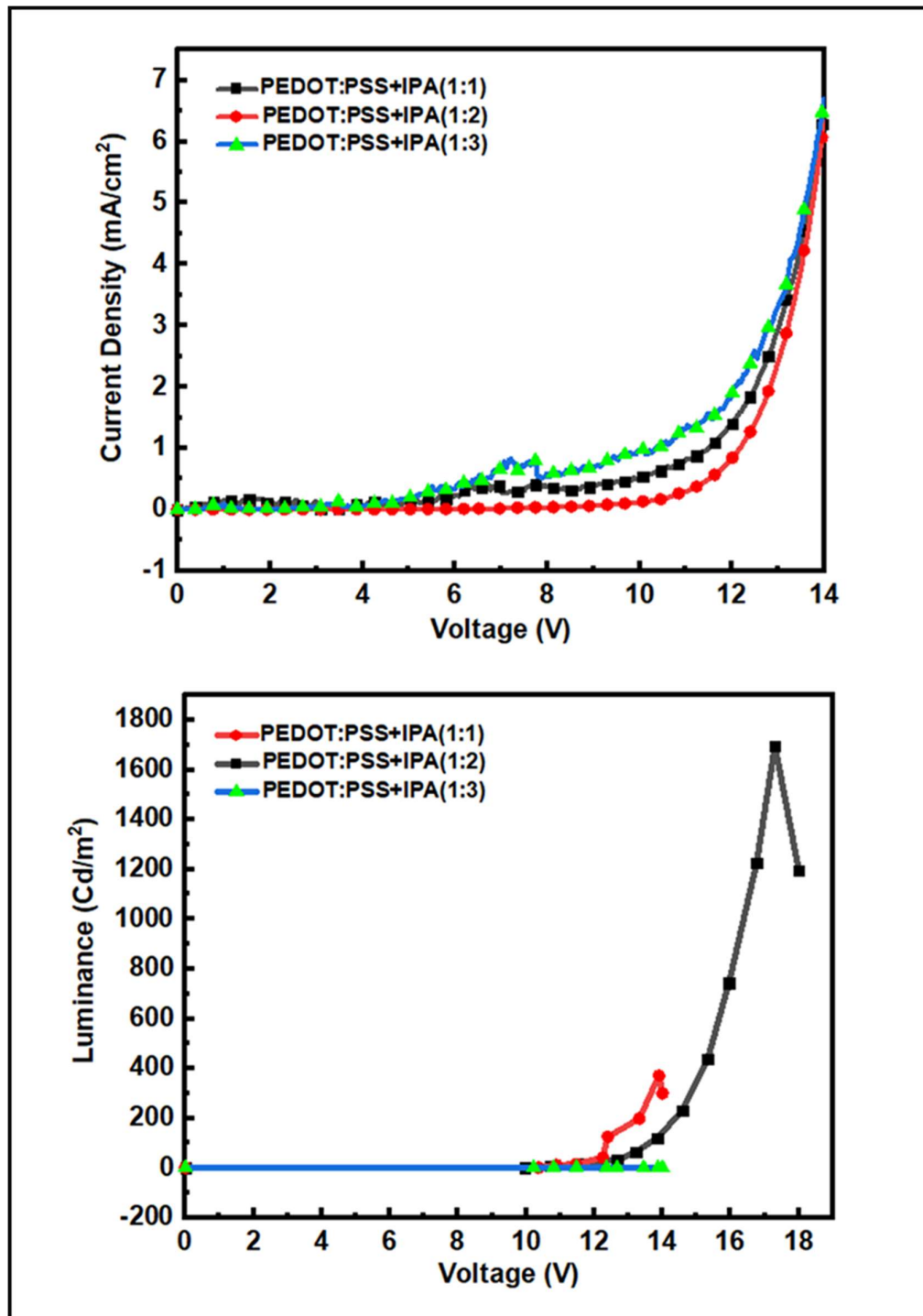


Figure 4.6. The J-V characteristic and luminance vs voltage curve of HIL thickness optimization with (1:1), (1:2), (1:3) ratios.

Our initial devices with the structure mentioned above gave either extremely low light output (best results obtained with 1:2 ratio) or devices degraded before any light emission. At this point, we attributed this poor performance to possible charge imbalance and shift of recombination zone (RZ) to the anode side. To mediate this problem, the electron transport layer (ETL) thickness optimizations were performed to improve the charge balance and RZ confinement.[71] A significant improvement was observed with this approach – from barely working devices to devices with EQEs over 20%, as detailed below – and the optimum thickness for ETL was determined to be 80 nm for graphene-based OLEDs. The ETL thickness optimization result is shown in figure 4.7.

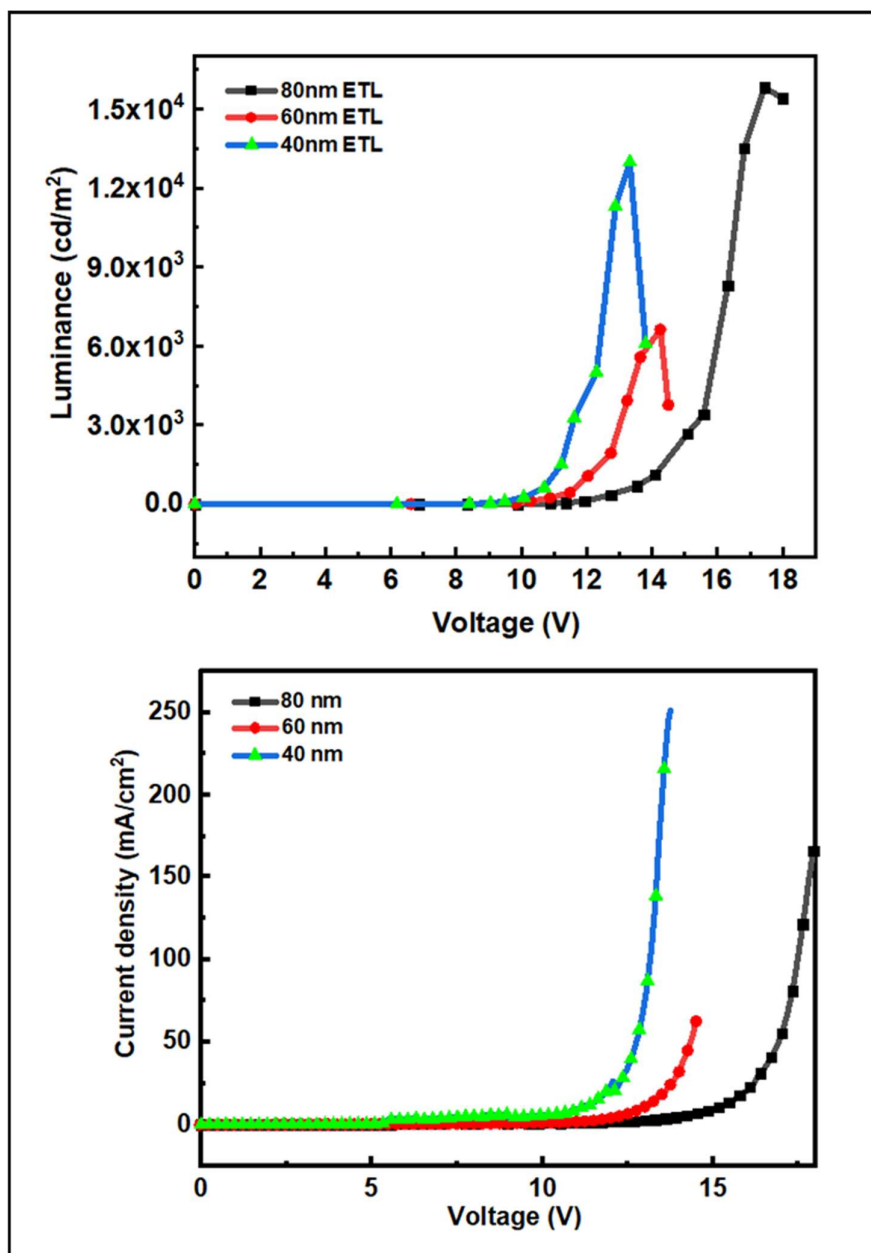


Figure 4.7. The J-V characteristic and luminance vs voltage curve of ETL thickness optimization.

The RZ expanded towards the cathode side as the thickness increased, causing redshift observed in the EL spectra (Figure 4.8).

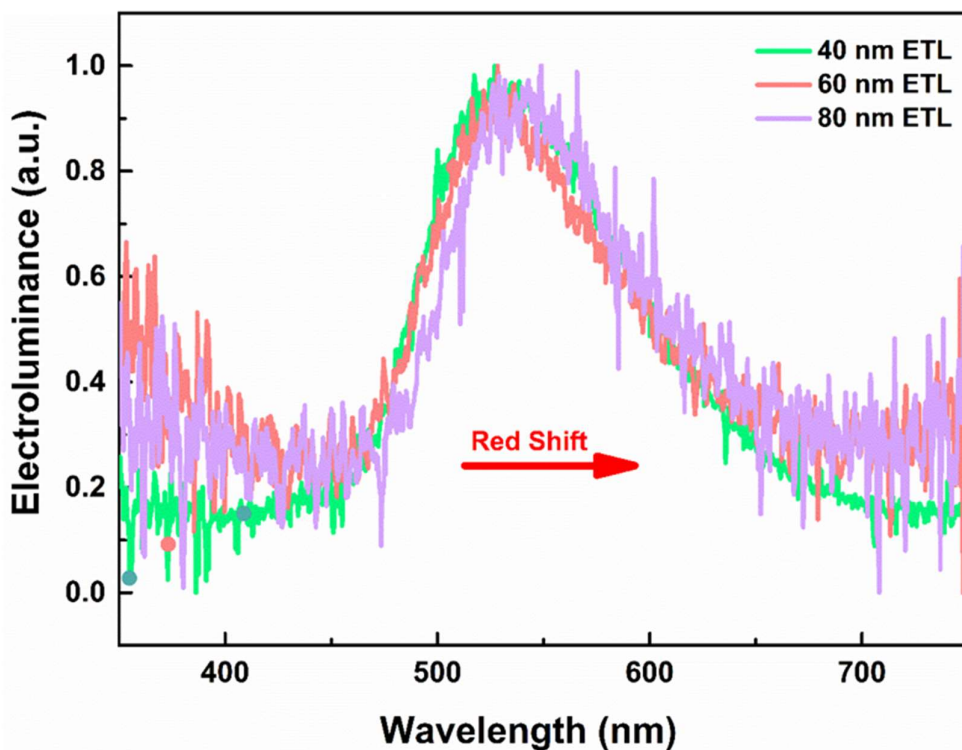


Figure 4.8. Electroluminescence vs wavelength graph for different ETL thicknesses

The device architectures and the energy level diagrams are given in Figure 4.9. The graphene on the pet substrate was first exposed to oxygen plasma for 5 minutes. The hole injection layer, which was made up of PEDOT:PSS and IPA in a 1:1.5 ratio, was spin-coated to create a 40-nm thick film on top of the anodes and then baked for 15 minutes in air at 80 degrees. The oxygen plasma time is 15 minutes for ITO-coated glasses. Organic layers are made up of α -NPD, which serves as an HTL, and TPBI, which works as ETL. The dopants SeDF-G, SeDF-B, and SeDF-YG are green, blue, and yellowish-green, respectively, and were deposited on the emissive layer next to the host material m-CBP. In all devices, the host-to-dopant ratio is 90:10 (v/v). Lithium fluoride (LiF) (0.6 nm)/aluminum (Al) (100 nm) cathode layers were deposited under high vacuum. All thermal vapor depositions were performed at a pressure of less than 10^{-6} torr. The device area was around 4-6 mm². Green, blue,

and yellowish-green OLEDs were successfully fabricated by using graphene and ITO anodes.

The device architecture of the former was PET/Graphene/HIL(40nm)/ α -NPD (40nm)/EML(20nm)/TPBI(80nm)/LiF(0.6nm)/Al(100nm). The latter's device architecture was Glass/ITO/ α -NPD (40nm)/EML(20nm)/TPBI(40nm)/LiF(0.6nm) /Al(100nm). All of the measurements were performed in a glove box.

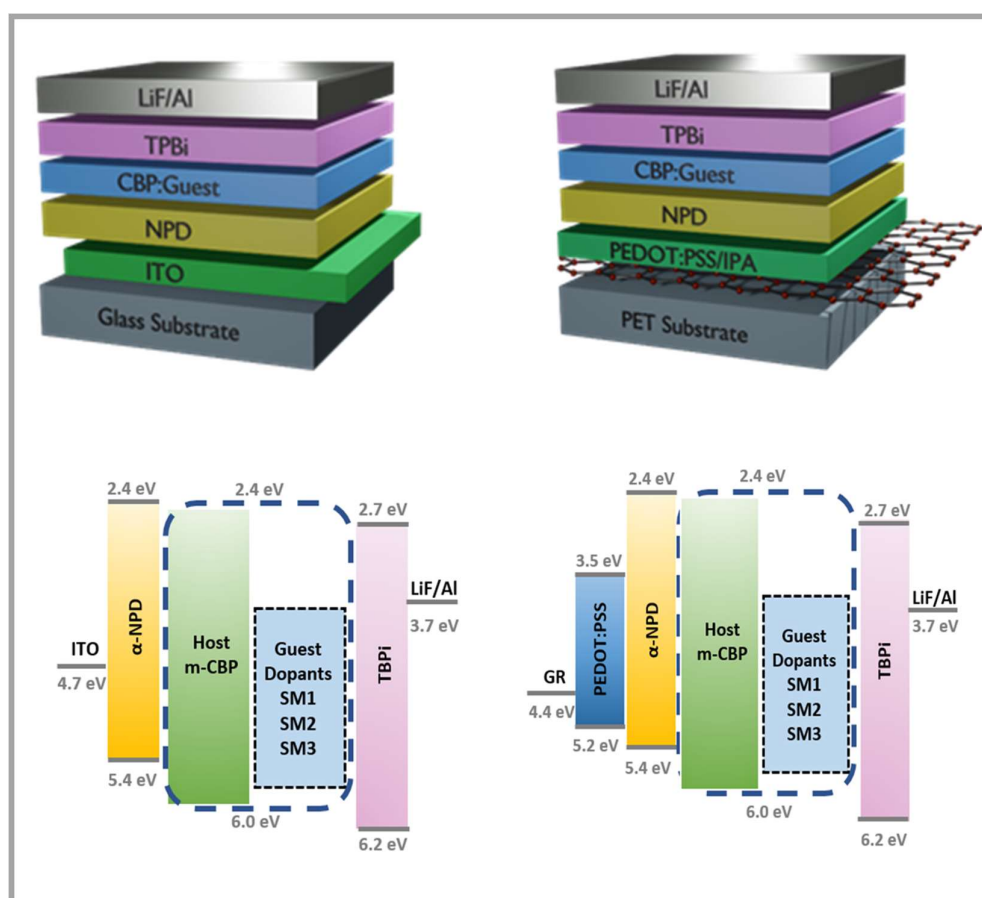


Figure 4.9. Device architectures of (a) ITO-based and (b) graphene-devices and energy band alignments of (c) ITO-based devices and (d) graphene-based devices.

The characterizations prove that (Figure 4.11 a) by mitigating the shortcomings of using graphene anodes for OLED fabrications, it is possible to reach the EQE values of ITO-based non-flexible devices. The reason for achieving high efficiency, almost as high as ITO-based devices, is that HIL is installed on graphene-based devices, reducing luminescence quenching and increasing device efficiency.[72] Once we obtained competitive results, we re-optimized our HIL layer. This time around, the optimum PEDOT:PSS/IPA ratio was determined to be 1:1.5 for graphene-based devices. There was no need to introduce HILs for the ITO-based devices since it has been shown in the literature that increased O₂ plasma durations (~15 minutes) increase the work function of the ITO to desired levels.[73], [74] It is also known that O₂ plasma treatment can modify the work function of graphene; however, longer plasma treatment durations result in peeling-off of the graphene layers and increases the sheet resistance. Hence a short O₂ plasma treatment (~5 minutes) to remove organic contaminants was performed on the graphene-coated PET substrates before PEDOT:PSS deposition.

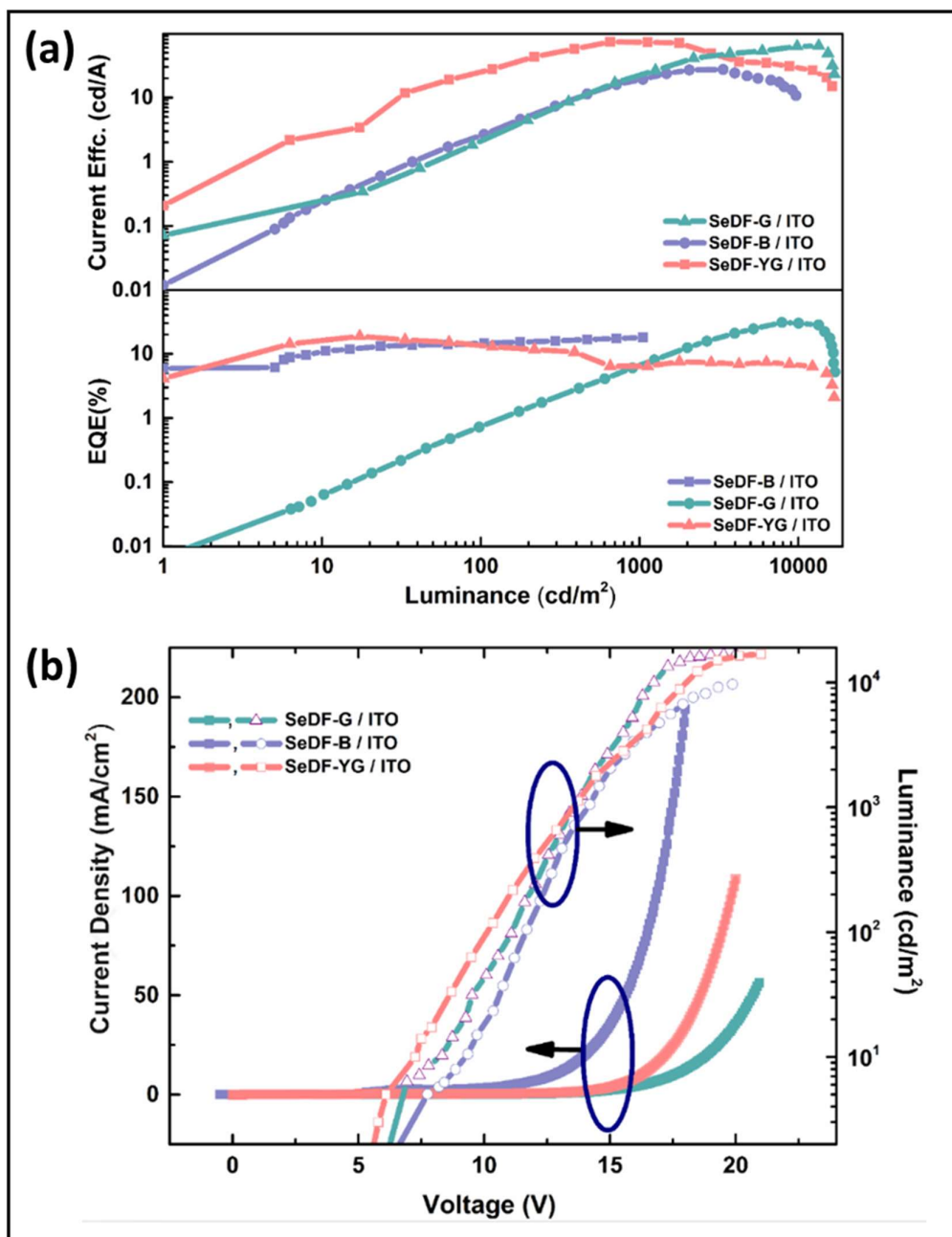


Figure 4.10. OLED characteristics, **a** Current Efficiency and EQE (%) vs. Luminance of devices ITO-SeDF-G, ITO-SeDF-B, and ITO-SeDF-YG, **b**. Current density–voltage–luminance (J–V–L) characteristics of ITO-based OLEDs.

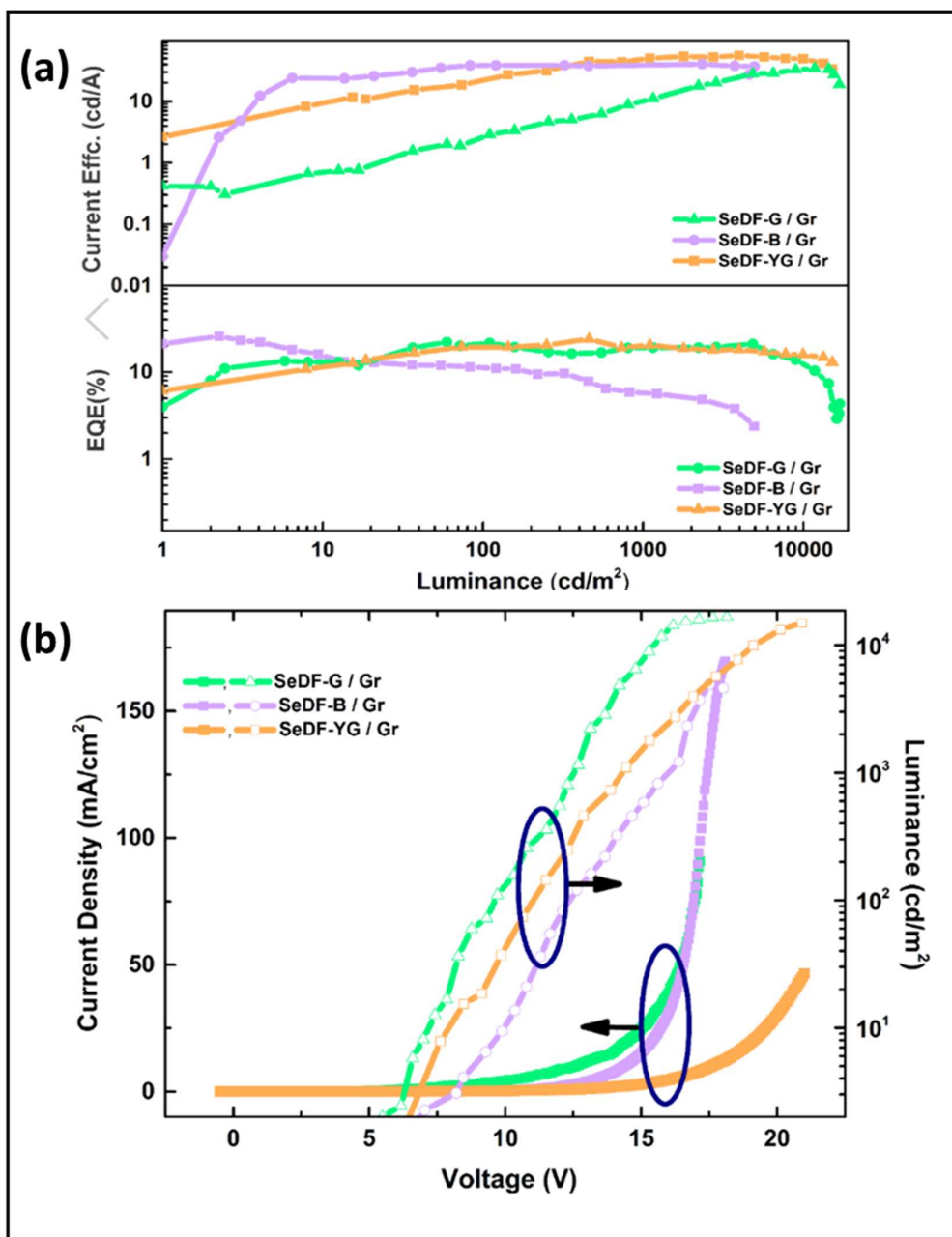


Figure 4.11. a. Current Efficiency and EQE (%) vs. Luminance of devices Gr-SeDF-G, Gr-SeDF-B, and Gr-SeDF-YG, b. Current density–voltage–luminance (J–V–L) characteristics of graphene-based OLEDs.

Once we settled our electrode transport layer optimizations, we moved to determine the potential of the TADF materials both with Gr and ITO-based anodes. Six different device sets were fabricated using three different emitting dopants (**SeDF-G**, **SeDF-B**, and **SeDF-YG**) and two different anodes (graphene and ITO). m-CBP was chosen as a host material for all systems because of its high triplet energy of 2.9 eV, aligned HOMO and LUMO energy levels, a wide energy bandgap, and high morphological stability.[75]

Table 4.1 Summary of OLED characteristics of champion devices, (average in parenthesis).

Device	Anode	Dopant	L_{MAX} (cd.m^{-2}) ^a	η_C (cd.A^{-1}) ^b	η_{EXT} (%) ^c	V_{on} (V) ^d	CIE (x, y) ^e
A	ITO	SeDF-G	17007 (16896)	64.0	30.8	4.3	(0.31,0.53)
B	Gr	SeDF-G	16870 (16290)	34.3	21.6	4.7	(0.36, 0.53)
C	ITO	SeDF-B	9662 (9641)	27.3	25.6	5.8	(0.17, 0.14)
D	Gr	SeDF-B	4594 (4508)	40.5	25.8	5.8	(0.19, 0.16)
E	ITO	SeDF- YG	16833 (16697)	73.5	18.8	5.4	(0.33, 0.48)
F	Gr	SeDF- YG	15144 (14222)	55.8	23.9	5.4	(0.37, 0.51)
Ref[76]	ITO	Px2BP*	86100	35.9	10.7	3.2	(0.37, 0.58)
Ref[76]	ITO	<i>p</i> - PxBBP**	57120	20.1	6.9	3.6	(0.49, 0.51)

Figure. 4.10 and figure. 4.11 illustrates the EQE and Current efficiency vs. Luminance and Current density vs. voltage vs. Luminance graphs for the fabricated devices, and Table 4.1 summarizes the results. The amount of emitter dopant dispersed was only 10% (v/v) to avoid exciton annihilation and high current density.[77] Among all device architectures, the highest EQE value was measured for **SeDF-G**-based OLEDs fabricated by using ITO as the anode (max EQE 30.8%), higher than its graphene counterpart. This observation can be correlated to the lower current density values measured for the aforementioned device architecture as it operates. Furthermore, improved hole injection from anode to emissive layer in **SeDF-G** / ITO could be another reason, which can be explained by the lower turn-on voltage of **SeDF-G** / ITO. Furthermore, the blue device with the graphene anode (**SeDF-B** / Gr) exhibited a much higher current efficiency (40.5 cd/A) than that with the ITO anode (27.3 cd/A) and coherent blue electroluminescence spectra with a Commission Internationale de l'Eclairage (CIE) coordinates (0.19, 0.16). According to Figure. 4.10a and 4.11a, when **SeDF-B** is used as the emitting dopant, the EQE values in both graphene- and ITO-based OLEDs decrease rapidly after reaching high luminance values. This efficiency roll-off at high current density is mainly attributed to excess T1 excitons in the emitting layer, which cause exciton quenching by triplet-triplet and/or singlet-triplet annihilation.[78] This study presents the purest blue color observed for a flexible TADF-based OLED in the literature. Moreover, a highly efficient flexible phosphorescent yellowish-green OLED was fabricated using graphene as the anode, in which the emitting dopant was **SeDF-YG**. The device showed much higher EQE values (23.9%) than the ITO-based device (18.8%). ITO-**SeDF-YG** has a lower EQE, although it has higher current efficiency and almost the same luminance and turn-on voltage as Gr-**SeDF-YG**. Lower EQE value could be explained by the increased joule heating during operation in ITO-**SeDF-YG**, although it shows superior charge injection characteristics.[79] The photographs of the working devices are shown in Figure. 4.12 a, and the color coordinates (x,y) are marked on the chromaticity diagram in Figure. 4.12 b. There is a noticeable red shift for graphene-based OLEDs compared to ITO-based devices in their EL spectrum

(Figure. 4.12 c), demonstrating that the recombination zones of graphene-based devices are closer to the cathode, a highly desirable phenomenon for increased efficiency.[80]

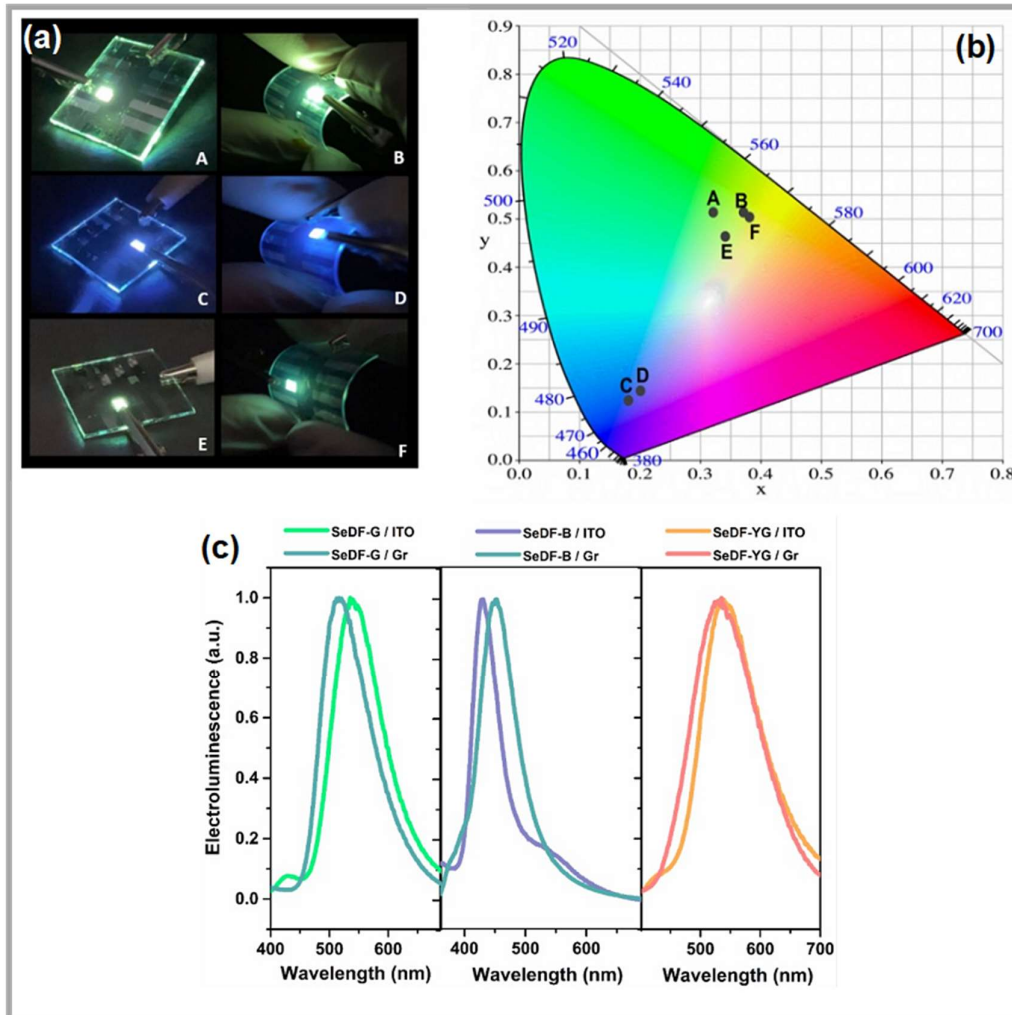


Figure 4.12., Photographs of ITO based and graphene-based OLED devices (A: **SeDF-G** / ITO, B: **SeDF-G** / Gr, C: **SeDF-B** / ITO, D: **SeDF-B** / Gr, E: **SeDF-YG** / ITO, F: **SeDF-YG** / Gr). **b**, Chromaticity diagram of OLED devices. **c**, Electroluminescence vs. wavelength graphs of devices: (**SeDF-G** / ITO and **SeDF-G** / Gr), (**SeDF-B** / ITO and **SeDF-B** / Gr), (**SeDF-YG** / ITO and **SeDF-YG** / Gr).

The results demonstrate that graphene/PET anodes are extremely promising candidates to replace ITO for next-generation flexible solid-state lighting device technologies. Last but not least, it is significantly important to note that EQEs observed from OLEDs utilizing **SeDF-G** and **SeDF-YG** (ITO/Glass) are almost three times higher than devices using their selenium free analogs (Px2BP and *p*-Px2BBP) with practically the same device structures (Table 2).[76] This clearly demonstrates the success of the rational design approach introduced in this work.

4.3 Graphene based OLEDs with commercial materials

In order to have working OLEDs with high EQEs and luminance, it's necessary to make sure about charge balance and broad recombination zone. When compared to a narrow recombination zone, a large electron-hole recombination zone results in a longer OLED operational lifetime. This makes sense since the recombination of large carriers confined in a narrow zone causes the device to heat up.

In OLEDs, the charge balance and recombination zone (RZ) are extremely sensitive to the thickness of the HTL, which must be controlled for increased device efficiencies.

The optimization of ETL thickness is applied in TADF OLEDs to solve narrow recombination zone which conclude with high efficiency OLEDs. Another solution to heating of the OLED devices is to design and synthesis emitters with low-turn on voltage. In order to do this, graphene-based OLEDs is fabricated by commercial polymers is used. PFOPV is kind of emitters which having turning-on voltages around 2,3 Volts. This emitter is spin coated on top of graphene anode. The thickness optimization of PFOPV is done and the results is summarized in figure 4.13.

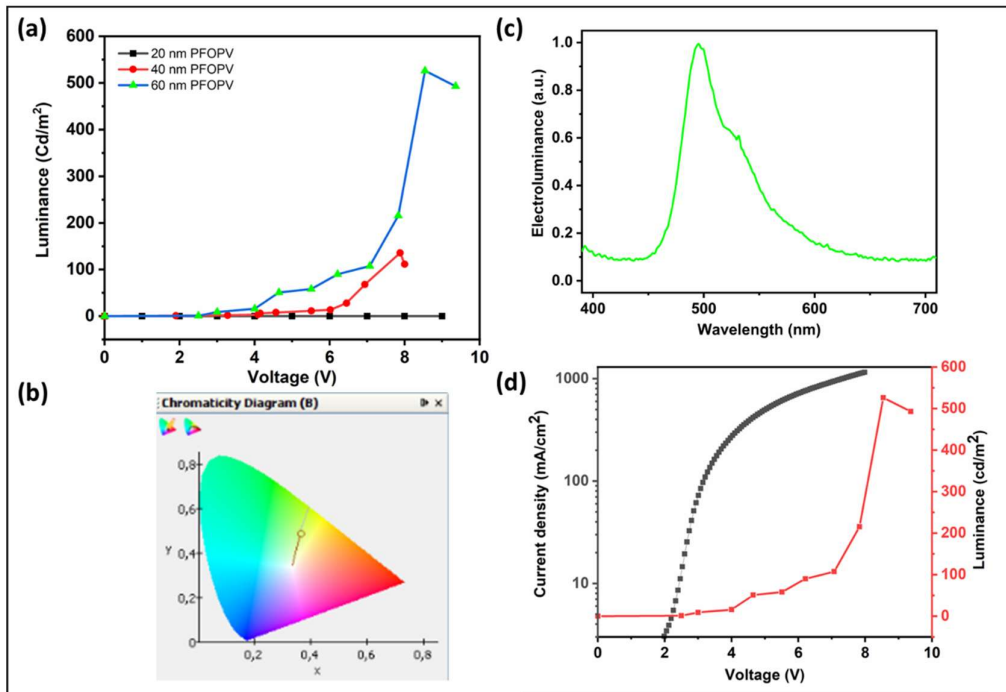


Figure 4.13. a. Luminance vs voltage plot of PFOPV thickness optimization, b. Electroluminescence spectrum of device, c. Chromaticity diagram of device, d. Current density–voltage–luminance (J–V–L) characteristics of graphene-based OLEDs.

CONCLUSION

In this thesis synthesis of single layer graphene is optimized and characterized with different characterization tools such as optical microscopy, Raman spectroscopy, SEM, optical transparency and hall effect measurement. In order to use graphene as transparent electrode in OLED application, it's necessary to reduce the sheet resistance of graphene. A doping method is optimized and investigated to decrease the sheet resistance of graphene. Last-layer doping is a method which 7 layer graphene is stacked layer by layer and transfer to PET substrate, and at the end last layer exposed to HNO_3 . As a result, a graphene anode with $29 \Omega/\square$ sheet resistance and 84 % optical transparency is achieved.

The key to achieve high efficiency OLEDs is to improve charge injection and transport to realize charge balance. In order to improve carrier injection and increase the work function of the graphene, many methods have been tried on the modification of anode surface such as: the treatment of oxygen plasma, the insertion of an ultra-thin buffer layer such as MoO_3 and PEDOT:PSS. Appropriate selection of the hole injection layer (HIL) is more important than electron transport layer. The work functions of graphene, and PEDOT:PSS are 4.4 eV, and 5.2 eV, respectively. PEDOT:PSS should be coated uniformly in the top of graphene but because of the hydrophobic property of graphene, it's not possible. To ignore this problem PEDOT:PSS was mixed by IPA (1:1.5). The mixture of PEDOT:PSS+IPA gave the best result.

The efficacy of RISC in TADF systems is proportional to HSO and inversely proportional to ΔEST . While different approaches have been pursued for minimizing ΔEST with transformative success, the effect of HSO in these systems has been largely overseen. Hence, TADF materials with heavy-atom selenium incorporation (SeDF-G, SeDF-B, SeDF-YG) which designed and synthesised in half of TUBITAK project is used in this work. The materials showed remarkable performance where EQEs over 30% were achieved with SeDF-G. OLEDs utilizing SeDF-G and SeDF-

YG are almost three times higher than devices using their selenium-free analogs with practically the same device structures. Additionally, first time in the literature, flexible graphene-based electrodes were developed for TADF based OLEDs and revealed almost ITO/glass like performance in most cases. Remarkably, graphene-based devices showed higher performance compared to their ITO analogs in pure blue OLED devices (EQEs, 25.6% vs. 25.8%).

REFERENCES

- [1] T. Kuilla, S. Bhadra, D. Yao, N. H. Kim, S. Bose, and J. H. Lee, “Recent advances in graphene based polymer composites,” *Prog. Polym. Sci.*, vol. 35, no. 11, pp. 1350–1375, 2010, doi: 10.1016/j.progpolymsci.2010.07.005.
- [2] L. Liao *et al.*, “High-speed graphene transistors with a self-aligned nanowire gate,” *Nature*, vol. 467, no. 7313, pp. 305–308, 2010, doi: 10.1038/nature09405.
- [3] M. F. El-Kady, V. Strong, S. Dubin, and R. B. Kaner, “Laser scribing of high-performance and flexible graphene-based electrochemical capacitors,” *Science (80-.)*, vol. 335, no. 6074, pp. 1326–1330, 2012, doi: 10.1126/science.1216744.
- [4] F. Bonaccorso, Z. Sun, T. Hasan, and A. C. Ferrari, “Graphene photonics and optoelectronics,” *Nat. Photonics*, vol. 4, no. 9, pp. 611–622, 2010, doi: 10.1038/nphoton.2010.186.
- [5] T. H. Han *et al.*, “Extremely efficient flexible organic light-emitting diodes with modified graphene anode,” *Nat. Photonics*, vol. 6, no. 2, pp. 105–110, 2012, doi: 10.1038/nphoton.2011.318.
- [6] N. Li *et al.*, “Efficient and bright organic light-emitting diodes on single-layer graphene electrodes,” *Nat. Commun.*, vol. 4, pp. 1–7, 2013, doi: 10.1038/ncomms3294.
- [7] T. H. Han *et al.*, “Approaching ultimate flexible organic light-emitting diodes using a graphene anode,” *NPG Asia Mater.*, vol. 8, no. 9, pp. 1–8, 2016, doi: 10.1038/am.2016.108.
- [8] T. Das and B. K. Sharma, “Graphene-based flexible and wearable electronics Graphene-based flexible and wearable electronics,” no. January 2018, 2020, doi: 10.1088/1674-4926/39/1/011007.

- [9] A. K. Geim and K. S. Novoselov, “The rise of graphene PROGRESS,” *Nat. Mater.*, vol. 6, no. 3, pp. 183–191, 2007.
- [10] K. S. Novoselov *et al.*, “Two-dimensional gas of massless Dirac fermions in graphene,” vol. 438, no. November, pp. 197–200, 2005, doi: 10.1038/nature04233.
- [11] Y. Zhang, Y. Tan, H. L. Stormer, and P. Kim, “Experimental observation of the quantum Hall effect and Berry ’ s phase in graphene,” vol. 438, no. November, pp. 201–204, 2005, doi: 10.1038/nature04235.
- [12] P. E. Allain and J. N. Fuchs, “Klein tunneling in graphene: Optics with massless electrons,” *Eur. Phys. J. B*, vol. 83, no. 3, pp. 301–317, 2011, doi: 10.1140/epjb/e2011-20351-3.
- [13] T. H. E. Royal, S. Academy, and O. F. Sciences, “compiled by the Class for Physics of the Royal Swedish Academy of Sciences Graphene,” vol. 50005, no. October, pp. 0–10, 2010.
- [14] A. H. C. Neto, “Two-dimensional crystals-based heterostructures : Materials with tailored properties,” no. April, 2016, doi: 10.1088/0031-8949/2012/T146/014006.
- [15] J. Basu, J. K. Basu, and T. K. Bhattacharyya, “The evolution of graphene-based electronic devices,” vol. 5411, 2010, doi: 10.1080/19475411.2010.510856.
- [16] Y. Hernandez *et al.*, “High-yield production of graphene by liquid-phase exfoliation of graphite,” *Nat. Nanotechnol.*, vol. 3, no. 9, pp. 563–568, 2008, doi: 10.1038/nnano.2008.215.
- [17] J. Penney and L. H. Tsai, “Elimination of senescent cells prevents neurodegeneration in mice,” *Nature*, vol. 562, no. 7728, pp. 503–504, 2018, doi: 10.1038/d41586-018-06677-7.
- [18] C. Berger *et al.*, “Ultrathin epitaxial graphite: 2D electron gas properties and

a route toward graphene-based nanoelectronics,” *J. Phys. Chem. B*, vol. 108, no. 52, pp. 19912–19916, 2004, doi: 10.1021/jp040650f.

- [19] W. Strupinski *et al.*, “Growth of graphene layers on silicon carbide,” *Mater. Sci. Forum*, vol. 615–617, pp. 199–202, 2009, doi: 10.4028/www.scientific.net/MSF.615-617.199.
- [20] S. Bae *et al.*, “Roll-to-roll production of 30-inch graphene films for transparent electrodes,” *Nat. Nanotechnol.*, vol. 5, no. 8, pp. 574–578, 2010, doi: 10.1038/nnano.2010.132.
- [21] T. Ozuluer, E. Pince, E. O. Polat, O. Balci, O. Salihoglu, and C. Kocabas, “Synthesis of graphene on gold,” *Appl. Phys. Lett.*, vol. 98, no. 18, pp. 18–21, 2011, doi: 10.1063/1.3584006.
- [22] B. J. Kang, J. H. Mun, C. Y. Hwang, and B. J. Cho, “Monolayer graphene growth on sputtered thin film platinum,” *J. Appl. Phys.*, vol. 106, no. 10, 2009, doi: 10.1063/1.3254193.
- [23] S. Y. Kwon *et al.*, “Growth of semiconducting graphene on palladium,” *Nano Lett.*, vol. 9, no. 12, pp. 3985–3990, 2009, doi: 10.1021/nl902140j.
- [24] K. Matsumoto, *Frontiers of Graphene and Carbon Nanotubes*. 2015.
- [25] X. Li *et al.*, “Large-area synthesis of high-quality and uniform graphene films on copper foils,” *Science (80-.)*, vol. 324, no. 5932, pp. 1312–1314, 2009, doi: 10.1126/science.1171245.
- [26] X. Li *et al.*, “Graphene films with large domain size by a two-step chemical vapor deposition process,” *Nano Lett.*, vol. 10, no. 11, pp. 4328–4334, 2010, doi: 10.1021/nl101629g.
- [27] G. H. Han *et al.*, “Influence of copper morphology in forming nucleation seeds for graphene growth,” *Nano Lett.*, vol. 11, no. 10, pp. 4144–4148, 2011, doi: 10.1021/nl201980p.

- [28] Z. Luo *et al.*, “Effect of substrate roughness and feedstock concentration on growth of wafer-scale graphene at atmospheric pressure,” *Chem. Mater.*, vol. 23, no. 6, pp. 1441–1447, 2011, doi: 10.1021/cm1028854.
- [29] I. Vlassioux *et al.*, “Role of hydrogen in chemical vapor deposition growth of large single-crystal graphene,” *ACS Nano*, vol. 5, no. 7, pp. 6069–6076, 2011, doi: 10.1021/nn201978y.
- [30] D. Bhat, “Chemical Vapor Deposition,” in *Coatings Technology*, CRC Press, 2006, pp. 36-1-36–11.
- [31] Z. Ni, Y. Wang, T. Yu, and Z. Shen, “Raman Spectroscopy and Imaging of Graphene,” 2008, doi: 10.1007/s12274-008-8036-1.
- [32] J. Lee, X. Zheng, R. C. Roberts, and P. X. L. Feng, “Scanning electron microscopy characterization of structural features in suspended and non-suspended graphene by customized CVD growth,” *Diam. Relat. Mater.*, vol. 54, no. 1, pp. 64–73, 2015, doi: 10.1016/j.diamond.2014.11.012.
- [33] Y. G. Shi, D. Wang, J. C. Zhang, P. Zhang, X. F. Shi, and Y. Hao, “Fabrication of single-crystal few-layer graphene domains on copper by modified low-pressure chemical vapor deposition,” *CrystEngComm*, vol. 16, no. 32, pp. 7558–7563, 2014, doi: 10.1039/c4ce00744a.
- [34] F. V. Kusmartsev, W. M. Wu, M. P. Pierpoint, and K. C. Yung, “Application of Graphene Within Optoelectronic Devices and Transistors,” no. June, pp. 191–221, 2015, doi: 10.1007/978-981-287-242-5_9.
- [35] J. Kang, D. Shin, S. Bae, and B. H. Hong, “Graphene transfer: Key for applications,” *Nanoscale*, vol. 4, no. 18, pp. 5527–5537, 2012, doi: 10.1039/c2nr31317k.
- [36] D. Senyildiz, O. T. Ogurtani, and G. Cambaz Buke, “The effects of acid pretreatment and surface stresses on the evolution of impurity clusters and graphene formation on Cu foil,” *Appl. Surf. Sci.*, vol. 425, pp. 873–878, 2017,

doi: 10.1016/j.apsusc.2017.07.092.

- [37] “Organic Light-Emitting Diodes (OLED) Have Many Potential Uses - Tech Briefs.”
<https://www.techbriefs.com/component/content/article/tb/supplements/ptb/briefs/29611> (accessed Jul. 01, 2021).
- [38] G. Hong *et al.*, “A Brief History of OLEDs—Emitter Development and Industry Milestones,” *Adv. Mater.*, vol. 33, no. 9, 2021, doi: 10.1002/adma.202005630.
- [39] S. F. Nelson, Y. Y. Lin, D. J. Gundlach, and T. N. Jackson, “Temperature-independent transport in high-mobility pentacene transistors,” *Appl. Phys. Lett.*, vol. 72, no. 15, pp. 1854–1856, Jun. 1998, doi: 10.1063/1.121205.
- [40] “DSCC details Samsung’s upcoming foldable OLED phones | OLED-Info.”
<https://www.oled-info.com/dscc-details-samsungs-upcoming-foldable-oled-phones> (accessed Jul. 01, 2021).
- [41] “Al Sharqiya.” <https://alsharqiya.com/en/news/launch-of-the-worlds-first-foldable-screen-tv> (accessed Jul. 01, 2021).
- [42] T. W. Hu, S. T. Chu, and K. H. Chu, “A study on application of OLED technology in development of product innovation,” *Proc. 4th IEEE Int. Conf. Appl. Syst. Innov. 2018, ICASI 2018*, no. November, pp. 762–765, 2018, doi: 10.1109/ICASI.2018.8394372.
- [43] “LG Display to Construct First 5th Generation OLED Light Panel Plant | Architect Magazine.”
https://www.architectmagazine.com/technology/lighting/lg-display-to-construct-first-5th-generation-oled-light-panel-plant_o (accessed Jul. 01, 2021).
- [44] D. Since, “Triplet Harvesting and Singlet Harvesting,” no. Iii, pp. 1–6.
- [45] “TADF: What is Thermally Activated Delayed Fluorescence?”

<https://www.edinst.com/us/blog/tadf-thermally-activated-delayed-fluorescence/> (accessed Jul. 02, 2021).

- [46] “Delorme & F. Perrin, *J. Phys. Rad. Ser.* 10, 177 (1929) - Google Scholar.” https://scholar.google.com/scholar?hl=en&as_sdt=0%2C5&q=Delorme+%26+F.+Perrin%2C+J.+Phys.+Rad.+Ser.+10%2C+177+%281929%29&btnG= (accessed Jul. 02, 2021).
- [47] G. N. Lewis, D. Lifkin, and T. T. Magel, “The Light Absorption and Fluorescence of Triarylmethyl Free Radicals,” *J. Am. Chem. Soc.*, vol. 66, no. 9, pp. 1579–1583, 1944, doi: 10.1021/ja01237a048.
- [48] H. Uoyama, K. Goushi, K. Shizu, H. Nomura, and C. Adachi, “Highly efficient organic light-emitting diodes from delayed fluorescence,” *Nature*, vol. 492, no. 7428, pp. 234–238, 2012, doi: 10.1038/nature11687.
- [49] S. Hirata *et al.*, “Highly efficient blue electroluminescence based on thermally activated delayed fluorescence,” *Nat. Mater.*, vol. 14, no. 3, pp. 330–336, 2015, doi: 10.1038/nmat4154.
- [50] J. Meyer *et al.*, “Metal oxide induced charge transfer doping and band alignment of graphene electrodes for efficient organic light emitting diodes,” *Sci. Rep.*, vol. 4, pp. 1–7, 2014, doi: 10.1038/srep05380.
- [51] J. Lee *et al.*, “Synergetic electrode architecture for efficient graphene-based flexible organic light-emitting diodes,” *Nat. Commun.*, vol. 7, pp. 1–9, 2016, doi: 10.1038/ncomms11791.
- [52] S. J. Kwon *et al.*, “Extremely stable graphene electrodes doped with macromolecular acid,” *Nat. Commun.*, vol. 9, no. 1, pp. 1–9, 2018, doi: 10.1038/s41467-018-04385-4.
- [53] P. Rajamalli, N. Senthilkumar, P. Gandeepan, C. C. Ren-Wu, H. W. Lin, and C. H. Cheng, “A Method for Reducing the Singlet-Triplet Energy Gaps of TADF Materials for Improving the Blue OLED Efficiency,” *ACS Appl.*

- Mater. Interfaces*, vol. 8, no. 40, pp. 27026–27034, 2016, doi: 10.1021/acsami.6b10678.
- [54] G. Kreiza *et al.*, “High efficiency and extremely low roll-off solution- and vacuum-processed OLEDs based on isophthalonitrile blue TADF emitter,” *Chem. Eng. J.*, vol. 412, no. January, 2021, doi: 10.1016/j.cej.2021.128574.
- [55] G. Xia *et al.*, “A TADF Emitter Featuring Linearly Arranged Spiro-Donor and Spiro-Acceptor Groups: Efficient Nondoped and Doped Deep-Blue OLEDs with CIE $y < 0.1$,” *Angew. Chemie*, vol. 133, no. 17, pp. 9684–9689, 2021, doi: 10.1002/ange.202100423.
- [56] K. Stavrou, A. Danos, T. Hama, T. Hatakeyama, and A. Monkman, “Hot vibrational states in a high-performance multiple resonance emitter and the effect of excimer quenching on organic light-emitting diodes,” *ACS Appl. Mater. Interfaces*, vol. 13, no. 7, pp. 8643–8655, 2021, doi: 10.1021/acsami.0c20619.
- [57] T. Serevičius *et al.*, “Achieving efficient deep-blue TADF in carbazole-pyrimidine compounds,” *Org. Electron.*, vol. 82, no. March, 2020, doi: 10.1016/j.orgel.2020.105723.
- [58] J. U. Kim *et al.*, “Nanosecond-time-scale delayed fluorescence molecule for deep-blue OLEDs with small efficiency rolloff,” *Nat. Commun.*, vol. 11, no. 1, 2020, doi: 10.1038/s41467-020-15558-5.
- [59] G. Kreiza *et al.*, “Realization of deep-blue TADF in sterically controlled naphthyridines for vacuum- And solution-processed OLEDs,” *J. Mater. Chem. C*, vol. 8, no. 25, pp. 8560–8566, 2020, doi: 10.1039/d0tc01637c.
- [60] T. Ohsawa *et al.*, “A Series of Imidazo[1,2-f]phenanthridine-Based Sky-Blue TADF Emitters Realizing EQE of over 20%,” *Adv. Opt. Mater.*, vol. 7, no. 5, pp. 3–8, 2019, doi: 10.1002/adom.201801282.
- [61] F. M. Xie *et al.*, “tert-Butyl substituted hetero-donor TADF compounds for

- efficient solution-processed non-doped blue OLEDs,” *J. Mater. Chem. C*, vol. 8, no. 17, pp. 5769–5776, 2020, doi: 10.1039/d0tc00718h.
- [62] T. Furukawa, H. Nakanotani, M. Inoue, and C. Adachi, “Dual enhancement of electroluminescence efficiency and operational stability by rapid upconversion of triplet excitons in OLEDs,” *Sci. Rep.*, vol. 5, p. 8429, 2015, doi: 10.1038/srep08429.
- [63] A. S. Malin and M. Hatherly, “Microstructure of cold-rolled copper,” *Met. Sci.*, vol. 13, no. 8, pp. 463–472, Aug. 1979, doi: 10.1179/030634579790438363.
- [64] R. Schlaf, “Tutorial on Work Function.”
- [65] A. Kasry, M. A. Kuroda, G. J. Martyna, G. S. Tulevski, and A. A. Bol, “Chemical doping of large-area stacked graphene films for use as transparent, conducting electrodes,” *ACS Nano*, vol. 4, no. 7, pp. 3839–3844, 2010, doi: 10.1021/nn100508g.
- [66] A. Rodriguez-Serrano, V. Rai-Constapel, M. C. Daza, M. Doerr, and C. M. Marian, “Internal heavy atom effects in phenothiazinium dyes: Enhancement of intersystem crossing via vibronic spin-orbit coupling,” *Phys. Chem. Chem. Phys.*, vol. 17, no. 17, pp. 11350–11358, 2015, doi: 10.1039/c5cp00194c.
- [67] D. Y. Kondakov, J. R. Sandifer, C. W. Tang, and R. H. Young, “Nonradiative recombination centers and electrical aging of organic light-emitting diodes: Direct connection between accumulation of trapped charge and luminance loss,” *J. Appl. Phys.*, vol. 93, no. 2, pp. 1108–1119, 2003, doi: 10.1063/1.1531231.
- [68] D. de Sa Pereira *et al.*, “The effect of a heavy atom on the radiative pathways of an emitter with dual conformation, thermally-activated delayed fluorescence and room temperature phosphorescence,” *J. Mater. Chem. C*, vol. 7, no. 34, pp. 10481–10490, 2019, doi: 10.1039/C9TC02477H.

- [69] Z. Wenjin, B. Ran, Z. Hongmei, and H. Wei, “The effect of the hole injection layer on the performance of single layer organic light-emitting diodes,” *J. Appl. Phys.*, vol. 116, no. 22, 2014, doi: 10.1063/1.4903752.
- [70] W. Zhang *et al.*, “Isopropanol-treated PEDOT:PSS as electron transport layer in polymer solar cells,” *Org. Electron.*, vol. 15, no. 12, pp. 3445–3451, 2014, doi: 10.1016/j.orgel.2014.09.026.
- [71] W. H. Lee *et al.*, “Improvement of charge balance, recombination zone confinement, and low efficiency roll-off in green phosphorescent OLEDs by altering electron transport layer thickness,” *Mater. Res. Express*, vol. 5, no. 7, 2018, doi: 10.1088/2053-1591/aacec6.
- [72] X. F. Peng *et al.*, “Modified conducting polymer hole injection layer for high-efficiency perovskite light-emitting devices: Enhanced hole injection and reduced luminescence quenching,” *J. Phys. Chem. Lett.*, vol. 8, no. 19, pp. 4691–4697, 2017, doi: 10.1021/acs.jpcclett.7b01992.
- [73] S. H. Chen, “Work-function changes of treated indium-tin-oxide films for organic light-emitting diodes investigated using scanning surface-potential microscopy,” *J. Appl. Phys.*, vol. 97, no. 7, 2005, doi: 10.1063/1.1884245.
- [74] J. Xin, P. Sun, F. Zhu, Y. Wang, and D. Yan, “Doped crystalline thin-film deep-blue organic light-emitting diodes,” *J. Mater. Chem. C*, vol. 9, no. 7, pp. 2236–2242, 2021, doi: 10.1039/d0tc05934j.
- [75] T. Furukawa, H. Nakanotani, M. Inoue, and C. Adachi, “electroluminescence efficiency and,” pp. 1–8, 2015, doi: 10.1038/srep08429.
- [76] S. Y. Lee, T. Yasuda, Y. S. Yang, Q. Zhang, and C. Adachi, “Luminous butterflies: Efficient exciton harvesting by benzophenone derivatives for full-color delayed fluorescence OLEDs,” *Angew. Chemie - Int. Ed.*, vol. 53, no. 25, pp. 6402–6406, 2014, doi: 10.1002/anie.201402992.
- [77] S. J. Yoon, H. J. Lee, K. H. Lee, and J. Y. Lee, “A study on the effect of a

- pyridine secondary acceptor on the emission properties of thermally activated delayed fluorescence emitters,” *J. Mater. Chem. C*, vol. 8, no. 22, pp. 7485–7491, 2020, doi: 10.1039/d0tc00318b.
- [78] Y. Zhang and S. R. Forrest, “Triplets contribute to both an increase and loss in fluorescent yield in organic light emitting diodes,” *Phys. Rev. Lett.*, vol. 108, no. 26, pp. 1–5, 2012, doi: 10.1103/PhysRevLett.108.267404.
- [79] A. Kirch, A. Fischer, M. Liero, J. Fuhrmann, A. Glitzky, and S. Reineke, “Experimental proof of Joule heating-induced switched-back regions in OLEDs,” *Light Sci. Appl.*, vol. 9, no. 1, 2020, doi: 10.1038/s41377-019-0236-9.
- [80] P. J. Jesuraj *et al.*, “Recombination Zone Control without Sensing Layer and the Exciton Confinement in Green Phosphorescent OLEDs by Excluding Interface Energy Transfer,” *J. Phys. Chem. C*, vol. 122, no. 5, pp. 2951–2958, 2018, doi: 10.1021/acs.jpcc.7b11039.

CURRICULUM VITAE

PERSONAL INFORMATION

Surname, Name: Parisa Sharif
Nationality: Iran
Date and Place of Birth: 19 September 1986, Urmia
Marital Status: Single
Phone: +90 5319846280
email: sharif.parisa@metu.edu.tr

EDUCATION

Degree	Institution	Year of Graduation
MS	METU Micro and Nanotechnology	2015
BS	Azad University Electrical Eng.	2009
High School	Zahra high school	2005

WORK EXPERIENCE

Year	Place	Enrollment
2016-Present	METU Physics.	Project Assistant
2014-2016	Bilkent Dept. of Electrical Eng.	Project Assistant
2012-2014	METU Dept. of Electrical Eng.	Project Assistant

FOREIGN LANGUAGES

English, Turkish, Farsi